AN ABSTRACT OF THE THESIS OF

Markus G. Graulich for the degree of Master of Science in

Electrical & Computer Engineering presented on Dec. 16, 1987

Title: Weather Influence on Loran-C

Abstract approved: Redacted for Privacy

R.S. Engelbrecht

The influence of weather on the long range radio navigation system Loran-C was investigated. The variables analyzed over a period of 255 days were: time differences (TDs), TD signal-to-noise ratios, TD standard deviations (measured at a fixed receiver location in Corvallis, Oregon), time interval numbers (TINOs) (measured at the transmitter locations), transmitter switching times from the U.S. West Coast Chain (9940), and weather data from the same geographical area over a period of 255 days.

The TDs are time differences between a pulse transmitted by the master station and a pulse transmitted by one of the three secondary stations W, X and Y, called TDW, TDX and TDY. The raw TD data showed a 28 day periodicity, which was found to be due to the master transmitter switchings. Only TDY showed a strong diurnal component.

The TD data were found to be significantly correlated with the TINO data, temperatures and, in the case of TDY, also with the α-factor (related to the vertical lapse rate of the refractive index n) and N Dry (the dry component of the refractive index n) in Winnemucca, Nevada.

The diurnal variations of TDY could be partially explained by the diurnal variations of the α-factor. The Local Phase Adjustments introduced by the System Area Monitors were estimated.

Using the (predicted) TINO, temperature, n and α values as control variates we were able to reduce the standard deviation of TDW by 12%, of TDX by 21%, and of TDY by 21%.

Weather Influence On Loran-C

by

Markus Günter Graulich

A THESIS

submitted to

Oregon State University

in partial fulfillment of
the requirements for the
degree of

Master of Science

Completed December 16, 1987

Commencement June 1988

APPROVED:

Redacted for Privacy

Professor in charge of major

Redacted for Privacy

Head of Electrical & Computer Engineering Department

Redacted for Privacy

Dean of Graduate School

Date thesis is presented: December 16, 1987

Typed by: Markus Graulich

ACKNOWLEDGEMENT

I wish to express my thanks to my major professor and thesis advisor Rudolf S. Engelbrecht for his help and encouragement throughout my studies at Oregon State University.

I would also like to thank my parents Günter and Waltraud Graulich in Stuttgart, West Germany for being so supportive and understanding.

Last, but not least, I would like to thank the Baden Württemberg - Oregon exchange program for giving me the opportunity to spend part of my higher education at the Oregon State University in Corvallis.

TABLE OF CONTENTS

LIST OF FIGURES

LIST OF TABLES

LIST OF SYMBOLS

a	radius of the earth = 6370 km
a_e	effective radius of the earth $a_e = a/\alpha$
ASF	Additional Secondary Phase Factor
c	signal propagation speed used by USNO: 299792458 m/s
C	Covariance of two RVs X and Y
CD_s	Coding Delay of secondary S [µs]
CSTD	Controlling Standard Time Difference: reference standard against which the SAM compares its observations
CV	Control Variate
e	partial water pressure [mbar]
E	Expected value
ED	Emission Delay of a secondary [µs]
d	distance between 2 stations [m]
DM	Daily Mean
DT	Day Time mean (9 am to 5 pm)
GRI	Group Repetition Interval Chain 9940: GRI=99400 µs
h	height above sea level [m]
LEN	Local Envelope Number, local transmission delay [µs]
Lkv	weather station in Lakeview, OR
LOP	Line Of Position, the hyperbola with constant TD
Loran	Long range navigation
Loran-C	more accurate than Loran-A, established in 1957
LPA	Local Phase Adjustments [µs]
LPA S	LPAs of secondary S
LV	weather station in Las Vegas, Nevada
m	number of control variates used
M	Master station in Fallon, NV
MFR	weather station in Medford, OR
M Sw	Master transmitter Switching times
MTINO W	Master TINO for secondary W, analogous for X and Y

n	refractive index on surface used by USNO: 1.000338 (standard atmosphere)
N	refractivity, deviation of the refractive index from unity (parts/million) $N=(n-1)*10^6$
N	Number of samples used
Ndry	dry term of the refractivity N
NT	Night Time mean (9 pm to 5 am)
Nwet	wet term of the refractivity N
p	atmospheric pressure in mbar
p	order of prediction
PF	Primary Phase Factor
R	Receiver in Corvallis, OR
r	cross-correlation coefficient
RH	Relative Humidity in %
RV	Random Variable
$r(\tau)$	autocorrelation coefficient at lag τ
$r_{x\,y}$	cross-correlation coefficient RV x and RV y
RXY	cross-correlation coefficient between TDX and TDY
RWX	cross-correlation coefficient between TDW and TDX
RWY	cross-correlation coefficient between TDW and TDY
SAM	System Area Monitor
SAM W	SAM in charge of secondary W in Pt.Cabrillo, CA
SAM XY	SAM in charge of sec. X and Y in Pt.Pinos, CA
SF	Secondary Phase Factor
SIG W	standard deviation of TDW, analogous for TDX, TDY
SLE	weather station in Salem, OR
SNR M	Signal-to Noise ratio for master signal
STINO W	Secondary TINO for secondary W
T	Temperature [K or °C]
$T_{a,b}$	propagation Time from location a to location b
TD	Time Difference [µs]: time interval between the receipt of a master station's pulse and secondary station's pulse from the same rate.
TDS	Phase Time Difference between Secondary S pulse and M pulse

TDW	Phase Time Difference between W pulse and M pulse
TDX	Phase Time Difference between X pulse and M pulse
TDY	Phase Time Difference between Y pulse and M pulse
TINO	Time Interval Number
TT	Transition Time mean (5 am to 9 am, 5 pm to 9 pm)
USNO	US Naval Observatory monitors chain performance
v	propagation velocity
VR	Variance Reduction
W	secondary station in George, WA
wss	wide-sense stationary
W Sw	secondary W transmitter Switching times
WMC	weather station in Winnemucca, NV
X	secondary station in Middletown, CA
X Sw	secondary X transmitter Switching times
Y	secondary station in Searchlight, Nevada
Y Sw	secondary transmitter Switching times
z	Gaussian random variable with $\mu=1$ and $\sigma=0$
α	α-factor
δ	generally used for the differential or difference delta
δ_M	time added to compensate for the master switchings
ϵ	dielectric constant
$\in$	expectation of a random variable
μ	mean
Φ	phase of the low frequency radio signal
σ	standard deviation
τ	lag τ (e.g. in multiples of 1 day)
τ_0	conductivity parameter

Weather Influence On Loran-C

I. INTRODUCTION

The influence of weather on the long range radio navigation system Loran-C was investigated. The measured time differences (TDs) (two TDs from different secondaries can be converted to a position in latitude and longitude) show seasonal and diurnal variations and have large standard deviations which result in time varying position errors. In order to reduce those position errors we need to understand the influence of weather on Loran-C. Then we can correct the measured TDs and so reduce their standard deviation.

Section I.1 explains the principles of the Loran-C system. Section I.2 explains the mathematical models estimating the signal propagation times. Since Loran-C is controlled by system area monitors we need to define how they influence the TDs (section I.3). The time interval numbers (TINOs) also need to be defined, since they reflect the propagation conditions on the paths between the transmitter stations and are correlated with the measured TDs (section I.4). The influence of weather on propagation conditions in general is explained in section I.5.

Sections II.1 - II.3 describe and analyze the measured TD, weather and transmitter data. Section II.4 attempts to explain the TD fluctuations using the observed weather fluctuations. Section II.5 determines the correlations between the TDs and the weather and transmitter data.

In section III. we reduce the time varying TD errors. Section III.1 introduces the theory of linear prediction and the theory of variance reductions using control variates. Section III.2 uses the (predicted) various weather and transmitter data as control variates and successfully reduces the standard deviations of the TDs and so the position errors.

I.1.1 Loran-C Principles

Loran-C is a pulsed, hyperbolic, all-weather long-range radio navigation system available day or night, on or over land and sea. It operates in a frequency band centered at 100 KHz. The system is organized into chains of usually four stations, each transmitting pulses that radiate in all directions. One station in each chain is designated as the master station M and transmits the master pulse; the others are secondary stations, called W,X and Y.

Master and secondary stations are usually separated by about 600 miles. The secondary stations always transmit in a set sequence after the master station with different predetermined fixed delays, called the emission delays (EDs). Thus at any receiver position the master pulses are always received first. Time differences between the master and the pulses from a secondary station increase from a minimum at the secondary station to a maximum at the master station and beyond. The locus of a constant time difference establishes a Loran Line Of Position (LOP), a hyperbola. A master station can be paired with two secondary stations and thus provide two LOPs. The intersection of these two LOPs gives the receiver's position.

A third secondary station can be used to provide an additional LOP to confirm and refine the estimated position.

A chain is characterized by its group repetition interval (GRI). Its number indicates the time interval between master pulses in μs. A receiver samples an incoming Loran-C pulse on the leading edge in order to differentiate between ground and sky waves. The ground wave signal will always be received before the sky wave.

The sky wave lag can be as short as 35 μs, making it necessary to use the leading edge of the pulse to ensure that the ground wave is measured before being contaminated by the effects of the sky wave signal. The ability to use ground waves without contamination from the sky wave permits use of precise techniques in time-difference measurement. It also allows the use of long base lines with high accuracy of synchronization between master and secondary stations. The operating range can exceed 1000 miles.

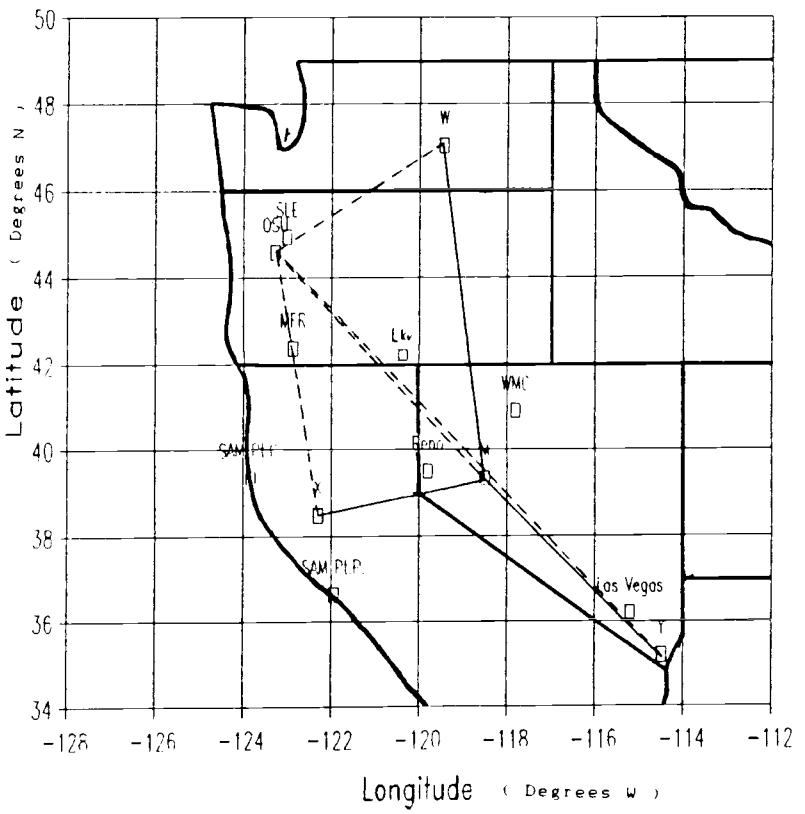

Figure 1.1 U.S. West Coast Loran-C Chain - GRI 9940, Station Map

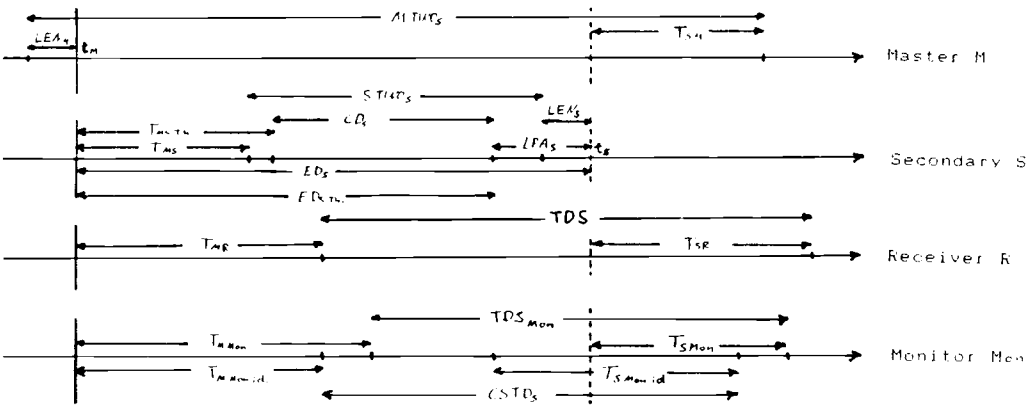

t_M time master actually transmits

t_S time secondary S actually transmits

$ED_S = T_{MS\ th.} + CD_S + LPA_S$

$ED_{S\ th.} = T_{MS\ th.} + CD_S$

$M\ TINO_S = LEN_M + ED_S + T_{SM}$

$S\ TINO_S = ED_S - LEN_S - T_{MS}$

$T_{MS} = (M\ TINO_S - S\ TINO_S)/2 - (LEN_M + LEN_S)/2$

$TDS = ED_S + T_{SR} - T_{MR}$

$TDS_{Mon} = ED_S + T_{SMon} - T_{MMon}$

$CSTD_S = TDS_{MON\ id.} = ED_{S\ th.} + T_{SMON\ id.} - T_{MMon\ id.}$

$LPA_S = (T_{SMon\ id.} - T_{SMon}) - (T_{MMon\ id.} - T_{MMon})$

Figure 1.2 Timing Relations in Loran-C

I.1.2 Specifics of the U.S. West Coast Chain GRI 9940

The U.S. West Coast Chain has a GRI of 99,400 μs. The geographical location of the stations and the weather stations used in this thesis can be seen in Fig.1.1.

The GRI 9940 specifications are given in Table 1.1:

Station	Function	Coordinates	Emm.Delay in μs
Fallon, NV	Master M	39°33'06.62'' N 118°49'56.37'' W	
George, WA	Second.W	47°03'47.99'' N 119°44'39.53'' W	13 796.90 = ED_W
Middletown, CA	Second.X	38°46'56.99'' N 122°29'44.53'' W	28 094.50 = ED_X
Searchlight, NV	Second.Y	35°19'18.18'' N 114°48'17.43'' W	41 967.30 = ED_Y
Pt.Pinos, CA	SAM for X and Y (SAM XY)	36°37'59.02'' N 121°56'05.58'' W	
Pt.Cabrillo,CA	SAM for W (SAM W)	39°20'55.27'' N 123°49'29.72'' W	

Table 1.1 GRI 9940 Station Locations and Emission Delays

The time difference data TDW, TDX and TDY (representing the time difference between the signal from secondary W,X and Y, respectively, and the master at any location) are calculated in the following way (see Fig. 1.2):

The emission delay of a secondary station:

$$ED_s = T_{MS\ ideal} + CD_s \qquad (1.1)$$

The TDs are:

$$TDW = ED_W + T_{WR} - T_{MR} \qquad (1.2)$$

$$TDX = ED_X + T_{XR} - T_{MR} \qquad (1.3)$$

$$TDY = ED_Y + T_{YR} - T_{MR} \qquad (1.4)$$

Special case:

The receiver R, the master and the secondary Y are nearly colinear (see Fig. 1.1):

TDY in Corvallis: $T_{YR} \approx T_{MY} + T_{MR}$ (1.5)

$\rightarrow$ TDY $\approx ED_Y + T_{MY}$ (1.6)

This approximation can be made since both paths are approximately within the first Fresnel zone (see Appendix II).

T_{WR}, T_{XR}, T_{YR} and T_{MR} represent the propagation times on the "base lines" between the stations W, X, Y, M and the Loran-C receiver which, for this experiment, was located on the Oregon State University campus in Corvallis, Oregon. The receiver antenna position is 44°34'03'' W and 123°16'28'' N. Using spherical geometry as described in [11,12] we can calculate the distance between any two locations. Using the free space velocity of $c=2.99792458\ 10^8$ m/s [18] the Loran-C signal has a theoretical free space propagation time of 333.56 µs / 100 km. In order to reduce the constant position errors it is necessary to use the following phase correction factors as defined in [6]:

1. A primary (phase) factor (PF) (included in equation 1.10a), which corrects for a propagation through a standard atmosphere over a perfectly conducting surface as opposed to propagation through free space, $\approx$ .1 µs / 100 km.

2. A secondary (phase) factor (SF), which reflects the amount in µs, by which the Loran-C signal is additionally delayed by propagation over an all sea-water path [11]:

$$S/F = T(1/0.9994 - 1.0) - .2 \quad (1.7)$$

where T is the theoretical propagation time through a standard atmosphere over a perfectly conducting surface [µs]. It amounts to $\approx$ 0.2 µs / 100 km.

3. An additional secondary (phase) factor (ASF) which

reflects the amount in µs, by which the Loran-C signal is additionally delayed by propagation over terrain of various conductivities. This correction varies and must be determined for each area empirically. It is listed in the "Loran-C Correction Tables", a Defense Mapping Agency publication. The corrections are applied to the TDs and are usually in the range of -0.5 to +0.5 µs, but can be as large as -9.9 to +9.9 µs in extreme cases.

The latest Loran-C charts have already been adjusted for all those corrections based on survey data and usually meet the one-quarter nautical mile (463 m) accuracy criteria established by the U.S. Coast Guard.

The theoretical TD values (SF added) calculated for the receiver position [11] are:

TDW = 12 871.49 µs (1.8a)

TDX = 28 022.79 µs (1.8b)

TDY = 43 928.19 µs (1.8c)

The distances and propagation times for all stations of this chain are:

Station to	Station	Distance [km]	Propagation Time [µs] (incl. SF)
M	W	837.8	2796.91
M	X	327.9	1094.53
M	Y	589.3	1967.32
M	R	667.3	2227.60
W	R	390.1	1302.18
X	R	645.8	2155.87
Y	R	1254.6	4188.48
M	SAM W	430.3	1436.35
W	SAM W	918.6	3066.94
M	SAM XY	423.1	1412.28
X	SAM XY	243.6	813.26
Y	SAM XY	659.1	2200.47

Table 1.2 Propagation Times and Distances

I.2 Propagation Equations

The phase velocity depends on various parameters such as ground conductivity, terrain variation and the refractive index profile of the atmosphere [15].

The electric field of a propagating electromagnetical wave is, among other factors, a function of the α-factor (equation A.18, Appendix IV). The α-factor is the ratio of earth radius and effective earth radius and is related to the lapse rate of the refractive index (see Appendix I):

$$\alpha = \frac{a}{a_e} = 1 + a \frac{dn}{dh} \qquad (1.9)$$

where

a = earth radius = 6370 km

a_e = effective radius of the earth due to atmospheric refraction [km]

n = atmospheric refractive index = $(1 + N\ 10^{-6})$

N = refractivity = $(n-1)\ 10^6$

h = height in 100 m units

The phase of a low frequency radio signal (Loran-C pulse) can be expressed as the sum of a primary phase Φ_p and a secondary phase correction Φ_c. Φ_c is caused by finite conductivity and refractive index discontinuities across the boundary along which the signal propagates (see Appendix IV):

$$\Phi_p = \frac{w}{c} nd \qquad (1.10a)$$

$$\Phi_c = (k_1 a)^{1/3}\ \alpha^{2/3}\ \tau_0\ \frac{d}{a} \qquad (1.10b)$$

where

n = surface refractive index

f = frequency of the Loran-C pulse = 100 KHz

c = 2.99792458 10^8 m/s free space velocity of light

$w/c = 2\pi f/c$ = 2.09584473 10^{-3} rad/m

d = distance from transmitter to receiver along smooth spherical earth [m]

k_1 = w/c*n, the wave number [rad/m]

α = α-factor (equation 1.9)

a = earth radius = 6370 km

τ_0 = ground conductivity parameter, derived from the boundary condition at the ground surface, typically ≈0.89 over average land [15], not constant

Φ = phase [rad]

The propagation time T over a path with length d is calculated in the following way:

$$T = \frac{\Phi}{w} = \frac{\Phi_P + \Phi_C}{2\pi f} = \frac{(\Phi_P + \Phi_C)10^{-5}}{2\pi} \quad [s] \qquad (1.11a)$$

The propagation velocity is

$$v = \frac{d}{T} = \frac{d\ 2\pi}{\Phi\ 10^{-5}} \quad [m/s] \qquad (1.11b)$$

A change of the refractive index N and the α-factor has the following effect on the propagation time on path of length d:

A change of the refractivity of ΔN mainly affects the primary phase Φ_P:

$$\Delta\Phi_P = (w/c)\ d\ 10^{-6}\ \Delta N \qquad (1.11c)$$

A change in N is accompanied by a change of the α-factor ($\Delta\alpha$), which influences only the secondary phase correction Φ_C:

$$\Delta\Phi_C = 2/3\ (k_1 a)^{1/3}\ \alpha^{-1/3}\ \tau_0\ d/a\ \Delta\alpha \qquad (1.11d)$$

The change in propagation time on the path is then

$$\Delta T = 10^{-5}\ (\Delta\Phi_P + \Delta\Phi_C)\ /\ (2\ \pi)\ [s] \qquad (1.11e)$$

I.3 Local Phase Adjustments

The propagation times of the master and secondary signals to the receiver can vary by several hundred ns due to weather influence and a frequency drift in the transmitters. To reduce these strong variations (resulting in time varying position errors), system area monitors SAMs are in employed. They keep the time difference that is established for their location (the once calibrated control standard time difference (CSTD)), from fluctuating too much by controlling the emission delays of the secondaries.

There are two SAMs in charge of the GRI 9940. Both are located at the coast, since Loran-C is traditionally used mainly by ships which require maximum precision navigation near the coast. Pt. Cabrillo monitors the performance of secondary W and Pt. Pinos monitors X and Y.

The expected TDW in Pt. Cabrillo is $CSTD_W$ = 15 428.14 µs. This value is called calibrated TD for this location or CSTD. In order to keep TDW, TDX and TDY within +/- 100 ns of the corresponding CSTD, LPAs (local phase adjustments) in 20 ns steps are performed when the 30 minute average of TD deviates from CSTD by more than 20 ns [Definition U.S. Coast Guard]. An adjustment of e.g. +20 ns (if TDS_{MON} is 20 ns below CSTD) is made by adding 20 ns to the coding delay of the corresponding secondary:

$$CD_s' = CD_s + LPA_s \qquad (1.12)$$

The result is that the SAM has forced its (measured) TDS again to meet the CSTD value, the calibration point. About eight adjustments/control steps are performed in a day. If there had been no transmitter drifts, the sum of all LPAs made would add up to zero over a longer period of time. An investigation showed that the first 148 days of the available LPA_W added up to 0, but in the following

days the LPAs made are mostly positive (adding LPAs to the coding delay). The next 162 daily LPA_M added up to +4.11 µs, a considerable drift. In the case of LPA_X the sum over 255 days was -7.64 µs and -8.04 µs for LPA_Y .
The CSTD for Pt. Pinos (monitors X and Y) are:

$TDX_{Pt.Pinos,calibrated} = CSTD_X = 27\ 494.29\ \mu s$

$TDY_{Pt.Pinos,calibrated} = CSTD_Y = 42\ 756.06\ \mu s$

In the following, TDS_a represents the time difference between the signal coming from secondary S and the master signal measured at location a, and T_{ab} means the time in which Loran-C pulse travels from point a to point b. The theoretical explanation of the LPAs is as follows:

ideal: $CSTD_S = TDS_{MON\ id.} = ED_{S\ Th.} + T_{SMON\ id.} - T_{MMON\ id.}$ (1.13)

real: $TDS_{MON} = ED_{S\ Th.} + LPA_S + T_{SMON} - T_{MMON}$ (1.14)

The difference ($CSTD_S$ - TDS_{MON}) is the deviation of TDS_{MON} from the calibrated value. This difference is kept at zero by performing LPAs.

$$TDS_{MON} - CSTD_S = TDS_{MON} - TDS_{MON\ id.}$$
$$= LPA_S + T_{SMON} - T_{SMON\ id.} - T_{MMON} + T_{MMON\ id.}$$
$$= 0\ !\qquad (1.15)$$

$$LPA_S = (T_{SMON\ id.} - T_{SMON}) - (T_{MMON\ id.} - T_{MMON}) \qquad (1.16)$$

In other words, the LPAs are the deviation of the propagation time secondary-monitor T_{SMON} from the ideal (calibrated) value minus the deviation of the propagation time master-monitor T_{MMON} from the ideal value. Fig. 1.2 explains the equations graphically.

In this estimation we ignore the fact that the LPAs also adjust for frequency drifts in the transmitters.

The daily sums of the LPAs LPA_M, LPA_X and LPA_Y were made available by the U.S. Coast Guard. We can calculate the residual TDs (if there had been no LPAs) by subtracting the LPA_S from the measured TDS::

$$TDS_{without\ LPAs} = TDS_{measured} - LPA_S \qquad (1.17)$$

In section II. we will determine whether the SAMs fulfill their purpose of improving the TD stability.

I.4 Time Interval Numbers

The Time Interval Number (TINO) is the time (measured in μs) between the remote signal tracked by the receiver at a master or secondary station and the local time base. It links the local Loran time base to the time of receipt of the remote signal. A secondary TINO is equal to the emission delay minus the baseline length minus the local envelope number (LEN), the TD measured at the secondary. LEN is the time from the signal being generated by the timer until it actually goes out to the transmitting antenna, also called the local transmission delay. A master TINO is the secondary TINO plus twice the baseline length [definition U.S. Coast Guard] plus LEN. The TINO is a good control figure for the performance of the Loran-C chain and can also be explained as the TD measurement at the master station for M TINO or the TD measurement at a secondary station for S TINO.

The theoretical TINOs are:

$$\text{M TINO W} = T_{MW} + CD_W + T_{WM} - T_{MM} + LEN_{MTINOW}$$
$$= ED_W + T_{WM} + LEN_{MTINOW} = 16\ 319.5\ \mu s \qquad (1.18a)$$

$$\text{S TINO W} = T_{MW} + CD_W + T_{WW} - T_{MW} - LEN_{STINOW}$$
$$= ED_W - T_{MW} - LEN_{STINOW} = 10\ 884.4\ \mu s \qquad (1.18b)$$

$$\text{M TINO X} = T_{MX} + CD_X + T_{XM} - T_{MM} + LEN_{MTINOX}$$
$$= ED_X + T_{XM} + LEN_{MTINOX} = 28\ 922.4\ \mu s \qquad (1.19a)$$

$$\text{S TINO X} = T_{MX} + CD_X + T_{XX} - T_{MX} - LEN_{STINOX}$$
$$= ED_X - T_{MX} - LEN_{STINOX} = 27\ 265.7\ \mu s \qquad (1.19b)$$

$$\text{M TINO Y} = T_{MY} + CD_Y + T_{YM} - T_{MM} + LEN_{MTINOY}$$
$$= ED_Y + T_{YM} + LEN_{MTINOY} = 43\ 660.5\ \mu s \qquad (1.20a)$$

$$\text{S TINO Y} = T_{MY} + CD_Y + T_{YY} - T_{MY} - LEN_{STINOY}$$
$$= ED_Y - T_{MY} - LEN_{STINOY} = 39\ 889.3\ \mu s \qquad (1.20b)$$

The deviations of the TINOs from the theoretical value (measured daily between 12-1 pm PST at the master and each secondary station by averaging over one hour)

were also made available for the time of the experiment. From M TINO S and S TINO S it is possible to determine the theoretical propagation delay on any base line, T_{MW}, T_{MX} and T_{MY}:

$$\text{M TINO W} = ED_W + T_{WM} + LEN_{MTINOW}$$

$$\text{S TINO W} = ED_W - T_{MW} - LEN_{STINOW} \qquad (1.21)$$

$$T_{MW} = (\text{M TINO W} - \text{S TINO W} - (LEN_{MTINOW} + LEN_{STINOW}))/2$$

$$\text{M TINO X} = ED_X + T_{XM} + LEN_{MTINOX}$$

$$\text{S TINO X} = ED_X - T_{MX} - LEN_{STINOX} \qquad (1.22)$$

$$T_{MX} = (\text{M TINO X} - \text{S TINO X} - (LEN_{MTINOX} + LEN_{STINOX}))/2$$

$$\text{M TINO Y} = ED_Y + T_{YM} + LEN_{MTINOY}$$

$$\text{S TINO Y} = ED_Y - T_{MY} - LEN_{STINOY} \qquad (1.23)$$

$$T_{MY} = (\text{M TINO Y} - \text{S TINO Y} - (LEN_{MTINOY} + LEN_{STINOY}))/2$$

LENs are not constant. A calculation of the exact propagation delays on the base lines would require having available the LENs as a function of time.

We express the TDs as a function of the TINO values at any receiver location R:

$$TDW = ED_W + T_{WR} - T_{MR}$$

$$\text{M TINO W} = ED_W + T_{WM} + LEN_{MTINOW}$$

$$\rightarrow ED_W = \text{M TINO W} - T_{WM} - LEN_{MTINOW}$$

$$TDW = \text{M TINO W} - T_{WM} - LEN_{MTINOW} + T_{WR} - T_{MR}$$

using (1.21):

$$TDW = (\text{M TINO W} + \text{S TINO W})/2 + (LEN_{STINOW} - LEN_{MTINOW})/2 + T_{WR} - T_{MR} \qquad (1.24)$$

analogous for TDX:

$$TDX = (\text{M TINO X} + \text{S TINO X})/2 + (LEN_{STINOX} - LEN_{MTINOX})/2 + T_{XR} - T_{MR} \qquad (1.25)$$

analogous for TDY:

$$TDY = (M\ TINO\ Y + S\ TINO\ Y)/2 + (LEN_{STINOY} - LEN_{MTINOY})/2 + T_{YR} - T_{MR} \quad (1.26)$$

For a receiver position on the extension of a baseline such as Corvallis (extension of the YM baseline) we obtain a special condition for TDY:

$$\begin{aligned} TDY &= ED_Y + T_{YR} - T_{MR} \\ M\ TINO\ Y &= ED_Y + T_{YM} + LEN_{MTINOY} \\ \rightarrow ED_Y &= M\ TINO\ Y - T_{YM} - LEN_{MTINOY} \\ TDY &= M\ TINO\ Y - T_{YM} - LEN_{MTINOY} + T_{YR} - T_{MR} \\ &= M\ TINO\ Y - LEN_{MTINOY} + T_{YR} - (T_{MR} + T_{YM}) \end{aligned}$$

and using (1.5): $T_{YR} \approx T_{MR} + T_{YM}$

$$TDY \approx M\ TINO\ Y - LEN_{MTINOY} \quad (1.27)$$

TDY is proportional to M TINO Y - LEN only, a result that will be confirmed later. The timing relations are shown in Fig. 1.2.

I.5 Influence of Weather

The propagation errors in Loran-C are a result of geophysical and metereological variations along the signal paths, atmospheric and man-made noise, and electromagnetic interference. In this research we look at the meterological variations, emphasizing the influence of the refractive index n and the lapse rate of the refractive index, which defines the α-factor.

The density of the atmosphere changes with altitude, due to water vapor, clouds, rain drops, sleet and sandy dust. The temperature decreases with altitude up to approximately 10 km. This portion of the atmosphere (the troposphere) accounts for more than 80 % of the mass. We need only to consider the propagation in the troposphere (groundwave) since Loran-C is designed as a pulse system, enabling it to separate the groundwave from the sky wave by rejecting sky-waves. Consequently it is necessary to study the effects of weather within the troposphere.

Weather parameters such as temperature T, air pressure p and humidity (partial water pressure e) influence the behavior of the atmospheric refractive index. The actual propagation velocity of any electromagnetic wave is a function of its velocity in vacuum ($c=2.997925\ 10^8$ m/s) and the refractive index n of the atmosphere:

$$v = \frac{c}{n} \quad [m/s] \qquad (1.28)$$

Radiometeorological studies commonly use the refractivity $N=(n-1)10^6$. The weather parameter can be related to N as follows [15]:

$$(n-1)10^6 = N = N_{Dry} + N_{Wet} = 77.6p/T + 3.73\ 10^5\ e/T^2 \qquad (1.29)$$

where T = absolute temperature [Kelvin]

p = atmospheric pressure [mbar]

e = partial water pressure [mbar]

A temperature decrease (as in winter) causes N Dry to increase, the propagation velocity (1.28) to decrease and hence the propagation time to increase. In order to estimate the α-factor we need to determine dN/dh:

$$\frac{dN}{dh} = -\left\{\frac{77.6*12.68}{T} + \frac{77.6}{T^2}\left[p + \frac{9620\ e}{T}\right]\frac{dT}{dh} + \frac{77.6}{T}\left[1 - \frac{4810}{T}\right]\frac{de}{dh}\right\} \quad (1.30)$$

where h = height in 100 m units

α itself is then (using 1.9)

$$\alpha = 1 + 0.06378\ \frac{dN}{dh} = k_1 - \{k_2 + k_3\ e\}\ \frac{dT}{dh} + k_4\ \frac{de}{dh} \quad (1.31)$$

An increase in α causes Ξ_c (1.10b) to increase, the propagation time (1.11a) also to increase and the propagation velocity v (1.11b) to decrease.

The temperature T and partial water pressure e from at least two altitude levels have to be used to estimate dT/dh and de/dh, assuming a linear variation of T and e with height.

Influence of rain, ice, snow on refractivity N:

We develop a first order approximation: The refractive index n is directly proportional to the square root of the dielectric constant ϵ.

The effective dielectric constant ϵ_{eff} of any medium can be approximated by the weighted sum of the dielectric constants of the components of the medium. Let us assume that the troposphere consists of p % air ($\epsilon \approx 1$) and 100 - p % liquid water ($\epsilon \approx 80$).

A typical raindrop has a diameter of 2 mm and a terminal velocity of 6.5 m/s. A typical rainfall produces

ca. .5 cm of precipitation per hour [1]. This results in a liquid water/air ratio of $2.1\ 10^{-7}$ and an effective dielectric constant of $\epsilon_{eff} = 1.000016$, an increase of $\delta\epsilon = +16\ 10^{-6}$.

Since $n \approx \epsilon^{1/2}$:

$$\delta n = 1/2\ \epsilon^{-1/2}\ \delta\epsilon \rightarrow \delta N \approx \delta\epsilon / 2\ 10^{6} \qquad (1.32)$$

The refractivity N will increase by 8 units.

For very heavy rainfall (d = 5 mm, v = 9 m/s, 5 cm/hour) [1] the refractivity N will increase by 61 units.

Various cloud layers have different compositions: High clouds above 6000 m, where it is cold and dry, are composed of ice crystals and are rather thin. Middle clouds (between 2km and 7 km) consist of small water droplets and some ice crystals. Low clouds (below 2 km) consist of water droplets (condensation nuclei), although in cold weather they may contain ice particles or snow.

Low clouds consist of large condensation nuclei, which typically have diameters of 2 µm, a negligible velocity; one cm^3 of air typically contains 100 particles [1]. This results in a liquid water/air ratio of $4\ 10^{-10}$ and an effective dielectric constant of $\epsilon_{eff} = 1.00000003$. This liquid water concentration is so small that the influence of clouds can be ignored.

Fog consists of cloud droplets with a diameter of typically 20 µm and a negligible velocity; one cm^3 of air typically contains 300 particles [1]. This results in a liquid water/air ratio of $1.3\ 10^{-6}$ and an effective dielectric constant of $\epsilon_{eff} = 1.000103$. The refractivity N will increase by 52 units.

Snowflakes can be considered to be floss silk made of ice (ϵ = 100 at p= 1000 mbar, T = -23 °C) and inflated with air. If snowflakes are ten times fluffier than typical rain drops, falling with a tenth of the velocity of rain drops (v=.65 m/s) and producing typically .8 cm of snow per hour [1], the snowflake/air ratio is 3.4 10^{-6}. The refractivity N will increase by 17 units, an effect comparable to the effect of rain.

A refractivity increase ΔN influences the propagation time as follows:

$$T = \frac{n}{c} d = \frac{(N\ 10^{-6} + 1)}{c} d \qquad [s] \qquad (1.33)$$

$$\Delta T = \frac{10^{-6}\ d}{c} \Delta N \qquad [s] \qquad (1.34)$$

	ΔN=10	ΔN=30	ΔN=50
d = 10 km	.3	1	2
d = 50 km	1.7	5	8
d = 100 km	3.3	10	17
d = 500 km	17.0	50	83

Table 1.3 Propagation Time Increases ΔT[ns] for Various ΔN

These propagation time increases seem to be large, but heavy rainfall and fog are not usually spread out over the whole length of a typical propagation path, so that the signal velocity v=c/n is reduced only in certain areas.

In the following the influence of rain, fog, clouds and snow has therefore been ignored but very heavy rain and fog can influence the propagation times noticeably.

II. MEASUREMENTS AND COMPUTATIONS

II.1.1 TD Data Collection

The data used were collected on the Oregon State University campus in Corvallis, Oregon (44°34'03'' N and 123°16'28'' W) over a period of 255 days, from 6/25/86 to 3/6/87.

A modified II Morrow Apollo II Model 611 Loran-C receiver outputs a data set TDW,TDX,TDY and the signal-to-noise ratios of master, secondary W and secondary X to an HP 87 every 1.1 seconds. The computer saves the following 12 parameters every 300 measurements (5 minutes) on a 5" disk in one "data set": the mean for TDW, TDX, TDY, the signal-to-noise ratios of the Master, W and X signals (SNRM, SNRW and SNRX), the calculated standard deviations of TDW, TDX and TDY (SIGW, SIGX, SIGY) and the calculated cross-correlation coefficients between signal TDW and TDX, TDW and TDY and TDX and TDY (RWX, RWY and RXY). In 1 hour the system collects 12 data sets, during the whole time period of 255 days 255*24*12=73440 data sets. Pacific Standard Time (PST) was used as a common time base for all data.

This system automatically saves the data sets for 69 days on one disk (providing there is no power failure) and gives enough relevant data to analyze the performance of a specific Loran-C chain for the particular receiver location. Missing data due to power and other failures (11 % of the data) was replaced by interpolated data. In the following, day 1 refers to 6/25/86 and day 255 to 3/6/87 etc. In order to reduce the amount of data to be saved only the fluctuation of the TD signal [ns] was stored. All TD times in the following are in ns and the actual TD value can be calculated by adding a constant time ΣTD:

	TDW	TDX	TDY
$\overline{TD}$ [μs]	12 869.8	28 022.8	43 930.1

Table 2.1 Constant Part of the TD Mean

II.1.2 Weather Data Collection

For the 255 day period the following data were recorded from the "Daily Weather Maps", published by the National Weather Service in a weekly series [17]: the maximum surface temperatures for the 12-hour period ending at 4 pm (PST) in Salem, OR, Medford, OR, and Lakeview, OR; the 4 am (PST) surface temperature, dew point and air pressure in Las Vegas, NV, and Reno, NV, (used to calculate the dry and wet component of the refractive index n).

To record the rainfall on the paths of the Loran-C pulses the "Precipitation Areas and Amounts Chart" (which shows areas with precipitation during the 24 hours ending at 4 pm) was used: for the paths W-R (R = receiver at OSU), X-R, M-R, M-W, M-X and M-Y was assigned a coefficient every day. The coefficient was 0.0 for no rain, 0.5 for some rain and 1.0 for heavy rain.

Detailed information about the temperature and dew point temperature distribution as a function of altitude is necessary to estimate the α-factor. To collect this information the soundings of the three weather balloons (which are being sent up at hundreds of locations all over the world at 4 am and 4 pm (PST) every day) were used. The data were accessible through the mainframe computer of the Department of Atmospheric Sciences at Oregon State University, which receives all U.S. soundings. The sounding locations used were Winnemucca, NV, Salem, OR, and Medford, OR, the only stations which are near the TDW, TDX and TDY paths of the GRI 9940 chain.

For a period of 70 days (12/27/86 - 3/6/87) the following data were recorded for all three locations using the 4 am and 4 pm data: temperature, dew point, air pressure and altitude at the following pressure levels:
1.) Surface (surface pressure [mbar] and surface altitude above sea level [m] for SLE: 1011 at 61 m; MFR: 970 mbar at 401 m; WMC: 870 mbar at 1312 m)
2.) 700 mbar (≈ 3 km above sea level)
3.) 250 mbar (≈ 10 km above sea level)

With this information N and α can be estimated

II.1.3 Transmitter Station Data Collection

The U.S. Coast Guard in Middletown, CA , made the following station data available for the same 255 day period:

The daily sum of local phase adjustments performed by the system area monitors Pt. Cabrillo (LPAW) and Pt. Pinos (LPAX and LPAY);

The Time Interval Numbers measured at the Master station (M TINO W, M TINO X and M TINO Y) and at the secondary stations (S TINO W, S TINO X and S TINO Y);

The transmitter switching times of the Master and the secondary transmitters W,X and Y (M Sw, W Sw, X Sw and Y Sw).

Each station has two identical AN/FPN-44A tube transmitters 1 and 2. Switching the transmitters routinely about every 14 days makes it possible for one transmitter to be used as a backup unit and is available for maintenance work. A +1 was assigned for transmitter 1 in operation and a -1 for transmitter 2.

II.1.4 Characteristics of the GRI 9940 Area

The diverse propagation conditions in the U.S. West Coast states are a result of the area's varied topographical and climatical zones: the desert areas in Nevada and Eastern Oregon with elevations between 1000 and 1500 m, extreme diurnal temperature variations and very low precipitation; the rugged Cascades with high peaks up to 2500 m; the Coast Range with high precipitation and the valleys with a mild climate dry and warm in the summer and cool and rainy in the winter.

The path WR crosses the Columbia Gorge and the Willamette Valley. The path XR travels along the coast range mountains and the south end of the Willamette Valley. The path YM is at a high altitude through the desert. The path MR crosses the desert, the Cascades and part of the Willamette Valley. This path has the most diverse propagation characteristics of any of the paths.

The diversity of landscapes in the GRI 9940 area make this chain especially susceptible to heterogeneous propagation conditions, which are hard to predict.

II.2 Analysis of the Receiver Data

Fig.2.1 shows the daily means (as measured in Corvallis, OR) of the time difference TDW. The daily means of TDX and TDY can be found in the Appendix.

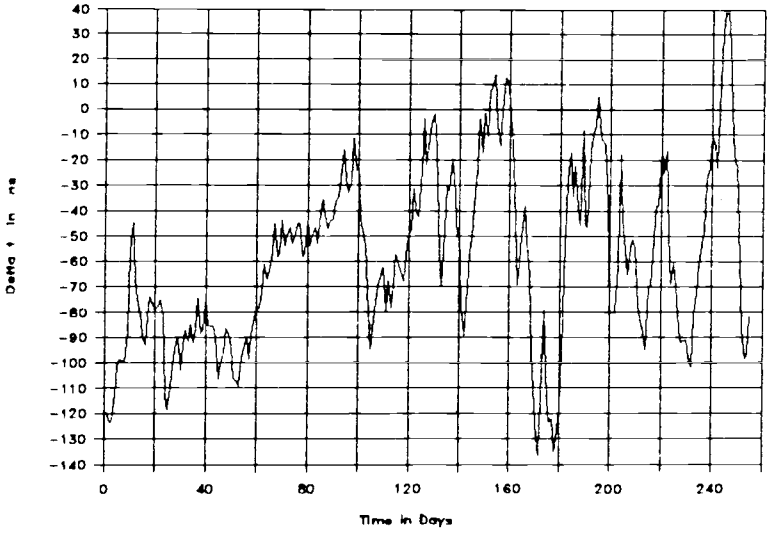

Figure 2.1 Daily Means of TDW Measured in Corvallis, OR

II.2.1 Distributions

The distributions of all TD hourly means appear to be close to normal (Fig. 2.2 and Appendix):

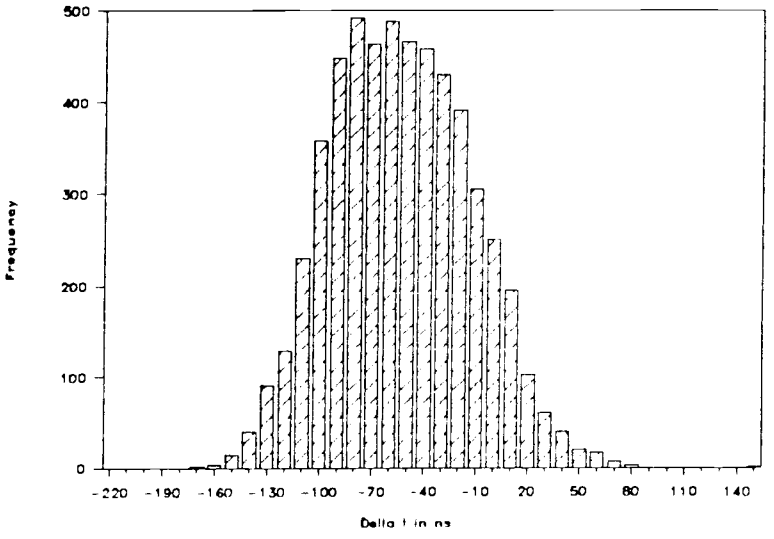

Figure 2.2 Distribution Hourly Means of TDW

This has to be proven: First we have to normalize our data by using the transformation

$$z = \frac{x - \mu}{\sigma} \qquad (2.1)$$

where x = TD value measured

μ = arithmetic mean of the TD data

σ = standard deviation of the TD data

The transformed random variable z has zero mean and a variance of 1. Now we have to prove the hypothesis

H_0: The data conform to a normal distribution (2.2a)

We can reject H_0, if $Chi^2 > Chi^2_{\alpha}\{k-1-m\}$ (2.2b)

$$\text{where } Chi^2 = \sum_{i=1}^{K} \frac{(fo - fe)^2}{fe} \qquad (2.3)$$

where k = number of categories

fo = observed frequency

fe = expected frequency

α = level of significance

m = number of population parameters estimated

In a normal distribution the expected frequency fe for an interval between z_1 and z_2 is the area under the normal curve between these class boundaries ($F(z_2)$-$F(z_1)$) multiplied by the number of samples N. We check our normal distribution by using hourly means, so we have N=24*255 = 6120 samples. We choose k=30 categories (-0.1 < z < 0.1, 0.1 < z < 0.3, etc.) in order to get a precise result. We choose a 95% significance level (area in the right tail of the Chi square distribution α=0.05). Since we use the sample mean and sample standard deviation (m=2) we have k-1-2=27 degrees of freedom and $Chi^2_\alpha(27)$ = 40.11.

The results of the calculations of Chi^2 are given in Table 2.2:

Time of day	DM	DT	TT	NT
TDW	119.8	104.4	76.1	47.4
TDX	70.8	29.0	73.8	56.0
TDY	235.1	172.1	117.2	47.2

Table 2.2 Chi^2 Test of TD at Various Times of the Day

where DM = daily mean
DT = day time, values between 9 am and 5 pm
TT = transition time, values between 5 am and 9 am and between 5 pm and 9 pm
NT = night time, values between 9 pm and 5 am

Since the hypothesis H_0 can be rejected (equation 2.2b), the daily means/DM have non-normal distributions. The TDY signal is farthest from normal. However, using the TD values at the same time every day and calculating the Chi^2 value, it is always below the $Chi^2_\alpha(27)$=40.11, confirming the hypothesis H_0.

Hourly mean at	TDW	TDX	TDY
7 am	36.79	24.30	27.84
7 pm	29.36	20.26	32.76

Table 2.3 Chi^2 Test Using TD Means at 7 am and 7 pm

Therefore the TD data, measured at the same time every day, can be considered to be normally distributed. This was expected because the signal propagates over a variety of landscapes and climatic zones. The propagation conditions are different in each zone. In other words, there are n independent random variables (RVs) that influence the propagation velocity. After the central limit theorem [13] the density of the sum of those RVs tends towards normal as $n \to \infty$.

The means μ [ns] and standard deviations σ [ns] used to calculate our Chi^2 value are shown in Table 2.4:

Time of day	DM	DT	TT	NT
TDW μ	-58.2	-62.3	-56.7	-55.5
TDW σ	40.2	39.0	40.2	40.9
TDX μ	-27.4	-26.2	-26.7	-29.3
TDX σ	40.0	29.9	32.0	33.8
TDY μ	-44.3	-29.6	-44.7	-59.5
TDY σ	48.3	45.0	41.6	53.3

Table 2.4 μ [ns] and σ [ns] of the TD Means

TDW and TDX do not show any significant diurnal variations, but TDY does. The night values definitely have a smaller mean and a higher standard deviation than the day values.

Distribution of the signal-to-noise ratios:

Time of day	DM	DT	TT	NT
SNRM μ	238.1	244.5	240.3	229.3
SNRM σ	8.7	2.7	6.1	7.6
SNRW μ	233.7	233.7	233.7	233.6
SNRW σ	1.2	1.4	1.1	1.0
SNRX μ	230.9	240.0	233.8	219.0
SNRX σ	11.2	3.7	7.9	8.3

Table 2.5 μ and σ of the Signal-to-Noise Ratios

In general the signal-to-noise ratio drops at night. This is explained by the higher noise level at night due

to heavy thunderstorms in the tropics. The secondary W is closest to our receiver location (390.1 km), so this signal-to-noise ratio is the strongest and shows hardly any diurnal variation. The signal from the secondary X has the smallest signal-to-noise ratio, the biggest diurnal variation and the highest standard deviations. Unfortunately (due to hardware constraints) it was not possible to record SNR of the secondary Y, which is 1,254.6 km away. The TDY signal dropped out 5.8 % of the time, mostly at night.

Assuming the signal-to-noise ratio x to have a normal distribution $f_x(x)$ the SNR [dB] defines a new RV $y=g(x)=\ln(x)$ with a distribution $f_y(y)$. The transformation $f_y(y) = f_x(x_i)/(|g'(x_i)|)$ [13], where $g'(x_i)$ is the derivative of g(x), yields the theoretical distribution for SNR:

$$f_y(y) = [\ 1/(\sigma \sqrt{2\pi}) \exp(-(e^y - \mu)^2/2\sigma^2)\ ]\ e^y \quad (2.4)$$

This distribution belongs to the family of lognormal distributions. The observed distributions of SNRM can be seen in Fig. 2.3. It can be explained as a superposition of the DT, TT and NT distributions (shown in Fig. 2.4). Fig. 2.5 shows the theoretical distribution (equation 2.4). The theoretical distributions agree reasonably well with the observed distributions.

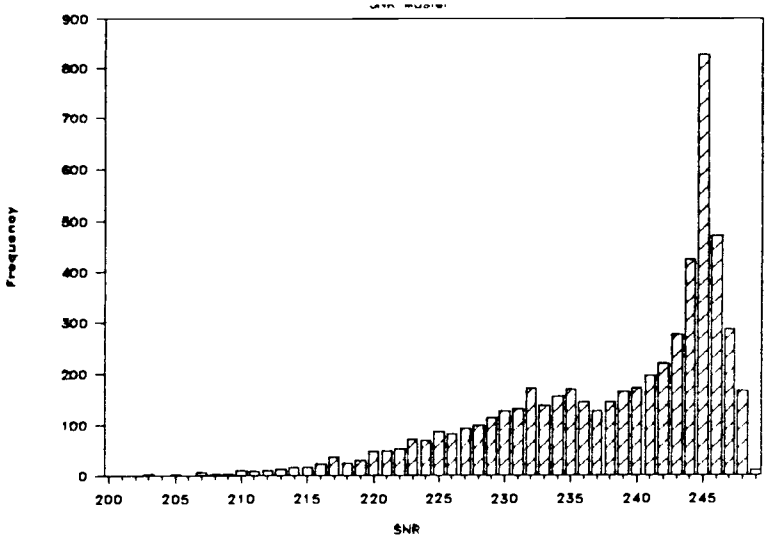

Figure 2.3 Observed Distribution of the SNRM

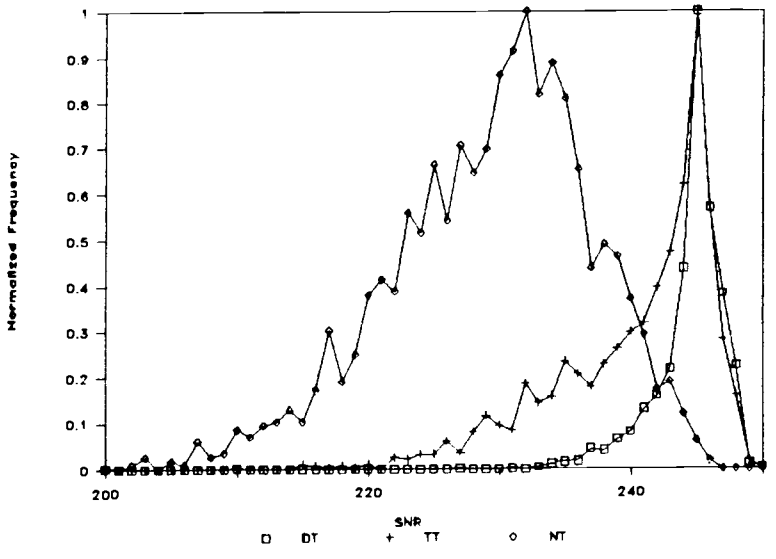

Figure 2.4 Observed Distribution of SNRM, Separated in DT, TT and NT Values

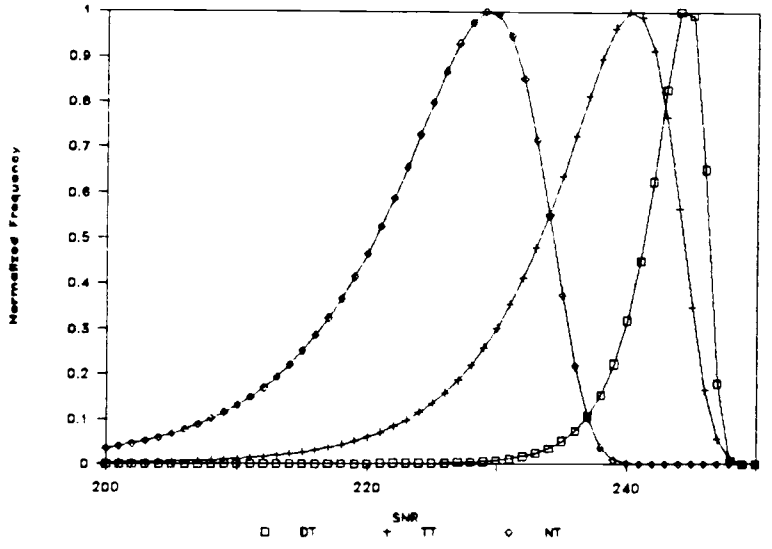

Figure 2.5 Theoretical Distributions of SNRM, Separated in DT, TT and NT Values

Distribution of the TD standard deviations:

Time of day	DM	DT	TT	NT
SIGW μ	19.4	15.1	17.5	25.7
SIGW σ	6.8	5.1	4.3	5.8
SIGX μ	28.3	20.8	25.4	38.7
SIGX σ	10.2	6.0	6.2	8.1
SIGY μ	46.2	33.0	40.8	64.6
SIGY σ	26.6	21.8	22.0	24.9

Table 2.6 μ [ns] and σ [ns] of the TD Standard Deviations

Day time (DT) TD values have a smaller variance than night time (NT) values, and the standard deviations of the sigmas observed during the night are higher than during the day. The distribution of SIGW can be seen in Fig. 2.6.

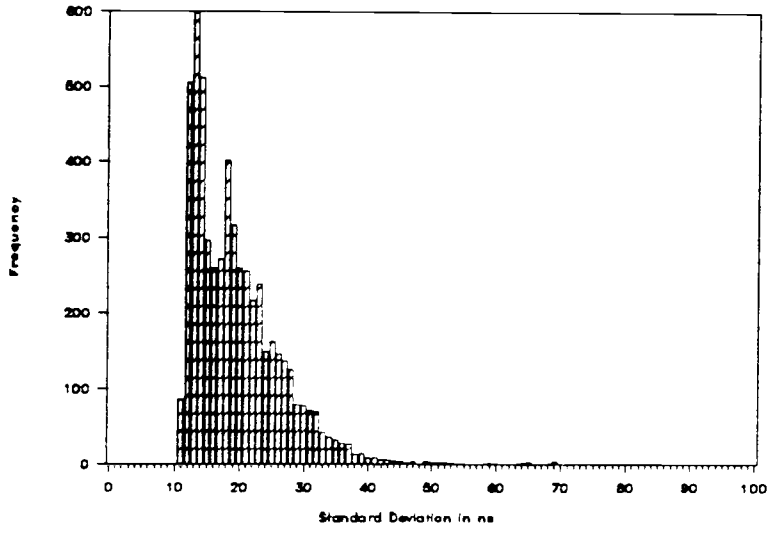

Figure 2.6 Distribution of the Hourly Means of SIGW

Again the distribution is a superposition of 3 distributions using the DT,TT and NT values,shown in Fig. 2.7 for the variances of TDY (distributions of the standard deviations of TDW and TDX are given in the Appendix).

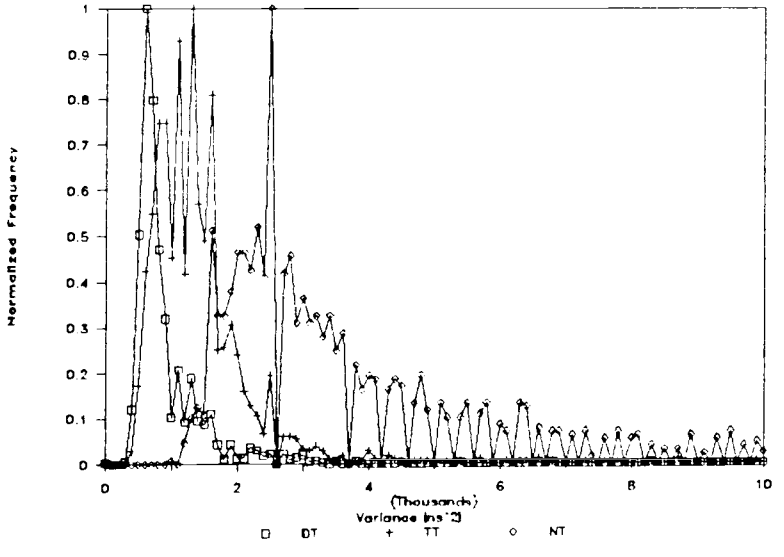

Figure 2.7 Variance of TDY, Separated in DT,TT and NT Values

Since the standard deviations are always positive, the distributions cannot be normally distributed. The

distribution of the variances of a normally distributed RV is a chi-square distribution. The distribution in Fig. 2.7 shows a fair agreement with a chi-square distribution.

The distribution of the cross-correlation coefficients:

Time of day	DM	DT	TT	NT
RWX μ	.480	.447	.475	.519
RWX σ	.070	.062	.061	.067
RWY μ	.151	.140	.150	.162
RWY σ	.065	.061	.061	.071
RXY μ	.122	.122	.123	.121
RXY σ	.069	.074	.066	.065

Table 2.7 μ and σ of the TD Correlation Coefficients

TDW and TDX show the strongest cross-correlation, r=0.48, TDW and TDY have a weak cross-correlation of r=0.15, and TDX and TDY have a cross-correlation of r=0.12. The cross-correlation at night is usually slightly stronger. The distribution of the cross-correlation coefficients is close to a normal distribution, as can be seen in Fig. 2.8 for RWX (and in Appendix for RWY and RXY).

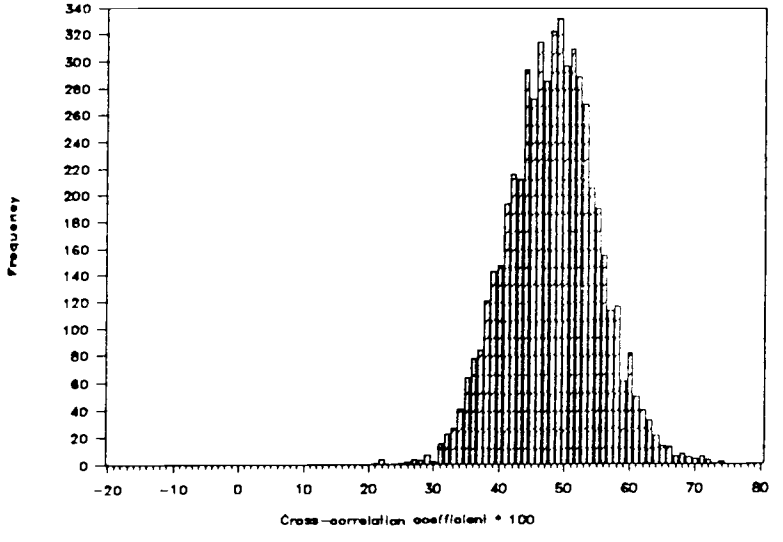

Figure 2.8 Distribution of the Hourly Means of RWX

II.2.2 TD Means, Standard Deviations

The plots of the daily TD means show a "monthly" periodicity, also a slight seasonal variation. The monthly averages (for TDX in Fig. 2.9, TDW and TDY in Appendix) show the seasonal variation even better: TDY does not show any strong seasonal variation, just a slight drop of TDY in December and January. For TDW and TDX the summer TD values are lower than the winter values.

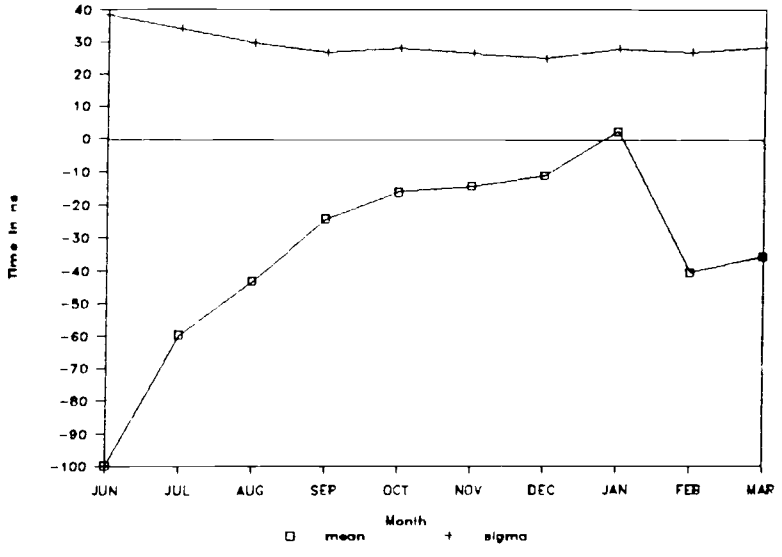

Figure 2.9 Monthly Averages of μ and σ for TDX

The following table shows the average TD values measured in July and January:

TD	μJul	σJul	μJan	σJan	$\delta = \mu$Jul-μJan
TDW	-86.3	15.3	-46.8	28.0	-39.5
TDX	-60.1	17.2	3.1	21.8	-63.2
TDY	-51.2	16.4	-66.8	38.1	15.6

Table 2.8 TD means in July and January [ns]

The following constant TD errors (resulting in constant position errors) can be observed (using Table 2.8 and 2.1): TDW is 1.75 μs below the expected value (equation 1.8a). TDY is 1.85 μs above the expected value (equation 1.8c). TDX agrees with the expected value

(equation 1.8b). In section II.4 we will explain those constant TD errors.

Assuming that the July values represent summer and the January values represent winter, and comparing these we recognize that the winter TDW is ca. 40 ns higher than the summer TDW, the winter TDX is ca. 60 ns higher than the summer TDX and the winter TDY is ca. 20 ns smaller than the summer TDY, a very small seasonal variation. The standard deviations in the summer are smaller than in the winter.

The diurnal variations of the TDs:

TD [ns]	μ4am	σ4am	μ4pm	σ 4pm	ξ=μ4pm-μ4am
TDW in July	-77.5	24.3	-96.4	17.1	-18.9
TDX in July	-61.9	20.2	-57.1	17.4	4.8
TDY in July	-78.3	23.9	-32.5	20.0	45.8
TDW in Jan.	-49.9	33.0	-50.4	32.9	-0.5
TDX in Jan.	-7.5	24.9	8.5	25.3	16.0
TDY in Jan.	-103.7	56.0	-44.1	61.9	59.6

Table 2.9 Diurnal/Seasonal TD Variations

The 4 am values represent day and the 4 pm values night conditions. TDW shows a ca. 20 ns increase during the night (compared to the day value) in the summer but no diurnal variation in the winter. TDX shows a very small diurnal variation in the summer and a ca. 15 ns decrease during the night in the winter, also quite small. Only TDY shows a strong diurnal variation: at night TDY drops by ca. 45 ns in the summer and in the winter by nearly 60 ns.

The monthly and hourly averages of the TD means (for TDY shown in Fig. 2.10, TDW and TDX cf. Appendix) again confirm a small seasonal influence for TDW and TDX and no distinct diurnal variation, but for TDY no obvious seasonal variation, but a certain diurnal variation. In section II.4 we will attempt to explain these variations.

Fig. 2.11 shows the monthly and hourly averages of the standard deviations of TDY (for TDW and TDX cf. Appendix). There is a strong diurnal variation: the standard deviations are smaller during the day by ca. 15 ns in the case of TDW, ca. 20 ns in the case of TDX and ca. 40 ns in the case of TDY. This confirms that the TD values are more stable during the day (as already anticipated in the previous section, since the signal-to-noise ratios are higher during the day).

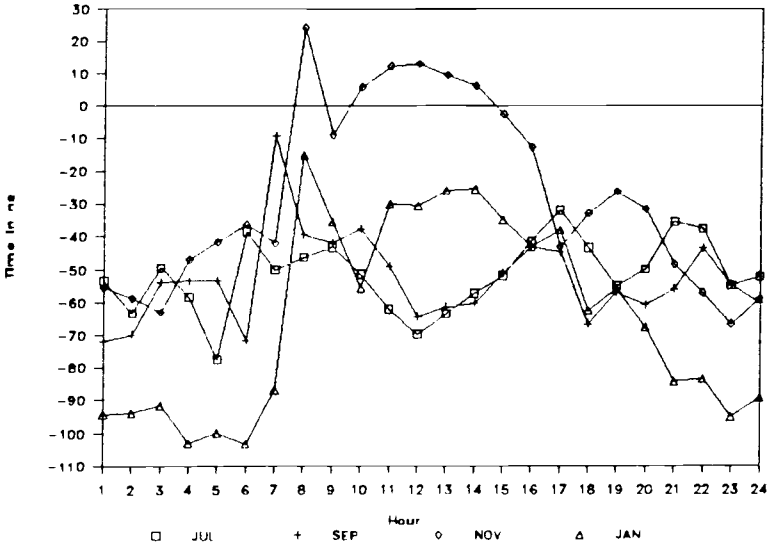

Figure 2.10 Monthly/Hourly Averages of TDY Means

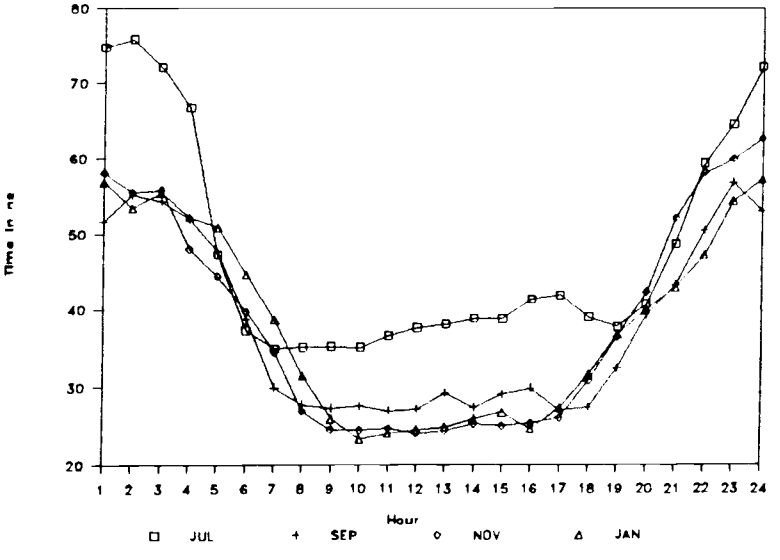

Figure 2.11 Monthly/Hourly Averages of SIG Y

II.2.3 TD Autocorrelations

In order to analyze the temporal variations of the TD signals we calculate the autocorrelation for various lags:

$$r(\tau) = \sum_{t=1}^{N-\tau} \frac{(TD(t) - \mu_{TD})(TD(t+\tau) - \mu_{TD})}{\sigma_{TD}^{\,2}} \qquad (2.5)$$

$$\sigma_{TD}^{\,2} = \frac{1}{N} \sum_{t=1}^{N} (TD(t) - \mu_{TD})^2 \qquad (2.6)$$

$$\mu_{TD} = \frac{1}{N} \sum_{t=1}^{N} TD(t) \qquad (2.7)$$

where μ_{TD} = sample mean of the TD signal

N = number of samples used

$\sigma_{TD}^{\,2}$ = sample variance of the TD signal

$r(\tau)$ = autocorrelation coefficient at lag τ

In order to get a good resolution and a significant result we take 4 hour means of our TD values and so get N = 255*6 = 1530 samples. Fig. 2.12 shows the autocorrelation coefficients of TDX as a function of the lag (autocorrelations of TDW and TDY cf. Appendix). All figures show a strong autocorrelation coefficient (especially in the case of TDX) at a lag of 28 days and multiples of that time period. This indicates a strong 28 day periodicity of the TD signal. The autocorrelation of TDY also shows a 24 hour periodicity.

Since the moon has a periodicity of 28 days, an influence of the moon can be suspected. We find that the transmitter switchings, which also occur in a ca. 28 day cycle, are responsible for this periodicity.

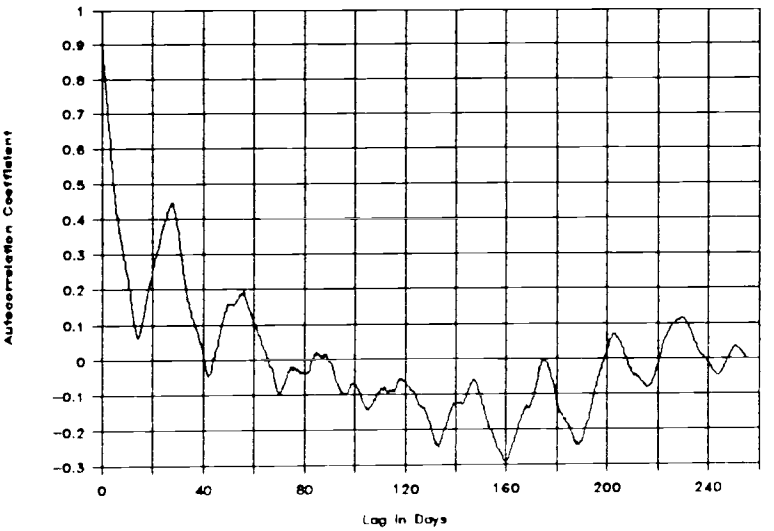

Figure 2.12 Autocorrelation of TDX using N=1530 Samples

II.2.4 TD Power Spectra

In order to find out how the energy of the TD signal is distributed over the spectrum we calculated the power spectrum, the Discrete Fourier Transform of the autocorrelation:

$$F(nw_o)=T_1 \sum_{m=0}^{N-1} f(mT_1)\exp(-j2\pi mn/N) \; ; \quad n=0,1,\ldots,N-1 \quad (2.8)$$

where N = number of samples = 1530

f(t) = autocorrelation function

T_1 = sampling interval of f(t)= 4 hours=.167 days

w_o = sampling interval of F(w) = $(2\pi)/(T_1 N)$

fo = sampling frequency of F(w)

$f_o = w_o/2\pi = 1/255$ [1/day]

$T=NT_1$ = period of f(t)

$w_1=Nw_o$ = period of F(w)

Fig. 2.13, the power spectrum of TDY (power spectra of TDW and TDX in Appendix) shows that the energy is mainly located in a band with a low frequency, (1/365 1/day),a yearly periodicity. There is also a strong periodicity of one day, confirming the diurnal variation in our TDY signal. TDW and TDX show no diurnal variations. All three signals also have a 28 day periodicity, as observed earlier.

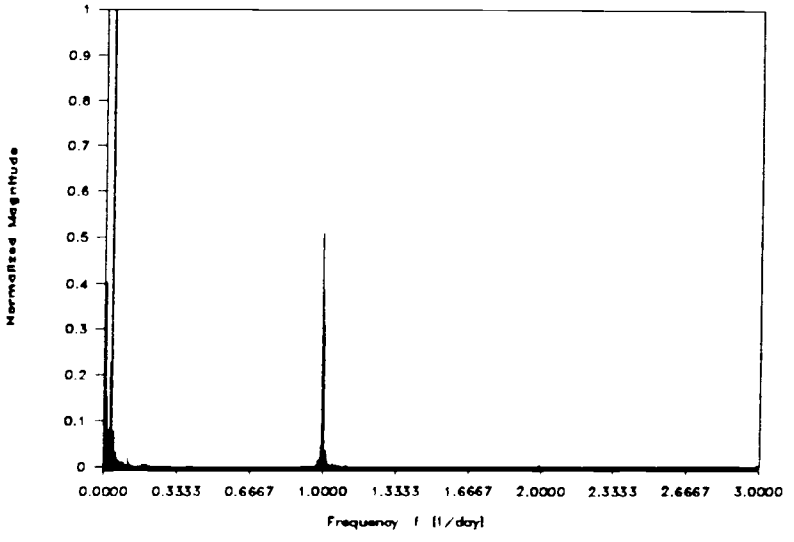

Figure 2.13 Power Spectrum of TDY

II.2.5 TD Stationarity

A stochastic process can be considered strict sense stationary, if its statistical properties are invariant to a shift of the origin. A less restrictive process, the wide sense stationary process (wss), has the following two conditions [13]:

1. The mean must be constant with time

2. The autocorrelation $Rxx(\tau) = E[X(t)X(t+\tau)]$ must be only a function of its lag τ, in other words independent of t: each sample autocorrelation, no matter at what time t taken, should result in the same autocorrelation.

For a stationary receiver the long term mean (at least 1 year) will remain constant, since the receiver is not moving and the TD values only fluctuate around the mean. We have only 70 % of one year's data available, so the first condition can not be completely met.

Fig. 2.14 shows the sample autocorrelation of TDW (for TDX and TDY in Appendix) calculated over a window of N=150 days, starting at various times. The autocorrelation coefficients are similar, but not identical for those various sample calculations. The standard error $s.e._r$ of a correlation coefficient r, estimated using n samples, is defined as

$$s.e._r = (1 - r^2)/\sqrt{n} \qquad (2.9)$$

The 95 % confidence interval is then

$$r - 1.96\ s.e._r \leq r \leq r + 1.96\ s.e._r \qquad (2.10)$$

Assuming n=150 samples used to estimate the autocorrelation coefficient and r=-0.3, the 95 % confidence interval is $-0.45 \leq r \leq -0.15$.

The calculated autocorrelation coefficients remain approximately within their confidence interval and so we can confirm the TD signals to be wide sense stationary.

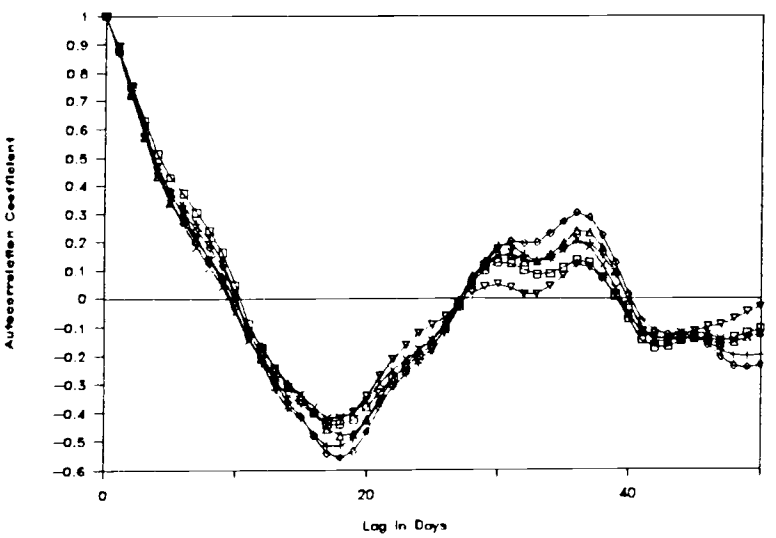

Figure 2.14 Sample Autocorrelations of TDW, N=150 Samples

II.3 Analysis of the Weather and Transmitter Data

The surface temperature T was available in [°C] and the air pressure p in [mbar]. The available surface dewpoint [°C] can be converted to the partial water pressure e [mbar] (see Appendix III). The relative humidity RH [%] was calculated (see Appendix III). The refractivity N and the α-factor were calculated using the results from section I.5.

Soundings from the stations in Salem, Medford and Winnemucca over a period of 70 days (12/27/86 - 3/6/87):

Parameter	μ 4am	σ 4am	μ 4pm	σ 4pm	μ4pm- μ4am
T SLE	3.4	4.3	9.2	3.0	5.8
T MFR	1.6	4.5	10.1	3.9	8.5
T WMC	-5.3	6.8	6.0	6.1	11.3
e SLE	7.5	2.2	8.3	2.5	.8
e MFR	6.3	1.7	6.6	1.9	.3
e WMC	3.5	1.6	4.2	1.5	.7
p SLE	1011.2	8.8	1010.6	8.4	-.6
p MFR	972.6	7.1	971.3	6.8	-1.3
p WMC	870.6	6.9	870.0	6.4	-.6
N Dry SLE	284.0	6.5	278.0	4.5	-6.0
N Dry MFR	274.9	5.9	266.3	4.5	-8.6
N Dry WMC	252.5	7.5	242.1	5.6	-10.4
N Wet SLE	36.1	9.7	38.8	11.0	2.7
N Wet MFR	30.7	7.5	31.4	8.6	.7
N Wet WMC	18.1	7.2	20.2	7.1	2.1
N SLE	320.1	4.7	316.8	8.7	-3.3
N MFR	305.6	4.8	297.6	8.0	-8
N WMC	270.6	3.5	262.3	7.4	-8.3
α SLE	.7473	.0161	.7613	.0193	.0139
α MFR	.7469	.0200	.7705	.0197	.0236
α WMC	.7366	.0297	.7806	.0300	.0439
RH SLE	92.0	7.1	70.5	13.9	-21.5
RH MFR	89.1	10.6	55.2	17.9	-33.9
RH WMC	79.6	11.2	47.1	19.9	-32.5

where μ4am is the 70 day average at 4am (PST) representing night values and μ4pm is the 70 day average at 4 pm (PST) representing the day values

Table 2.10 Weather Data 12/27/86 - 3/6/87 (Obtained from Soundings, Twice a Day)

Weather data obtained from daily weather maps collected over a period of 255 days (6/25/86 - 3/6/87):

Parameter	μ255	σ255	μJul	σJul	μJan	σJan	μJul-μJan
T SLE	17.1	8.4	24.5	3.3	8.1	3.0	16.4
T MFR	19.1	11.0	30.6	3.3	8.8	3.3	21.8
T Lakeview	15.1	10.8	27.3	3.1	1.6	2.9	25.7
T Reno	3.5	7.8	12.2	2.8	-4.2	5.4	16.4
T Las Vegas	13.7	9.6	25.1	2.5	3.0	3.5	22.1
e Reno	5.9	2.7	9.5	2.4	3.6	1.2	5.9
e Las Vegas	6.8	3.7	8.9	4.6	4.6	1.8	4.3
p Reno	1018.1	6.4	1015	3.7	1022	8.3	-7.3
p Las Vegas	1015.1	6.3	1011	3.0	1020	6.7	-9.2
N Dry Reno	286.0	9.4	276.1	3.5	295.3	7.8	-19.2
N Dry Las Veg.	275.1	10.4	263.2	2.8	286.9	4.9	-23.7
N Wet Reno	28.2	11.6	43.4	10.8	18.5	5.7	24.9
N Wet Las Veg.	30.4	15.2	37.3	19.5	22.2	8.5	15.1
N Reno	314.1	7.3	319.6	11.4	313.8	5.6	5.8
N Las Vegas	305.5	13.4	300.5	19.7	309.1	6.5	-8.6
RH Reno	71.2	16.4	67.1	16.5	79.2	15.6	-12.1
RH Las Vegas	44.4	21.7	28.1	16.2	58.4	17.4	-30.3
Rain: path W-R	.45	.47	.19	.37	.56	.49	-.37
Rain: path X-R	.36	.43	.10	.23	.58	.44	-.58
Rain: path M-R	.27	.39	.08	.18	.50	.44	-.42
Rain: path M-W	.23	.36	.05	.15	.39	.43	-.34
Rain: path M-X	.19	.35	.00	.00.	48	.47	-.48
Rain: path M-Y	.09	.27	.11	.30	.13	.31	-.02

where μ255 is the average over the 255 day period, μJan is the January average, representing winter conditions and μJul is the July average, representing summer conditions.

Table 2.11 Weather Data 6/25/86 - 3/6/87 (Obtained from the Daily Weather Maps, Once a Day)

Comments:

1. The Salem, Medford and Winnemucca weather stations are located at 61, 401 and 1312 m above sea level, respectively. The measured air pressures confirm the rule that the air pressure decreases about 10 mbar for an altitude increase of 100 m.

The diurnal variation of p is very small, p at night is .6 - 2 mbar higher than during the day, as expected, because p and T are inversely proportional. The seasonal variation of p is also small, p in the winter is 7 - 10 mbar higher than in the summer. The air pressure

fluctuates less in the summer (smaller σ).

2. The temperatures show strong diurnal variations, with night values 5 - 12 °C below day time values. In desert areas this variation is especially high. The seasonal variation is even larger: the summer values exceed the winter values by 16 - 26 °C. The temperature in desert areas is usually warmer and more stable (smaller standard deviation σ).

3. The partial water pressure shows a small diurnal variation, the night pressures are .2 - 1.0 mbar lower. The seasonal variation is much larger: the summer pressures exceed the winter pressures by 4 - 6 mbar.

4. The dry component of the refractivity shows diurnal variations: N Dry decreases by 6 - 12 units during the day, compared to the night value. The seasonal change is even larger: N Dry decreases by 19 - 24 units in the summer, compared to the winter value. N Dry is inversely proportional to the temperature, so increasing temperatures mean a decreasing N Dry.

5. The wet component of the refractivity behaves differently: the diurnal variation shows an N Wet increase by .5 - 3 units during the day compared to the night value, a very small variation. Again, the seasonal change is much larger. N Wet increases by 15 - 25 units in the summer, compared to the winter value. Since N Wet is proportional to the partial water pressure e, an increase of e in the summer or at night means an increase of N Wet.

6. The refractivity N itself shows smaller variations than N Dry, since the decrease of N Dry and the increase of N Wet during day/summer values compared to the night/winter values partly cancel each other. The diurnal and seasonal variations are between 3 and 8 units. One interesting aspect is that N Wet accounts for about 13% of N in the summer and for only about 6% in the winter, since the partial water pressure is larger in the summer.

7. The α-factor was estimated using equation (1.30).

To estimate dT/dh and de/dh, the temperature and partial water pressure must be known at two altitude levels in order to perform a linear interpolation. Samaddar [15] recommends using the surface value and a value at an altitude of 2-3 wave lengths, about 9 km. The α-factors calculated using the values at an altitude of 10 km do not show any temporal or regional variations. Temperature and partial water pressure at that altitude do not fluctuate as much. Using the data at the surface and the data at an altitude of 3 km (700 mbar pressure level) gives more meaningful results. The diurnal variation of α in the desert (in WMC) is three times the diurnal variation of α in SLE. The lapse rate of the partial water pressure de/dh is more or less the same in SLE, MFR and WMC, $\approx$ -.15 mbar/100 m at 4 am and .025 mbar/100 m below that at 4 pm. The temperature lapse rates dT/dh are quite different in SLE, MFR and WMC, as can be seen in Table 2.12:

	dT/dh 4 am	dT/dh 4 pm	dT/dh 4 pm - dT/dh 4 am
SLE	-.34	-.54	-.20
MFR	-.30	-.60	-.30
WMC	-.06	-.69	-.63

Table 2.12 Diurnal/Regional dT/dh [°C/100 m] Variations

Since the temperature decreases very fast with height in the desert at night, dT/dh is quite small there during the night and the diurnal variation of dT/dh large.

8. The relative humidity shows strong diurnal and seasonal variations: The relative humidity is ca. 20 - 35 % higher at night compared to the day time, and ca. 12 - 35 % higher in the winter compared to the summer.

9. The mean of the rain coefficient (defined in section II.1.2) indicates that the path with the most rainy days per year is W-R. In general, the paths across the Cascades and the Coast Range have the most precipitation. The driest path is the desert path in Nevada between secondary Y and the master station.

10. Fig. 2.15 shows the temperature in Lakeview over

a period of 255 days (1 sample/day), and Fig. 2.16 shows the α-factor in WMC over a period of 70 days (2 samples/day).

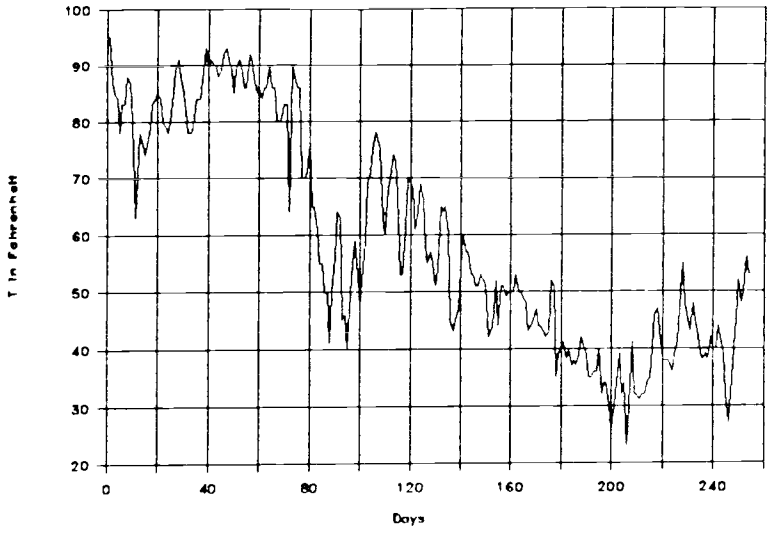

Figure 2.15 Daily Maximum Temperature in Lakeview, OR

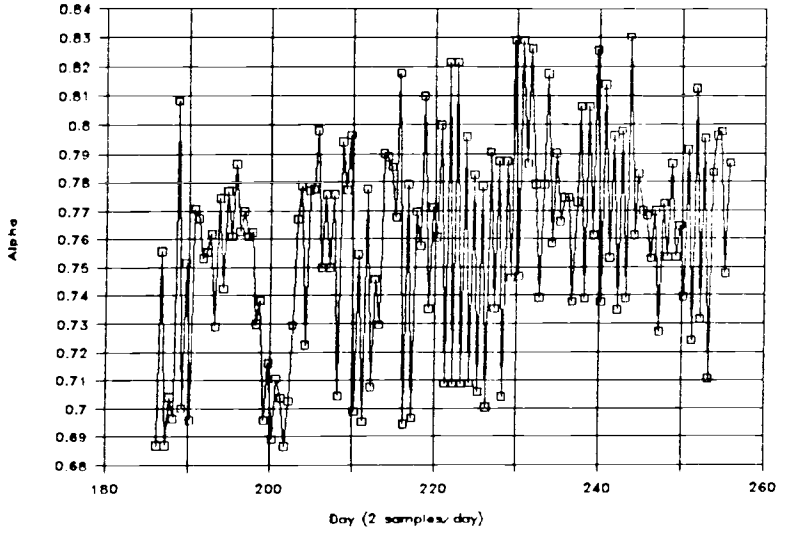

Figure 2.16 α-Factor in Winnemucca, NV

Fig. 2.17 shows the distribution of N Dry in Las Vegas. The distributions are far from being normal. If we had more samples available, the distribution would tend more towards normal.

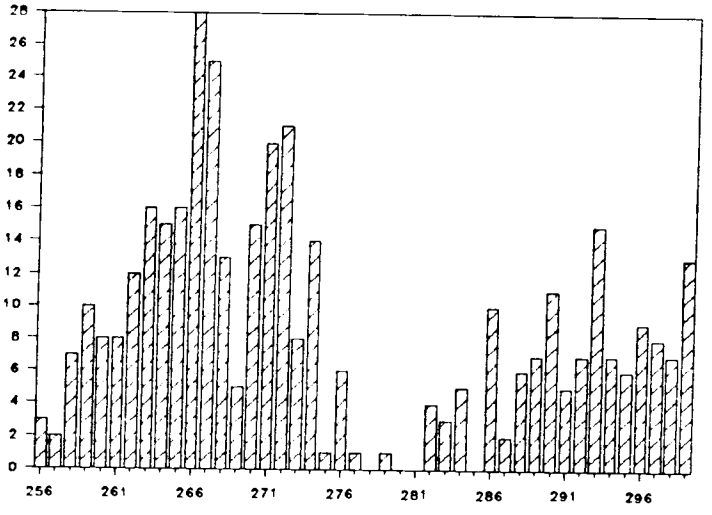

Figure 2.17 Distribution of N Dry Measured in Las Vegas

The autocorrelations and power spectra illustrate the periodicities of the weather data and are shown in the appendix.

Two time series are used, one with 255 daily samples and one with 140 samples (twice a day). The frequency of the n-th line in the power spectrum is

$f = n\, f_o$,

where $f_o = 1/(n\, t_i)$ (2.11)

n number of samples

t_i sampling interval

$f_o(n=255) = 0.00392$ [1/day]

$f_o(n=140) = 0.0143$ [1/day]

The autocorrelations of air pressure time series show basically no diurnal component and a 7 day periodicity, the duration of a typical pressure system.

The autocorrelations of surface temperatures in Salem, Medford and Winnemucca (2 samples/day) show a strong positive correlation for a lag of one day, the diurnal variation. In the case of temperatures in Salem, Medford, Lakeview, Reno and Las Vegas, where only one value a day was available, the autocorrelations for small lags are high. The temperatures, measured at the same time

each day, do not change rapidly, but gradually.

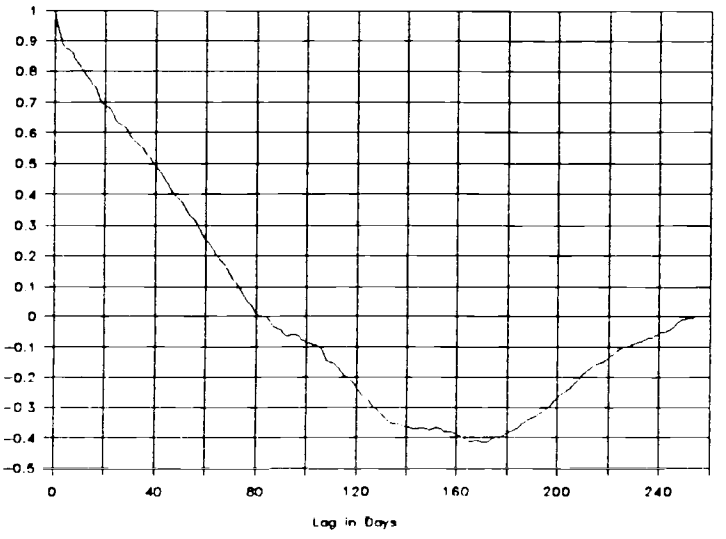

Figure 2.18 Autocorrelation Temperature in Lakeview

The power spectra of the temperature data where two samples/day were available clearly show a strong diurnal variation. This frequency can be detected since we sampled the temperature twice a day. In the case of temperatures, where only one datapoint was available per day, the power spectra show only a periodicity of 1/365 days. The diurnal variations cannot be detected, since we did not sample with at least with twice the highest frequency (2 * 1/day), which is necessary in order to detect the diurnal variations.

Similarly, the autocorrelations and power spectra of the dewpoint temperatures indicate almost no diurnal variations.

Autocorrelations of the lapse rate α at Salem and Medford show a weak diurnal variation and a very weak autocorrelation for any lag. But in the case of α in Winnemucca a strong diurnal periodicity is visible. The power spectra further confirm this. The power spectrum of α in Salem shows no diurnality,but the power spectrum of α in Winnemucca shows a strong frequency of 1/day (diurnality).

The autocorrelations and power spectra indicate the diurnal variations of the relative humidity and the strong diurnal variations of N Dry, especially N Dry in Winnemucca.

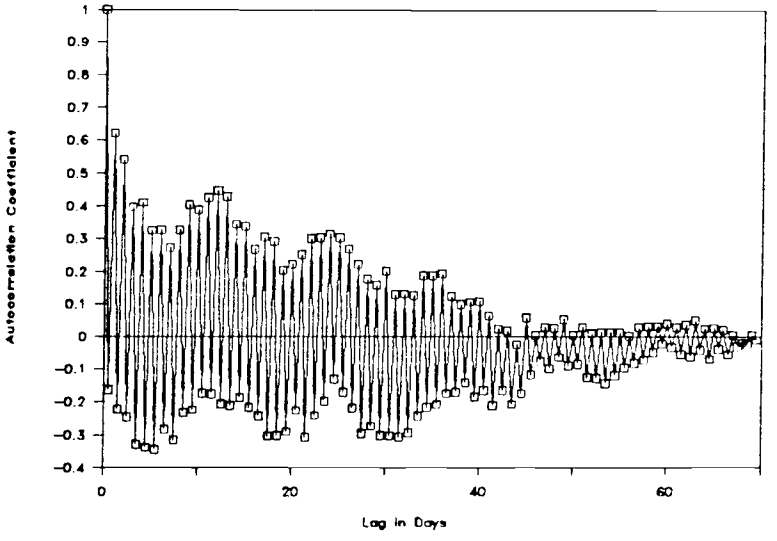

Figure 2.19 Autocorrelation α-Factor in WMC

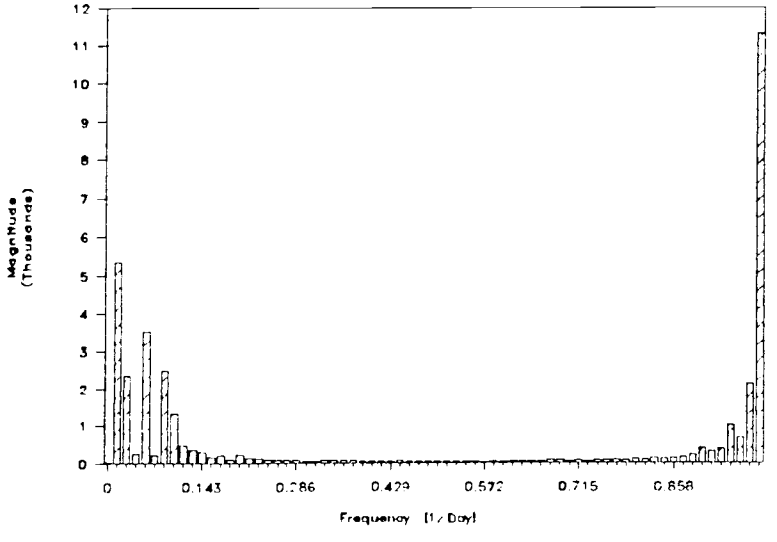

Figure 2.20 Power Spectrum N Dry in Winnemucca

The autocorrelations and power spectra of N Wet show that N Wet has almost no diurnal variations, and the power spectra of the refractivities N show that the diurnal variation is by far strongest in WMC.

The Loran-C transmitter data analysis:

Parameter	μ	σ	μJul	σJul	μJan	σJan
M TINO W	9350.7	54.3	9372.9	19.9	9312.3	61.8
S TINO W	3957.4	175.0	3802.9	40.4	3967.4	36.7
M TINO X	2301.8	52.2	2343.2	26.6	2230.0	71.0
S TINO X	5621.8	70.1	5542.9	33.0	5692.3	17.5
M TINO Y	309.4	93.1	281.9	22.2	334.8	47.5
S TINO Y	9248.1	48.5	9231.6	30.2	9304.2	22.7
LPA W	16.1	59.2	-10.3	43.1	60.6	39.5
LPA X	-30.0	88.1	-141.9	54.1	47.1	38.9
LPA Y	-31.5	62.2	-132.9	53.6	-12.2	35.1

Table 2.13 Overview over the Loran-C Station Data Used (6/25/86 - 3/6/87) All Values [ns]

The distribution of the TINO data are clearly not normal. Over a very long time period the distributions would approach normal distributions. The distribution of M TINO Y is shown in Fig. 2.21.

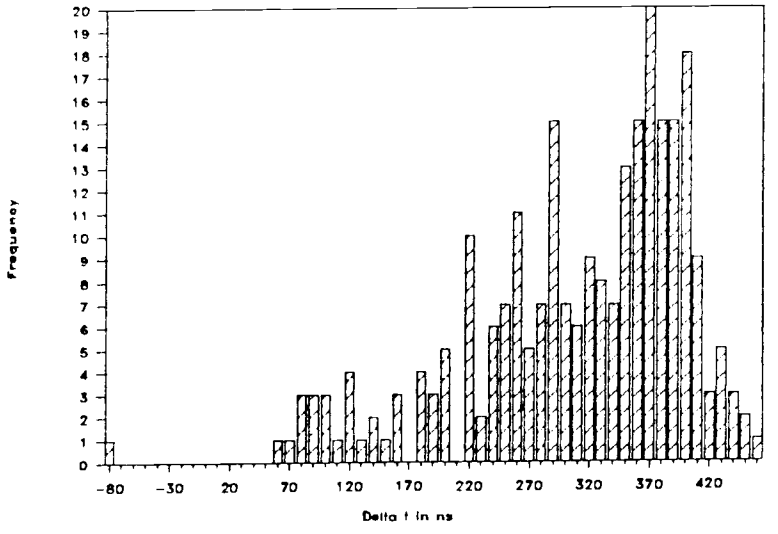

Figure 2.21 Distribution of M TINO Y

The power spectra of the TINOs (cf. Appendix) show that the signal power is located in a band with frequencies between 1/365 and 1/28 [1/day].

The power spectra of the transmitter switching functions, in Fig. 2.22 for the case of M Sw, others in Appendix, show that the stations switch back to the same transmitter every 28 days. The width of the peak indicates how precisely the stations switch transmitters every 14 days. The peak of W Sw has the smallest width. Y Sw has the widest peak, indicating that this secondary station does not switch exactly every 14 days, which can also be seen in Fig. 3.1. Master M Sw and Secondary X Sw have a fairly narrow peak. A transmitter switching exactly every 14 days would result in just one line for a frequency of 1/28 [1/day]. Master and Secondary X do not switch precisely every 14 th day either, making the switchings hard to predict.

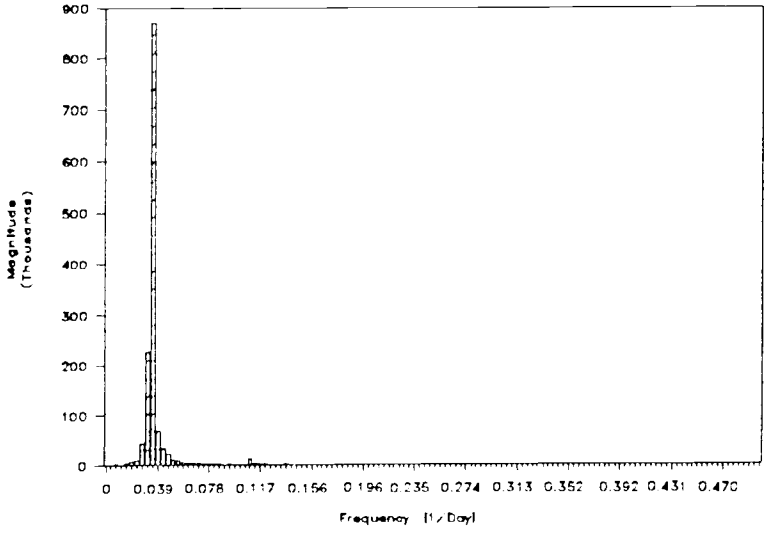

Figure 2.22 Power Spectrum of Master Switching Times

Can the weather data considered to be wide sense stationary (wss)? Fig. 2.23 shows sample autocorrelations using N=30 samples starting at various points in time. Over the short periods of time we are considering, the weather and transmitter data can clearly not be considered wss, since the autocorrelations are not invariant to a shift in time origin.

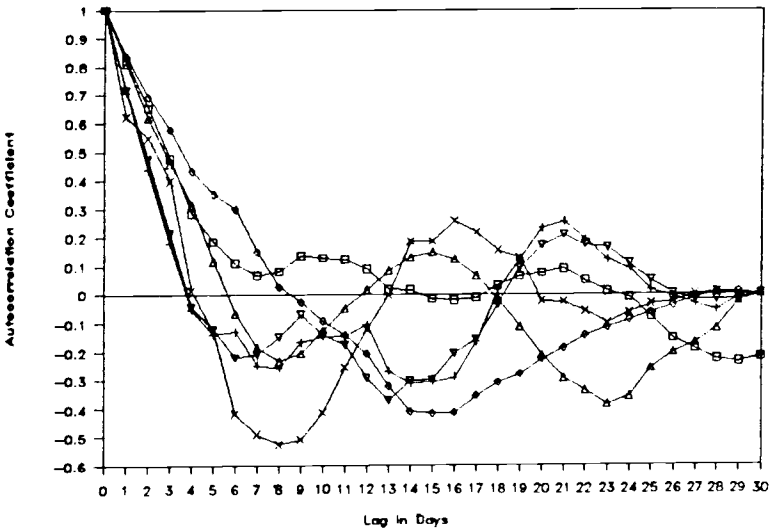

Figure 2.23 Sample Autocorrelations of Daily Means of N Dry in WMC, N=30 Samples Used

Other sample autocorrelations can be found in the Appendix. Can the processes, however, be considered cyclostationary (or periodically stationary)? If its statistics are invariant to a shift in time origin by integral multiples of a constant period [13], then they are cyclostationary. Assuming that weather data (measured at the same time every day, so diurnal variations do not have to be considered) are periodical with a period of one year, we can assume a wide sense cyclostationarity. Within the short periods of time at which we are looking, the weather data can not be considered stationary.

II.4 Explanation of TD Variations

Since the emission delays are computed at the secondary transmitters using local clocks (cesium standards), the TDs do not depend on the propagation conditions along the Master-Secondary paths. In the following we assume that any changes in propagation conditions occur uniformly over the whole chain area rather than over one path. The TDs then depend only on a path with the length Secondary-Receiver path (length d_{SR}) minus Master-Receiver path (length d_{MR}) (see equations 1.2, 1.3 and 1.4) and for our receiver in Corvallis we obtain (using the distances in Table 1.2):

	$d_{SR} - d_{MR}$ [km]
TDW	-277.2
TDX	-21.7
TDY	+589.3
TDW at SAMW	+488.3
TDX at SAMXY	-179.5
TDY at SAMXY	+236.0

Table 2.14 Distances Path SR Minus Path MR

TDW obviously depends mainly on the path MR (negative difference), TDX is influenced almost equally by the conditions on both paths (small difference) and TDY depends almost exclusively (see Appendix II) on the path YM.

The TDW measured at SAMW depends mainly on the propagation conditions on path W-SAMW, TDX measured at SAMXY depends mainly on the path M-SAMXY and TDY measured at SAMXY depends mainly on the path Y-SAMXY. Already we suspect that the system area monitor SAMY improves the TDY in Corvallis the most, since the TDY measured in Corvallis and the TDY measured at the SAMXY location both mainly depend on the propagation conditions in south-west Nevada.

We observed constant TD errors of -1.75 μs for TDW, +1.85 μs for TDY and about 0 for TDX. An additional propagation delay (ASF) on the path causes a negative constant TD error for TDW, because TDW depends on a path with a negative length (negative difference $d_{WR} - d_{HW}$). For TDY the constant TD error is positive (positive difference $d_{YR} - d_{HY}$). There is a negligible constant TD error for TDX, since $d_{XR} - d_{HX}$ is very small, propagation delays cancel each other out.

According to equations (1.10a) and (1.10b) there are three main factors that influence the phase of a low frequency ground wave:

1. The refractive index n
2. The α-factor
3. The ground conductivity parameter τ_0

N changes with a change of T,e or p in the following way (using equation 1.29):

$$\delta N_p = 77.6/T \; \delta p \qquad (2.12)$$

$$\delta N_T = \{-77.6p/T^2 - 7.46\ 10^5\ e/T^3\}\ \delta T \qquad (2.13)$$

$$\delta N_e = 3.73\ 10^5/T^2\ \delta e \qquad (2.14)$$

$$\delta N = \delta N_p + \delta N_T + \delta N_e \qquad (2.15)$$

Table 2.15 shows the diurnal/seasonal variations of p, T and e (as observed in Table 2.10):

	Diurn. Min	Diurn. Max	Seas. Min	Seas. Max
δp [mbar]	-.5	-2	-5	-10
δT [°C]	+5.0	+15	+16	+26
δe [mbar]	+.2	+1	+3	+8

where the diurnal variations are the 4 pm minus the 4 am values and the seasonal variations are the July values minus the January values

Table 2.15 Diurnal/Seasonal Variations of p, T and e

The following table shows how changes of p, T and e influence N:

	δN_T	δN_e	δN_p	δN
Minimal diurnal:	-5.5	+0.9	-0.1	-4.7
Maximal diurnal:	-16.4	+4.5	-0.5	-12.4
Minimal seasonal:	-17.4	+13.5	-1.4	-5.3
Maximal seasonal:	-24.9	+36.0	-2.7	+8.4

Table 2.16 Diurnal/Seasonal Variations of δN

The refractivity N decreases by about 4 to 13 units during the day/summer compared to the night/winter; in extreme cases the seasonal change can even be positive, +8 units. The δN_p, refractivity fluctuations due to changes in the air pressure, are negligible compared to δN_T and δN_e. An increase in temperature is usually accompanied by an increase in dew point temperature (partial water pressure, see Appendix III), i.e. the terms δN_T and δN_e cancel each other somewhat and keep the fluctuations of the refractivity N small.

Change in weather / propagation conditions influence propagation time t_p over a path of length d=100 km; t_p is the standard propagation time (equation (1.11a)) for a 100 km path and δt_p is its deviation from the standard t_p for various propagation conditions.

Diurnal / seasonal changes in refractivity of δN = +8 to -13 result in δt_p =+3 ns to δt_p =-4 ns. Diurnal

changes in the α-factor of as little as $\delta\alpha$=.014 and as much as $\delta\alpha$=.044 result in δt_p = +5 .. +17 ns.

Since a change in weather conditions changes the refractive index and the α-factor, the δt_p's have to be added to estimate the full variations in propagation conditions. Here again, the influences cancel each other somewhat due to the opposite signs.

A change in the conductivity coefficient of $\delta\tau_0$ =-.1 would cause a δt_p of -51ns, a magnitude above the influence of N and α. This calls for further research, which is, however, beyond the scope of this project.

Now let us look at the variation of the TDs due to variations in N and α. To obtain realistic results we need to include the local phase adjustments performed by the system area monitors. For standard conditions the CSTD is calculated for each monitor station. A change in propagation / weather conditions results in LPAs (equation 1.16) added to the coding delay of each secondary (equation 1.12). In this simulation we assume that the LPAs performed adjust only for changing weather / propagation conditions, not for transmitter drifts. Using the adjusted coding delays we then calculate the TDS deviations from the standard mean value in Corvallis δTDs [ns].

In the following we assume uniform weather changes in the whole chain area: a change of δN = -3 would result in a δTDW of 8 ns (includes a LPAW of 5 ns). A change of $\delta\alpha$=.014 would result in a δTDY of 19 ns (includes a LPAY of -12 ns). However a decrease of N is always accompanied by an increase in α (equations 1.30 and 1.31).

We now simulate how a change in N and α affects the TDs measured in Corvallis.

	W	X	Y
estimated ΔTDS [ns]	-33	7	15
LPA for this Sec. [ns]	-21	8	-10
ΔTDS without LPAs [ns]	-12	-1	25

Table 2.17 ΔTDS Variations Due to $\Delta\alpha$ =.014, ΔN = -3

	W	X	Y
estimated ΔTDS [ns]	-96	20	44
LPA for this Sec. [ns]	-61	22	-29
ΔTDS without LPAs [ns]	-35	-2	73

Table 2.18 ΔTDS Variations Due to $\Delta\alpha$ =.044, ΔN = -13

In Table 2.9 we observed the following night-to-day fluctuations: an increase of 50 to 60 ns during the day (compared to the night value) for TDY, an increase of 5 to 15 ns during the day for TDX and a decrease during the day of 0 to 20 ns for TDW. The estimations, assuming a uniform change in propagation conditions over the whole area, explain the diurnal variations of TDY and TDX, but not the variations of TDW. The propagation conditions are too different on the various paths; a uniform change in propagation conditions in the whole chain area does not estimate the observed TDs very well.

We now estimate the effect of weather on night-to-day TD fluctuations ΔTDS. Instead of assuming uniform changes in weather conditions the whole chain area, we use the weather stations in Salem, Medford and Winnemucca to estimate the weather conditions on the paths of TDW, TDX and TDY, respectively. Using the diurnal changes observed ($\Delta\alpha$SLE=.014, $\Delta\alpha$MFR=.024, $\Delta\alpha$WMC=.044, ΔNSLE=-3.3, ΔNMFR=-8, ΔWMC=-8.3, Table 2.10) we obtain the following:

	W	X	Y
estimated ΔTDS [ns]	-32	10	50
LPA for this Sec. [ns]	-21	11	-33
ΔTDS without LPAs [ns]	-11	-1	83

Table 2.19 TD Variations Due to Changes in α and N

	W	X	Y
observed night-to day ΔTDS [ns]	0..-20	5..15	50..60
estimated ΔTDS [ns]	-32	10	50

Table 2.20 Comparison Observed and Estimated ΔTDS

The observed diurnal variations of TDY and TDX can therefore be estimated quite well. For TDW, the weather station in SLE is not a very good representative for the weather conditions on the MR and WR paths; consequently the estimation is not a good one. It would have been ideal if the weather conditions on all propagation paths had been known.

The seasonal variations (increase of TDW by 40 and of TDX by 60 ns in the winter (compared to the summer) and a decrease of TDY by 15 ns in the winter cannot be fully explained by a change in α and N. For diurnal variations the influence of the slowly fluctuating ground conductivity (τ_0) can be ignored, but for seasonal TD variations a consideration of a change in ground conductivity is quite important and requires a thorough investigation.

Table 2.19 shows that the SAMY for Secondary Y reduces the observed ΔTDY and so improves the TDY in Corvallis and not only the coastal area for which it is calibrated (ΔTDY in this case reduced by 40 %).

SAMX deteriorates the observed TDX (in this case increases the observed ΔTDX fluctuations by 11 ns). Assuming uniform weather changes on the MR and XR paths the weather changes would cancel each other almost for a

receiver location like Corvallis, where $T_{MR} \approx T_{XR}$, if no SAM had corrected the emission delay.

The SAMW also deteriorates the observed TDW appreciably (in this case increases the ΣTDW 21ns).
This proves that system area monitors do not necessarily improve the accuracy of the time difference for receiver locations far away from the SAM (again assuming they adjust for changing propagation conditions only).

They especially deteriorate the TD accuracy for receiver locations where $T_{MR} \approx T_{SR}$.

They do improve the situation for receiver locations close to the system area monitors and for receiver locations where TDS and the TD measured at the SAMs location depend mainly on propagation paths in the same geographical area.

In our case this is true for TDY.

II.5 Correlation between TD Data and Weather and Transmitter Data

The covariance C of two wide-sense stationary (wss) random variables (RVs) x and y at lag τ is calculated in the following way:

$$C(\tau) = \frac{1}{N} \sum_{t=1}^{N+\tau} (x(t-\tau) - \mu_x)(y(t) - \mu_y) \quad \text{for } \tau < 0$$

$$C(\tau) = \frac{1}{N} \sum_{t=1}^{N-\tau} (x(t) - \mu_x)(y(t+\tau) - \mu_y) \quad \text{for } \tau \geq 0 \qquad (2.16)$$

where N = number of samples used

$\mu x, \mu y$ = sample means of the RVs x and y

The correlation coefficient r_{xy} at lag τ is then defined by the ratio

$$r_{xy}(\tau) = \frac{C}{\sigma_x \sigma_y} \qquad (2.17)$$

where $\sigma x, \sigma y$ = sample standard deviations of the RVs x and y

First let us look at the correlation coefficients of the station data (TINO's and transmitter switching times):

The following correlation coefficients are calculated at lag 0 using the RV x (TINO data, measured at 12 pm PST every day) and the RV y (12 pm hourly mean of the TD data) over a time of 255 days:

$r_{x,y}$	TDW	TDX	TDY
M TINO W	+.06		
S TINO W	+.29		
M TINO X		-.10	
S TINO X		+.47	
M TINO Y			+.57
S TINO Y			+.32
(M TINO W + S TINO W)/2	+.30		
(M TINO X + S TINO X)/2		+.44	
(M TINO Y + S TINO Y)/2			+.57
(M TINO W - S TINO W)/2	-.27		
(M TINO X - S TINO X)/2		-.36	
(M TINO Y - S TINO Y)/2			+.43

Table 2.21 Cross-Correlations TINO's and TDs

All correlations have their maximum at lag 0. As expected (equations 1.24 - 1.26), the sum of the M TINO and the S TINO for each secondary is significantly correlated with the corresponding TD value. In the case of TDY the TD is significantly correlated with M TINO Y, as expected (equation 1.27). Since TDY depends almost only on $T_{M,Y}$, we obtain a high correlation between TDY and (MTINOY - STINOY)/2, as expected (equation 1.23). Since TDW and TDX depend not only on the master-secondary path, the cross-correlation with (MTINO - STINO)/2 is weaker.

The 95% confidence interval for a sample correlation coefficient of .57 obtained using 255 samples is (using equation 2.10) $.49 \leq r' \leq .65$.

The following correlation coefficients are calculated at lag 0 using the RV x (transmitter switching times) and the RV y (daily mean of the TD data) over a time of 255 days:

$r_{x,y}$		TDW	TDX	TDY
M Switching Times	M Sw	-.45	-.31	-.56
W Switching Times	W Sw	-.13		
X Switching Times	X Sw		+.42	
Y Switching Times	Y Sw			+.06

Table 2.22 Cross-Correlations Switching Times and TDs

All correlations have their maximum at lag 0, except

for the correlation of TDX and M Sw. It is maximum at lag -7: $r_{xy}(-7)=+.46$. TDW and TDY show a high positive correlation with M Sw and a weak correlation with the secondary transmitter switching times. Obviously TDW and TDY are mainly influenced by the master transmitter switching times. In the case of TDX there is a strong correlation with X Sw at lag 0 and also a strong correlation with M Sw at lag -7. A closer look at the transmitter switching times (Fig. 3.1) shows that M, W and Y switch at about the same time, but X switches seven days later. TDX depends almost equally on X Sw and at a lag of -7 days on M Sw.

Now let us look at the cross-correlations of the TD data at 4 am/4 pm and the weather soundings in Salem, Medford and Winnemucca at 4 am/4pm at lag 0 (used to calculate α, N and the relative humidity RH). The soundings were available for 70 days, so we use 140 sample points (twice a day).

r_{xy}		TDW	TDX	TDY
Salem:	α	+.31	+.11	+.07
	N Dry	+.21	+.04	-.42
	N Wet	-.37	-.18	+.30
	N	-.36	-.23	+.06
	RH	-.18	-.14	-.21
Medford:	α	+.11	+.02	+.20
	N Dry	+.26	+.04	-.51
	N Wet	-.34	-.16	+.28
	N	-.13	-.13	-.16
	RH	+.05	-.04	-.33
Winnemucca:	α	-.05	-.16	+.40
	N Dry	+.26	+.16	-.52
	N Wet	-.17	-.10	+.23
	N	+.13	+.09	-.39
	RH	+.31	+.14	-.49

Table 2.23 Cross-Correlations Soundings 4am/4pm and TDs

The 95% confidence interval for a sample correlation coefficient of -.52, obtained using 140 samples, is (using equation 2.9) $-.64 \leq r' \leq -.40$.

We observe fairly strong negative correlations

between the dry component of the refractive index in Salem, Medford and Winnemucca with TDY, also significant positive correlations of the α-factor in Winnemucca with TDY. Since TDY depends only on the path M-Y we expect it to be significantly correlated with N and α. N Wet has negative correlations with the TDs, as expected, and N itself has a much smaller correlation with the TD values than N Dry.

We realize that the influence of N Dry on the TDs is much more important than the influence of N Wet or N but the theory of radio wave propagation predicts that a change in TD is correlated with N. This indicates that the ground wave of the Loran-C signal is influenced by the refractivity N at some height above the surface more than by the surface value. At a certain height N Dry is more indicative than N Wet, since the humidity (and therefore N Wet) decreases with height.

A significant negative correlation of -.49 at lag 0 between RH in Winnemucca and TDY, and weaker correlations with TDW and TDX can also be observed.

Since TDW and TDX depend on more than one path, the correlations are much smaller between weather data and TDW and TDX.

In the case of the correlations between the weather data and TDY, the correlation coefficients are slightly higher at a lag of -8, four days. The weather change leads the TD change by four days (e.g. X=N Dry SLE, Y= TDY: $r_{xy}(0)=-.42$ and $r_{xy}(-8)=-.61$). This could indicate a gradual change in ground conductivity as a result of the weather change.

Next we need to examine whether or not our correlation coefficients agree with what we had expected. The regression curve of two RVs Y (the TD values) and X (the weather parameters, called a control variate) is calculated in the following way:

$$Y = a\,X + b \qquad (2.19a)$$

$$\Delta Y = a\,\Delta X \qquad (2.19b)$$

where $a = r_{XY}\,(\sigma_X/\sigma_Y)$, the slope of the regression curve

$b = \mu x - a\,\mu y$

ΔY is the increase of Y, if X increases by ΔX

The slope of the regression curve using control variate α in the case of e.g. WMC is (σ_{TDY}=57 ns, σ_α=.03, $r_{TDY\ \alpha}$=.4) a = 760 [ns/α-unit]. An increase of $\Delta\alpha$=.014 results in an increase of TDY of a$\Delta\alpha$ = 11 ns, in fair agreement with section II.4, where an increase of α alone by $\Delta\alpha$=.014 was predicted to change TDY by +19 ns. But since N decreases at the same time α increases the increase of TDY is not as large.

The slope of the regression curve using control variate N, e.g. in SLE, is (σ_{TDW}=36 ns, σ_N=5.5, $r_{TDW\ N}$=-.36) a=-3.5 [ns/N-unit]. A decrease of ΔN=-3 causes TDW to increase by a ΔN = 10 ns, a fair agreement with the predicted change of ΔTDW = 8 ns. We have therefore confirmed the validity of some correlation coefficients.

It is rather obvious that a uniform change in N, α or τ_0 over the whole chain area does not precisely reflect the actual changes along particular pathways.

A solution is the mixed path propagation [14]. Each path has to be divided into m different climatical/propagation zones, where m can be as low as 1 for a propagation path over an area, where the climatical/ propagation conditions stay pretty much the same or as high as 5 for propagation over high deserts (e.g. desert of Nevada), high mountains (e.g. Cascades), valleys (e.g. Willamette Valley), low mountains (e.g. Coast Range) and seawater (e.g. Pacific). The actual propagation time on a path with such a diversity of propagation conditions can

then be estimated better by the superposition of the m different propagation conditions on the path. This, however, requires very detailed weather informations for each zone.

The following table shows the cross-correlations between the TD data (hourly means at 12 pm) and temperature measurements at various locations at lag 0 for N=255 data points:

r_{xy}	TDW 12 pm	TDX 12 pm	TDY 12 pm
T Salem daily max	-.33	-.45	-.47
T Medford daily max	-.41	-.48	-.45
T Lakeview daily max	-.45	-.50	-.43
T Reno 4 am	-.32	-.45	+.36
T Las Vegas 4 am	-.36	-.54	-.46

Table 2.24 Cross-Correlations Temperatures and TDs

The temperatures show a significant negative correlation with TDW and TDX. The slope of the regression curves range from -.7 to -1.8 ns/°C in the case of TDW and TDX.

The observed summer/winter differences of ca. -20 °C would result in TD changes of +14 to +32 ns, confirming high seasonal variations for TDW and TDX with a considerable increase of TD in the winter.

The following table shows the correlations of N Dry, N Wet, N and the relative humidity, measured in Reno and Las Vegas over a period of 255 days with the TD values at 12 pm:

r_{xy}		TDW 12 pm	TDX 12 pm	TDY 12 pm
Reno:	N Dry	+.28	+.43	+.32
	N Wet	-.36	-.44	-.36
	N	-.22	-.15	-.15
	RH	+.11	+.23	+.19
Las Vegas:	N Dry	+.31	+.53	+.45
	N Wet	-.21	-.27	-.25
	N	-.00	+.10	+.07
	RH	+.18	+.36	+.31

Table 2.25 Cross-Correlations N and TDs

The significant positive correlation of N Dry and TDY obtained using two samples/day can be confirmed.

The correlations of dewpoint / partial water pressure and the air pressure and the TDs are quite small.

The rain - TD correlations (over a period of 255 days) are:

r_{xy}		TDW DM	TDX DM	TDY DM
Rain on path	W-R	.35	.22	+.23
	X-R	.30	.26	+.19
	M-R	.34	.19	+.11
	M-W	.26	.12	+.09
	M-X	.06	.12	-.01
	M-Y	.09	-.09	-.11

Table 2.26 Cross-Correlations Rain and TDs, 255 days

All correlations are quite small. Even rain on the path M-Y has only a very small correlation with TDY. So we can confirm our decision to ignore the effect of rain. But the effect of rain on the ground conductivity has to be investigated.

Concluding Comments:

1. The major cross-correlations are: A strong cross-correlation between the TD values and the master transmitter switching times, in the case of TDX also with the secondary X switching times; a strong negative cross-correlation between TDY and N Dry in Winnemucca, a positive correlation with the α-factor. This makes sense

since TDY is only dependent on the path MY and therefore is only dependent on the weather conditions there. We also observed a significant positive correlation with M TINOY.

2. It can be confirmed that the influence of N Wet is smaller than the influence of N Dry, as described by Samaddar [15].

3. A correlation test of the 4 am/4 pm (PST) weather data with the 4 am/4 pm TD data results in correlation coefficients at lag 0 between TDY and N Dry WMC of -.52 and between TDY and α WMC of .40. An observed decrease of N by e.g. 8 units decreases the primary phase time T_P on a 100 km path by 3 ns (equation 1.11c). It is accompanied by an observed increase in α of +.044, resulting in a strong positive phase correction T_c of 17 ns (equation 1.11d). The total propagation time increase on the 100 km path is 17-3=14 ns, thus explaining the positive correlation with α and the negative correlation with N. Fig. 2.24 shows clearly how a diurnal weather change (diurnal variation of N Dry and α) causes the TDY value to change (diurnally).

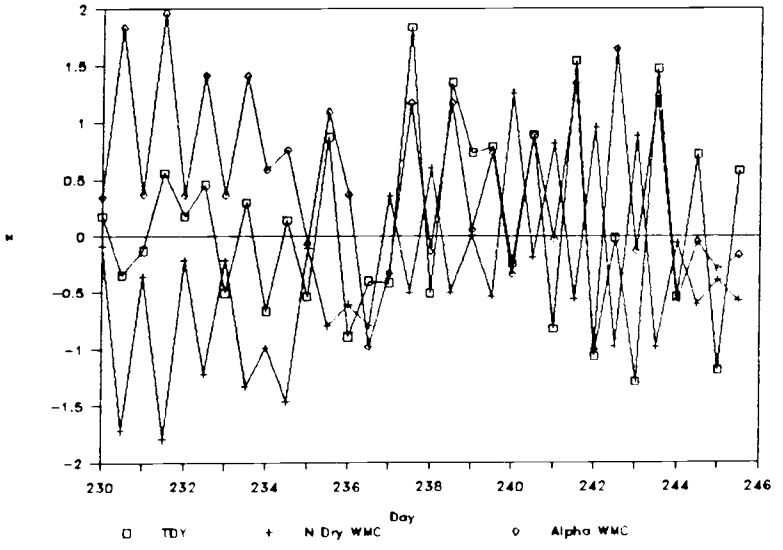

Figure 2.24 TDY, N Dry and α in WMC at 4am and 4 pm (Variables are Normalized Using $z=(x-\mu)/\sigma$)

If the weather data were available 24 hours a day the direct correlation could be shown even better. Although it

is not practical to gather weather data 24 hours a day, it would be practical to measure the TINO values 24 hours a day and broadcast them. In section III. we will show how those (broadcasted) TINO values can be used as control variates to reduce the variance of the received TDs.

Since TINO and weather data are strongly correlated we should be able to show a strong correlation at each hour of the day.

The next step is to determine if the TD values and the control variates, as we call the weather/station data, are jointly wss. In order to do this we need to perform several sample cross-correlations over several periods within the year.Two random processes are jointly wss if each process is wss and their cross-correlation depends only on $\tau=t_2-t_1$ [13]:

$$R_{x,y}(t_1,t_2)=E[x(t_1)y(t_2)] = R_{x,y}(\tau) = E[x(t+\tau)y(t)] \quad (2.19)$$

Fig. 2.25 and Fig. 2.26 show two examples for sample cross-correlations, starting at different days. Obviously the two processes are not jointly wss (it was shown earlier that the weather CVs are not wss in the short time period of our observation). The cross-correlations between the TD values and our control variates (weather, TINOs) are seasonally dependent.

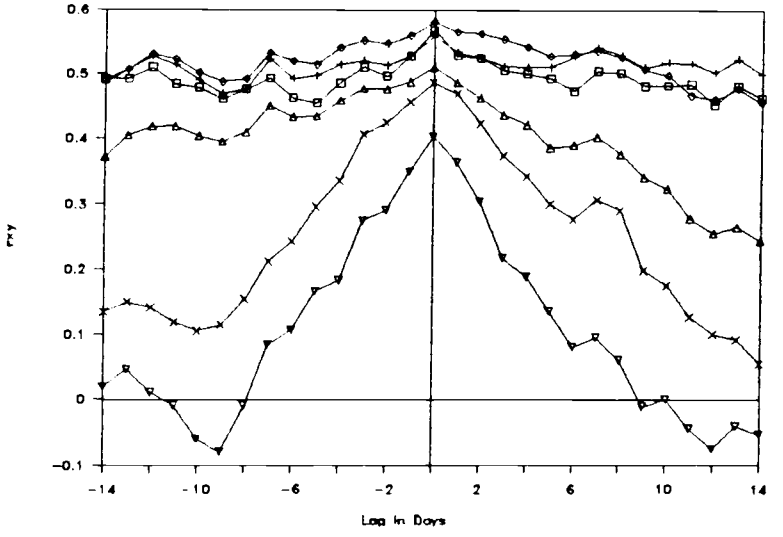

Figure 2.25 Sample Cross-Correlation Coefficients of TDY and M TINO Y Using N=150 Samples

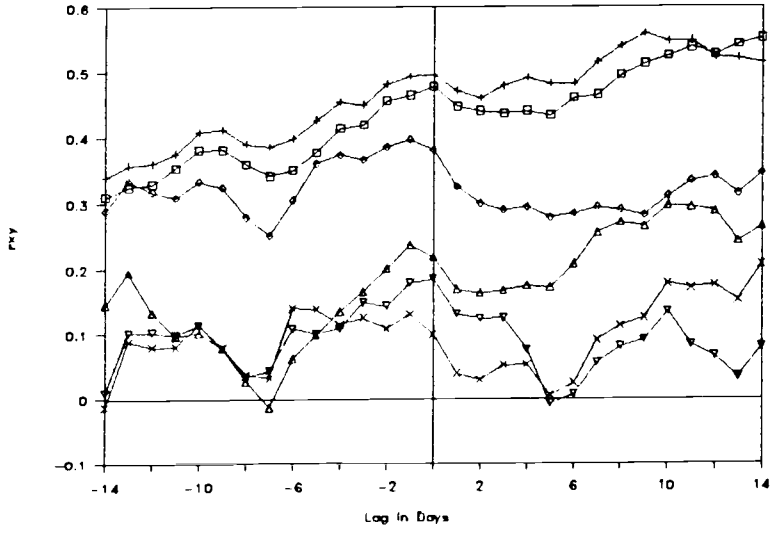

Figure 2.26 Sample Cross-Correlation Coefficients of TDX and N Dry in Las Vegas Using N=150 Samples

The cross-correlations are seasonally dependent. The calculated cross-correlations indicate which weather data show significant correlations with the TDs and can therefore be used as control variates (CVs). In the next section we will use the most significant CVs to reduce the standard deviation of the measured TDs.

III. TD ERROR REDUCTION

III.1 Theory of Optimal Prediction and Variance Reduction

We want to correct the measured TD values of a Loran-C receiver which moves around in a certain geographical area by using various weather and TINO data as so-called control variates (CVs).

We assume that the means and autocorrelations of all CVs, as well as the cross-correlations between them, are known from previous long-term measurements as a function of time (e.g. for each month of the year), since we showed in section II. that the CVs and the TDs are not jointly wide sense stationary. We also assume that the covariances between TD measurements and the CVs are known from prior long-term measurements for the same general geographic region and the same time intervals. We assume that within this geographic region these covariances are constant, i.e. independent of specific receiver locations.

From a set of consecutive control variate values we wish to optimally correct the TD values measured with a Loran receiver (reduce the TD variance). Since the CVs are usually not available at the time the TD measurements are made, they need to be predicted.

In the following we outline the theory of optimal prediction and variance reduction (VR):

Let the random variable (RV) S be the output TD of our Loran-C receiver. Our goal is to estimate the mean of S (μ_S) by using another RV X (a so called control variate CV), which is correlated with S to reduce the variance (V) of μ_S. A result of the VR is also that S_c is uncorrelated with the CV X. We assume that the covariance C (X,S) and the mean of the CV X, μ_x are known.

The control variate method to reduce the variance of a signal can be explained as follows: good CVs should be strongly correlated with S, either positively or negatively. Then if the observed value of X_1 is larger than the (known) μ_{x1}, we have the information that the observed value of X is quite likely to be either above the unknown μ_S (if $C[S,X_1] > 0$) or below μ_S (if $C[S,X_1] < 0$) and the control variate technique makes use of this information to obtain a variance reduction.

Let S_c be defined as

$$S_c = S - a\,(X - \mu_x) \qquad (3.1)$$

Then S_c is an unbiased estimator of μ_S [9].

Using the relations

$$V[X - Y] = V[X] + V[Y] - 2\,C[X,Y] \qquad (3.2)$$

and $$V[a\,g(x) + b] = a^2\,V[g(x)] \qquad (3.3)$$

we obtain the variance of our estimator:

$$V[S_c] = V[S] + a^2\,V[X] - 2\,a\,C[S,X] \qquad (3.4)$$

Obviously the variance of our estimator $V[S_c]$ is smaller than the the variance of our measured value V [S], if

$$2\,a\,C[S,X] > a^2\,V[S] \qquad (3.5)$$

Which value for a minimizes $V[S_c]$?

$$\partial V[S_c]/\partial a = 0: \quad 2a\,V[X] - 2\,C[S,X] = 0$$

$$\Rightarrow \qquad a = C[S,X]/V[X] = r_{Sx}\,\sigma_S/\sigma_x \qquad (3.6)$$

where r_{Sx} = cross-correlation coefficient of S and X

σ_s, σ_x are the standard deviations of S and X

We obtain a residual variance of

$$V[S_c] = (1 - r_{sx}^2)\, V[S] \qquad (3.7a)$$

and a residual standard deviation of

$$\sigma[Sc] = \sqrt{(1 - r_{sx}^2)}\ \sigma[S] \qquad (3.7b)$$

The higher the cross-correlation between our signal and the control variate, the larger the VR. For RVs with a normal distribution (which we assumed) the minimum mean square error is a linear estimate.

The VR can be even greater if m independent CVs are used.

$$S_c = S - \sum_{l=1}^{m} a_l\, (X_l - \mu_{xl}) \qquad (3.8)$$

Each of the CVs X_l is individually correlated with S. The CVs are also correlated with each other. In order to use m independent CVs we need to orthogonalize those CVs using the Gram-Schmidt orthogonalization method [8]:

We have m independent vectors $x_1, x_2, \ldots x_m$ and we want to create a set of m orthogonal vectors $y_1, y_2, \ldots y_m$:

We choose $y_1 = x_1$ (3.9)

$$y_j = x_j - \sum_{k=1}^{j-1} c_{kj}\, y_k \qquad j = 2, 3, \ldots N \qquad (3.10)$$

and $$c_{kj} = \frac{y_k \cdot x_j}{|y_k|^2} \qquad (3.11)$$

The vectors y_j are uncorrelated, if the vectors x_j have zero mean.

The present CVs are usually not readily available, which makes it necessary to predict them. Let us assume that we use the values of the last p days (which can be published) in order to perform a one-step linear prediction of today's CV x:

$$x_{pred\ n} = -\sum_{k=1}^{p} a_k\ x_{n-k} \qquad (3.12)$$

where $x_{pred\ n}$ = the predicted CV x for day n

x_{n-k} = CV x at date k days before day n

a_k = parameters, yet to be determined

Then the error between the actual value x_n and the predicted value $x_{pred\ n}$ is given by

$$e_n = x_n - x_{pred\ n} = x_n + \sum_{k=1}^{p} a_k\ x_{n-k} \qquad (3.13)$$

also known as the residual. In the method of the least squares the parameters a_k are obtained as a result of the minimization of the mean of the total squared error with respect to each of the parameters. Our signal x_n is a sample of an underlying random process, so the error is also a sample of a random process:

$$E = \in(e_n\hat{}2) = \in(x_n + \sum_{k=1}^{p} a_k\ x_{n-k})^2 \qquad (3.14)$$

where $\in(x)$ is the expectation of x. Now we have to minimize the mean square error with respect to each of the parameters:

$$\partial E/\partial a_i = 0 \qquad 1 \leq i \leq p \qquad (3.15)$$

We obtain p equations for the p unknown a_k s:

$$\sum_{k=1}^{p} a_k\ \in(x_{n-k}\ x_{n-i}) = -\in(x_n\ x_{n-i}) \qquad 1 \leq i \leq p \qquad (3.16)$$

This set of equations is called YULE-WALKER equations [13].

The minimum mean square error is then given by

$$E_p = \epsilon(x_n^2) + \sum_{k=1}^{p} a_k \, \epsilon(x_n \, x_{n-k}) \qquad (3.17)$$

For a stationary process $\epsilon(x_n \, x_{n-k}) = R(i-k) = R(\tau)$, where $R(\tau)$ is the autocorrelation of that stationary process. As shown in section II our CVs cannot be considered stationary. Therefore

$$\epsilon(x_{n-k} \, x_{n-i}) = R(n-k,n-i) \qquad (3.18)$$

where $R(t,t')$ is the nonstationary autocorrelation between times t and t'. $R(n-k,n-i)$ is a function of the time index n. Without a loss of generality we can estimate the YULE-WALKER equations at time n=0 [10]:

$$\sum_{k=1}^{p} a_k \, R(-k,-i) = -R(0,-i) \qquad 1 \leq i \leq p \qquad (3.19)$$

or in matrix form:

$$(R)_{p \times p} \, (a)_{1 \times p} = (B)_{1 \times p}$$

$$\rightarrow (a)_{1 \times p} = (R)^{-1}_{p \times p} \, (B)_{1 \times p} \qquad (3.20)$$

The minimum mean square error is then

$$E_p' = R(0,0) + \sum_{k=1}^{p} a_k \, R(0,-k) \qquad (3.21)$$

We consider the nonstationary CVs to be locally stationary and we can estimate the autocorrelation function with respect to a point in time as a short-time average [10], e.g. over one month.

The autocorrelations therefore are calculated the following way (covariance method, [10]):

$$R(-k,-i) = \frac{1}{N} \sum_{n=0}^{N-1} x_{n-i} \, x_{n-k} \qquad 1 \leq i \leq p, \; 1 \leq k \leq p \qquad (3.22)$$

Note that the matrix (R) is not Toeplitz, the elements on each diagonal are not identical. But the matrix is symmetric, which allows the use of simplified matrix inversion algorithms.

Note that rounding errors which occur when inverting the matrix can add up and introduce a large error. It is therefore necessary to solve the YULE-WALKER equations using double precision.

Note also that the values of the signal x_n must be known for $-p \leq n \leq N-1$, a total of p+N samples. We assume that enough samples are available to solve the YULE-WALKER equations for each month.

III.2 TD Error Reduction Performed

In the following all times are in PST, ignoring daylight savings time. For TDW, TDX and TDY we remove the transmitter switching influence first, pick the 3 major CVs that have the greatest influence on that particular TD, predict the CVs of each day (by using the published values of the preceding 14 days), orthogonalize those 3 CVs and then reduce the variance of the measured TD signal by using the control variate method, which reduces the variance and removes the correlation of the TD signal with the CVs.

Since the available TINO CVs are averaged from 12 pm to 1 pm PST every day over a period of 255 days and we want to perform a linear prediction using the 14 preceding days, we use as our first TD time series the 12 pm to 1 pm PST hourly means of day 15 to 255 (1 sample/day).

The soundings are available twice a day at 4 am and 4 pm PST over a period of 70 days (day 186 to 255). We need to leave 14 samples for the linear prediction, so we use as the second TD time series the 4am/4pm means (averaged over one hour) of day 193 to 255 (2 samples/day).

III.2.1 Removal Of The Transmitter Switching Influence

Cross-correlation coefficients between the master transmitter switching times and the TD's (at lag 0) are -.45 for TDW, -.31 for TDX and -.56 for TDY (see section II.5). The cross-correlations with the transmitter switching times of the secondaries W and Y are negligible, but not so the cross-correlation between TDX and X Sw. This cross-correlation coefficient is .42 at lag 0. The cross-correlation of TDX and M Sw is strongest at lag -7, +.46. Therefore TDX seems to be approximately equally influenced by the transmitter switchings X Sw and M Sw and TDW and TDY are mainly influenced by the master switchings.

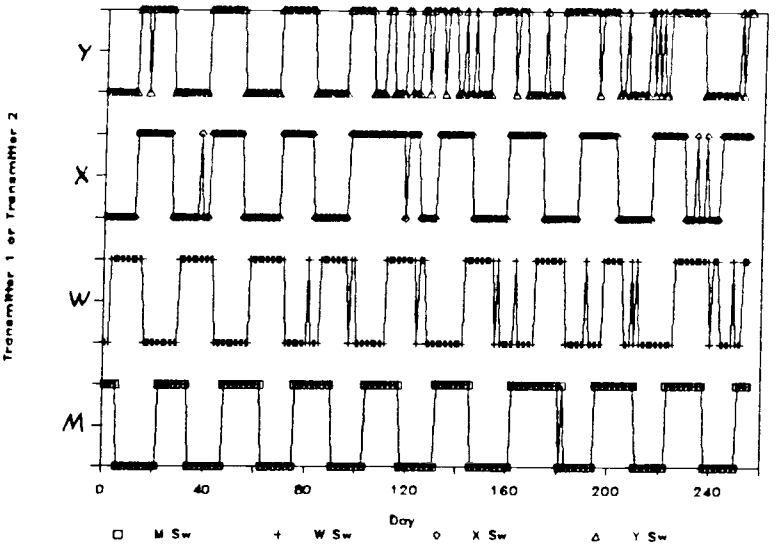

Figure 3.1 Transmitter Switching Times

Fig. 3.2 shows for the case of TDW how the master switchings influence the TD signal (Figures for TDX and TDY in Appendix).

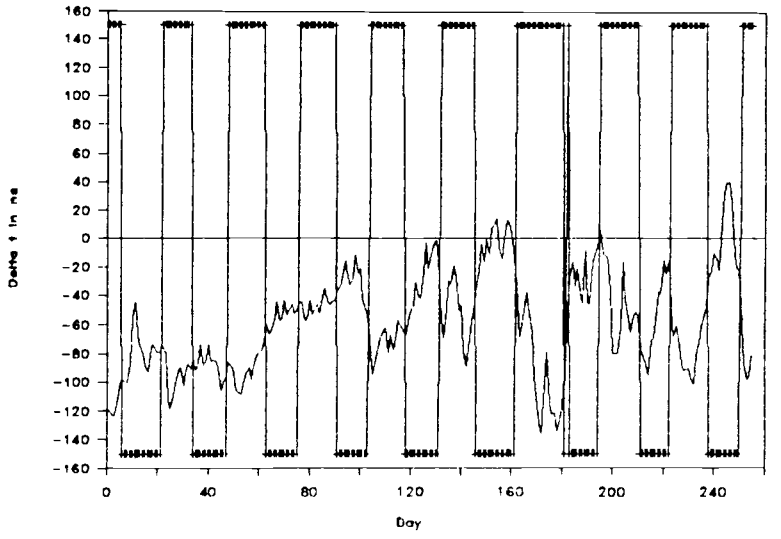

Figure 3.2 TDW Daily Mean and Master Switching Times

Before we use the weather CVs to reduce the variance of the TD signal we will remove the transmitter switching influence. Since the transmitter switching CVs are rectangular functions, we compensate each time interval by adding / subtracting a ξ [ns] each time a certain transmitter is used and thus take care of the negative / positive drift this particular transmitter introduces. If, for example, transmitter 1 tends to make the TD signal drift towards a higher value and transmitter 2 drifts towards a lower value. We then perform the following correction:

$$\begin{aligned} &\text{Transmitter 1 used:} \quad TDs1 = TDs - \xi \\ &\text{Transmitter 2 used:} \quad TDs1 = TDs + \xi \end{aligned} \qquad (3.23)$$

TDW and TDY mainly depend on the master switchings: The optimum ξs, which bring the largest VRs and remove the correlations of TDW and TDY with M Sw, are iteratively found to be (using the first time series, the 12 pm TD values of day 15 - 255):

TD	TDW 12 pm	TDY 12 pm
μ [ns]	-62.2	-32.1
σ [ns]	38.1	48.9
cross-corr. TD - M Sw	-0.45	-0.29
optimum δ [ns]	+17	+15
μ of residual TD [ns]	-61.5	-31.5
σ of residual TD [ns]	34.1	46.7
cross-corr. TD - M Sw	0.00	.01
σ improved by [ns]	4.0	2.2

Table 3.1 Removal of Master Switching Influence,
(1 Sample/Day)

We reduced the variance of the TD signals considerably, and TDW and TDX are now uncorrelated with the master switchings.

In the case of TDX, where the signal fluctuations are dependent on master and secondary X switching times, we have to proceed as follows:

$$TDX = TDs +/- \delta m +/- \delta x \qquad (3.24)$$

Master Station: Transmitter 1 used: + δm
Transmitter 2 used: - δm
Secondary X : Transmitter 1 used: + δx
Transmitter 2 used: - δx

Through iteration the optimum δm and δx were found as follows:

	TDX 12 pm
μ [ns]	-25.2
σ [ns]	28.8
cross-corr. TD - M Sw	-0.36 (lag 0),0.42 (lag 7)
cross-corr. TD - X Sw	+0.39 (lag 0)
optimum δm [ns]	+12
optimum δx [ns]	+13
μ of residual TD [ns]	-26.3
σ of residual TD [ns]	23.6
cross-corr. TD - M Sw	-0.01 (lag 0)
cross-corr. TD - X Sw	+0.01 (lag 0)
σ improved by [ns]	5.2

Table 3.2 Removal of Master and X Switching Influences,
(1 Sample/Day)

The standard deviation of TDX was improved by ca. 5 ns. This success invites us to try to remove the influence of M Sw and W Sw from TDW and also the influence of M Sw and Y Sw from TDY. The improvements are negligible, however, which was to be expected, since TDW and TDY have very small cross-correlations with their secondary transmitter switching times.

The second time series, containing two samples per day of TD at 4 am and 4pm, show similar cross-correlations with the transmitter switching times. Their influence can be removed in exactly the same way as for the time series with one sample per day:

	TDW 4am/pm	TDY 4am/pm
μ [ns]	-49.0	-59.6
σ [ns]	41.3	58.5
cross-corr. TD - M Sw	-0.40	-0.29
optimum δ [ns]	+17	+15
μ of residual TD [ns]	-46.6	-57.5
σ of residual TD [ns]	37.8	55.9
cross-corr. TD - M Sw	+0.01	-0.04
σ improved by [ns]	3.5	2.6

Table 3.3 Removal of Master Switching Influence,
(2 Samples/Day)

	TDX 4am/pm
μ [ns]	-21.6
σ [ns]	35.4
cross-corr. TD - M Sw	-0.36 (lag 0),-0.48 (lag 7)
cross-corr. TD - X Sw	+0.42 (lag 0)
optimum δm [ns]	+12
optimum δx [ns]	+13
μ of residual TD [ns]	-22.2
σ of residual TD [ns]	29.6
cross-corr. TD - M Sw	-0.03 (lag 0)
cross-corr. TD - X Sw	+0.07 (lag 0)
σ improved by [ns]	5.8

Table 3.4 Removal of Master and X Switching Influences,
(2 Samples/Day)

Since we also get similar VRs for the time series with two samples per day, we proved that the corrections applied to remove the transmitter switching influences can be performed at any time of the day.

III.2.2 Further Variance Reduction Using Control Variates

We can use m CVs to reduce the variance of the TD time series (transmitter switching influence removed) even more, as outlined in section III.1. As an illustration, we decide on m=3 CVs for each TDS: we pick CVs which have the strongest correlations with the TDS in order to obtain large VRs.

We choose the following CVs for the time series containing one sample per day:

	1. CV	2. CV	3. CV
TDW	(M TINO W + S TINO W)/2	T Lkv	N Dry LV
TDX	(M TINO X + S TINO X)/2	T Lkv	N Dry LV
TDY	M TINO Y	T Lkv	N Dry LV

Table 3.5 CVs for Time Series, (1 Sample/Day)

The cross-correlations of the TDs with the CVs are still evident in spite of the switching influence removal:

	1. CV	2. CV	3. CV
TDW	.26	-.47	.33
TDX	.40	-.60	.59
TDY	.58	-.45	.49

Table 3.6 Cross-Correlations CVs and TDs for Time Series, (1 Sample/Day)

Before we reduce the variance of our measured data we need to predict the CVs for each day. We assume that the autocorrelations (equation 3.22) for each month are known, as described in section III.1 and thus can solve the YULE-WALKER equations (3.19). The solutions are the a_k prediction coefficients, and with equation (3.12) we can predict today's CV , if we know the CV values of the previous p days. In order to reduce the mean square error in equation (3.21) we have to use a large p. With p =14 days we get the following errors:

The means of the residual, defined in equation (3.13) are (e.g. in July):

CV	σ of CV	μ residual
M TINO Y	17 ns	13 ns
T Lakeview	4.6 °F	2.0 °F

Table 3.7 σ of CV and μ (CV Minus Predicted CV)

The residuals have always a smaller mean than the standard deviation of the signal to be predicted, proving the accuracy of the prediction.

The prediction coefficients a_k are recalculated each month, since the CVs are not stationary and we assumed that the autocorrelations of all CVs were available for each month. The prediction of the temperatures in Lakeview can be seen in Fig. 3.3:

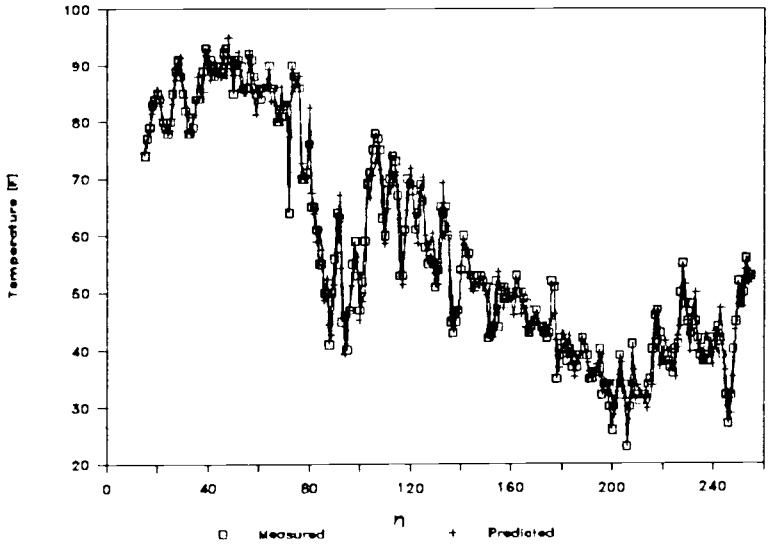

Figure 3.3 Measured and Predicted Temperatures in Lakeview [°F] (1 Sample/Day)

The plot of M TINO Y and its predicted value can be found in the Appendix.

Table 3.8 shows the cross-correlations of the predicted CVs with the TDS.

	1. CV	2. CV	3. CV
TDW	.24	-.45	.32
TDX	.35	-.60	.58
TDY	.58	-.47	.54

Table 3.8 Cross-Correlations Predicted CVs and TDs for Time Series 1 Sample/Day

The correlations have hardly changed, further evidence of the quality of our predicted CVs.

Applying equation (3.1) to our residual TDY using the (predicted) CV M TINO Y reduces the σ of TDY by another 8.7 ns, from 46.7 ns to 38.0 ns, which is exactly the standard deviation predicted in equation (3.7b). If we also used some weather CVs, by how much further would this reduce the σ?

We need independent CVs, but the CVs themselves are strongly correlated (e.g. T Lkv and N Dry LV have r=-.89). We orthogonalize the (predicted) CVs first, using equations (3.9 - 3.11).

	r_1	r_2	r_3	r_{12}	r_{13}	r_{23}
TDW and CV before orth.:	+.24	-.45	+.32	-.51	+.44	-.89
TDW and CV after orth.:	+.24	-.38	-.17	.00	.00	.00
TDX and CV before orth.:	+.35	-.60	+.58	-.51	+.54	-.89
TDX and CV after orth.:	+.35	-.48	+.11	.00	.00	.00
TDY and CV before orth.:	+.58	-.47	+.54	-.56	+.67	-.89
TDY and CV after orth.:	+.58	-.17	+.12	.00	.00	.00

where r_i is the cross-correlation between the i-th CV and the respective TD and r_{iu} is the cross-correlation coefficient between the i-th and the u-th CV.

Table 3.9 Cross-Correlations between TDs and CVs before and after the Orthogonalization, 1 Sample/Day

Now let us look at the three VR (equation 3.8) operations again, one for each CV, in the order of decreasing correlation with the TD signal:

Signal:	TDY
Original measured μ=-32.1,	σ=48.9
After Master Switching influence reduction:	σ=46.7
After VR using 1. CV (r=.58)	σ=38.0
Remaining correlations of TD residual with	
2. CV:	r=-.21
3. CV:	r=.14
After VR using 2. CV (r=-.21)	σ=37.2
Remaining correlations of TD residual with	
3. CV:	r=.14
After VR using 3. CV (r=.14)	σ=36.8
Remaining correlation of TD residual with	
1. CV:	r=0
2. CV:	r=0
3. CV:	r=0
M Sw:	r=-.03
Y Sw:	r=+.03
Total σ reduction [ns]	12.1
[%]	25
σ reduction using CVs [ns]	9.9
[%]	21

Table 3.10 TDY Variance Reductions (1 Sample/Day)

Note that in each VR step the standard deviation is reduced exactly by the theoretically predicted value (equation 3.7b).

TDW and TDX depend on many different paths, thus there are no CVs that show a strong correlation. But the proposed CVs show a significant correlation, and we will now apply the same methods to them:

Signal:	TDW
Original measured μ=-62.2,	σ=38.1
After Master Switching influence reduction:	σ=34.1
After VR using 2. CV (r=-.39)	σ=31.4
Remaining correlations of TD residual with	
1. CV:	r=.25
3. CV:	r=-.19
After VR using 1. CV (r=.25)	σ=30.5
Remaining correlations of TD residual with	
3. CV:	r=-.19
After VR using 3. CV (r=-.19)	σ=29.9
Remaining correlation of TD residual with	
1. CV:	r=-.01
2. CV:	r=0
3. CV:	r=0
M Sw:	r=-.02
W Sw:	r=-.13
Total σ reduction [ns]	8.2
[%]	22
σ reduction using CVs [ns]	4.2
[%]	12

Table 3.11 TDW Variance Reductions (1 Sample/Day)

Signal:	TDX
Original measured μ=-25.2,	σ=28.8
After M Sw and X Sw influence reduction:	σ=23.6
After VR using 2. CV (r=-.48)	σ=20.7
Remaining correlations of TD residual with	
1. CV:	r=.40
3. CV:	r=.12
After VR using 1. CV (r=.40)	σ=18.9
Remaining correlations of TD residual with	
3. CV:	r=.14
After VR using 3. CV (r=.14)	σ=18.7
Remaining correlation of TD residual with	
1. CV:	r=.01
2. CV:	r=0
3. CV:	r=0
M Sw:	r=-.02
X Sw:	r=.03
Total σ reduction [ns]	10.1
[%]	35
σ reduction using CVs [ns]	4.9
[%]	21

Table 3.12 TDX Variance Reductions (1 Sample/Day)

The VR is successful in each case. The stronger the correlations of signal and CVs, the greater the VRs possible. Any number of CVs can be used, as long as they are orthogonalized first.

We also found significant correlations between our TDs measured at 4 am/pm and the weather data available from the soundings, especially α and N Dry. We will now perform the VR on the second time series using the following (most significant) weather CVs:

	1. CV	2. CV	3. CV
TDW	α SLE	N SLE	RH WMC
TDX	α SLE	N SLE	RH WMC
TDY	N Dry WMC	RH WMC	α WMC

Table 3.13 CVs for Time Series, (2 Samples/Day)

The cross-correlations of the TD time series containing 4am/4pm values (after removing the transmitter switching influences) with the CVs are:

	1. CV	2. CV	3. CV
TDW	.28	-.36	.34
TDX	.10	-.26	.07
TDY	-.58	-.57	.47

Table 3.14 Cross-Correlations CVs and TDs for Time Series, (2 Samples/Day)

Unfortunately we do not have the CVs TINO available twice a day at 4am/pm. We would expect significant correlations and also had another strong CV available. Therefore in this case we can only use weather data as CVs.

Applying the 12 pm TINO corrections at 4am and 4 pm deteriorates the variance and introduces an additional noise component.

We predict the CVs in the same way recalculating the a_k s every month and using the preceding 14 data points (7 days) to predict the CV of any day. We then orthogonalize our (predicted) CVs again:

	r_1	r_2	r_3	r_{12}	r_{13}	r_{23}
TDW and CV before orth.:	+.29	-.31	+.37	-.56	-.06	-.06
TDW and CV after orth.:	+.29	-.18	+.37	.00	.00	.00
TDX and CV before orth.:	+.29	-.38	+.13	-.56	-.06	-.06
TDX and CV after orth.:	+.29	-.26	+.12	.00	.00	.00
TDY and CV before orth.:	-.55	-.57	+.48	+.70	-.72	-.68
TDY and CV after orth.:	-.55	-.26	+.04	.00	.00	.00

where r_i is the cross-correlation between the i-th CV and the respective TD and r_{iu} is the cross-correlation coefficient between the i-th and the u-th CV.

Table 3.15 Cross-Correlations between TDs and Predicted CVs before and after the Orthogonalization for time series, (2 Samples/Day)

We then reduce the variance of TDY, TDW and TDX by using the orthogonalized CVs in the order of decreasing correlation coefficients (equation 3.8):

Signal:	TDY
Original measured μ=-59.6,	σ=58.5
After Master Switching influence reduction:	σ=55.9
After VR using 1. CV (r=-.55)	σ=46.9
Remaining correlations of TD residual with	
2. CV:	r=-.31
3. CV:	r=.05
After VR using 2. CV (r=-.31)	σ=44.6
Remaining correlations of TD residual with	
3. CV:	r=.05
After VR using 3. CV (r=.05)	σ=44.5
Remaining correlation of TD residual with	
1. CV:	r=0
2. CV:	r=0
3. CV:	r=0
M Sw:	r=-.04
Y Sw:	r=-.09
Total σ reduction [ns]	14
[%]	24
σ reduction using CVs [ns]	11.4
[%]	20

Table 3.16 TDY Variance Reductions (2 Samples/Day)

Signal:	TDW
Original measured μ=-49.0,	σ=41.3
After Master Switching influence reduction:	σ=37.8
After VR using 3. CV (r=.37)	σ=35.1
Remaining correlations of TD residual with	
1. CV:	r=.31
2. CV:	r=-.19
After VR using 1. CV (r=.31)	σ=33.4
Remaining correlations of TD residual with	
2. CV:	r=-.20
After VR using 2. CV (r=-.20)	σ=32.7
Remaining correlation of TD residual with	
1. CV:	r=0
2. CV:	r=0
3. CV:	r=0
M Sw:	r=.07
W Sw:	r=-.02
Total σ reduction [ns]	8.6
[%]	20.8
σ reduction using CVs [ns]	5.1
[%]	14

Table 3.17 TDW Variance Reductions (2 Samples/Day)

Signal:	TDX
Original measured μ=-21.6,	σ=35.4
After M Sw and X Sw influence reduction:	σ=29.6
After VR using 1. CV (r=.29)	σ=28.3
Remaining correlations of TD residual with	
2. CV:	r=-.28
3. CV:	r=.12
After VR using 2. CV (r=-.28)	σ=27.3
Remaining correlations of TD residual with	
3. CV:	r=.13
After VR using 3. CV (r=.13)	σ=27.1
Remaining correlation of TD residual with	
1. CV:	r=0
2. CV:	r=0.01
3. CV:	r=0
M Sw:	r=.06
W Sw:	r=.07
Total σ reduction [ns]	8.3
[%]	23
σ reduction using CVs [ns]	2.5
[%]	9

Table 3.18 TDX Variance Reductions (2 Samples/Day)

The covariance method in combination with predicting the CVs was successful. In the case of one sample/day and in the case of two samples/day we reduced the standard deviations of the TD signals by 20 - 30 % while keeping the mean constant. The residual TD signals (after using all three CVs on the TDs) are also uncorrelated with the major CVs and have lost their periodicity due to transmitter switchings.

The original and residual of TDX with a 35 % improved standard deviation is shown in Fig. 3.4:

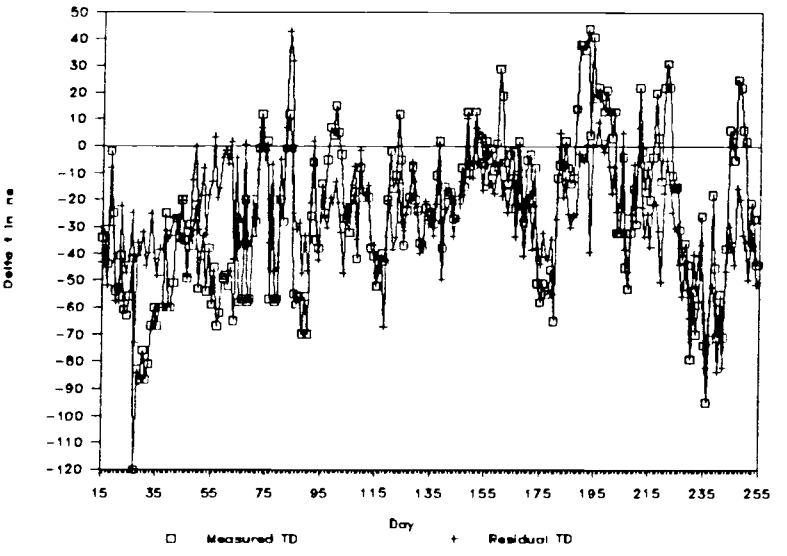

Figure 3.4 Observed and Residual of TDX (1 Sample/Day)

The autocorrelation of the residual of TDX in Fig. 3.5 shows that the 28-day periodicity has disappeared (compare with Fig. 2.12).

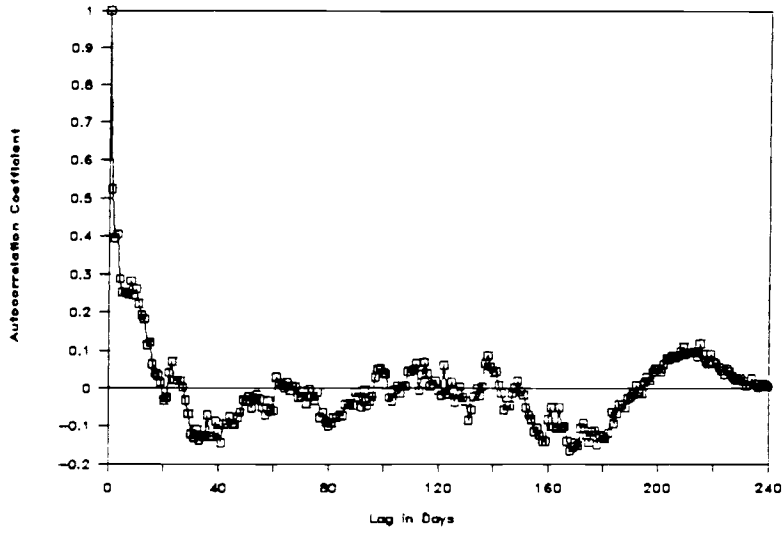

Figure 3.5 Autocorrelation of TDX Residual, 1 Sample/Day

The power spectrum of TDY in Fig. 3.6 shows (peak at frequency 1/day) that the 28-day periodicity has disappeared, but the diurnality of TDY is still present.

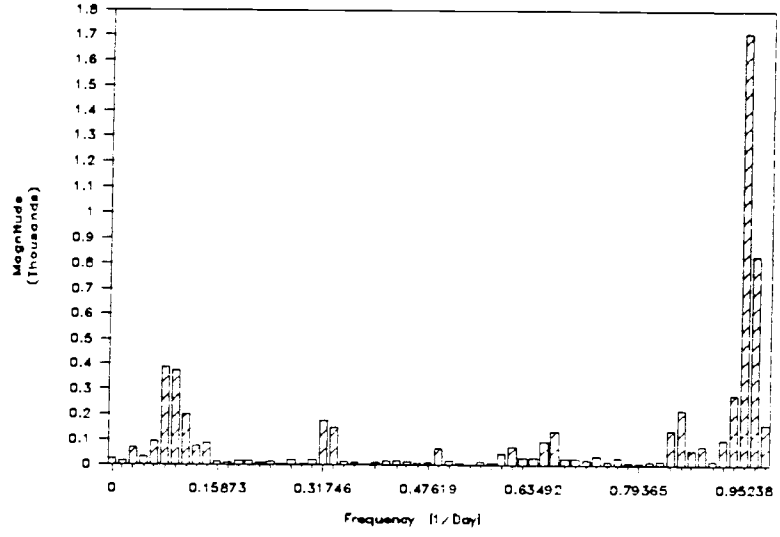

Figure 3.6 Power Spectrum of TDY, (2 Samples/Day)

IV. CONCLUSIONS AND RECOMMENDATIONS

TD data (TDW, TDX TDY) were analyzed from U.S.-chain 9940 at a fixed location over a period of 255 days. Weather and transmitter station data were also collected. All TD data showed a 28 day periodicity, which could be explained by the transmitter switchings.

When the new generation of solid state transmitters (ideally with no frequency drift) are in use, this problem will be eliminated.

A constant TD error in the case of TDW and TDY was observed. The observed time varying TD error had standard deviations of 30 to 60 ns.

Only TDY showed a diurnal variation, which could be explained by the diurnality of the α-factor in the Nevada desert. TDY is only dependent on the path MY and therefore shows significant correlations with the weather conditions on this path, especially with α and N Dry. TDW and TDX showed somewhat lower correlations with the weather data, since their signal depends on several paths.

The TD data also showed significant correlations with TINOs. These reflect the propagation conditions on the base lines and, if measured and transmitted 24 hours a day, they would give the user a good control variate to further reduce the variance of the TD signal without the need of predicting a control variate. Since TINOs are strongly correlated with weather data, they can replace weather data from the propagation paths as control variates.

After removing the transmitter switching influences, predicted (orthogonalized) control variates (CVs) were used to successfully reduce the variance of the time varying TD error. Standard deviation reductions of

9 - 21 % (21 % in the case of TDY where strongly correlated CVs were available) were obtained..

It was also shown that in the case of TDY the LPAs performed by the SAMY improve the measured TD values in Corvallis, but in the case of TDW and TDX the SAM deteriorate the TD values (introducing larger errors than if no LPAs were introduced at all). For a specific location, the LPAs performed by the SAM can be predicted and the user can feel free to adjust for those LPAs, providing the TD signal is averaged over at least 3 hours (since LPAs are usually performed only about 8 times a day, a LPA about every 3 hours).

Land and air-over-land applications of Loran-C are increasing (airplanes, cars). LPAs mainly improve the TDs for locations off-shore and in the general area of the SAMs, but not further inland. It would be useful for SAMs to broadcast their corrections so users (in areas where the LPAs deteriorate the accuracy) could adjust their measured TDs. If SAMs were located on base lines, the LPAs performed due to changing weather conditions on the base lines would result in adjustments that were not disadvantageous to users anywhere in the chain area.

To reduce the TD errors even more and to explain the offset between measured TD value and predicted value for that location, further topics need to be investigated:

* The estimation of the α-factor by using a higher order approximation to estimate dN/dh. (Several radiosonde measurements along the path MY, measured 24 hours a day, would be an ideal base.)
* The influence of the ground conductivity, especially the factor τ_0 on the seasonal fluctuations.
* The influence of strong sun-spot activities on radio wave propagation.

* The influence of very heavy rain or snow on a particular path.
* The influence of transmitter system synchronization errors.
* The influence of propagation errors due to geophysical variations along the signal paths.
* The influence of atmospheric noise, man-made noise and electromagnetic interferences.
* The influence of receiver measurements. (Two identical receivers should be used at the same location and the results be compared.)
* The influence of various antenna environments.

Loran-C still has a lot of potential, and with falling receiver prices the number of users of this easy-to-use radio navigation sytem will further increase in spite of the new (more expensive, more complex) satellite navigation aids.

BIBLIOGRAPHY

[1] C.D.Ahrens "Meterology Today", West Publishing Company, 1985

[2] B.R.Bean and E.J.Dutton, "Radio Metereology", NBS Monograph 92, 1966

[3] H.Bremmer,"Terrestrial Radio Waves", Elsevier Publishing Company,Inc., 1946

[4] R.H.Doherty and J.R.Johler, "Meteorological influences on Loran-C ground wave propagation", Journal of Atmospheric and Terrestrial Physics Vol.37,pp.1117 to 1124, Dec. 1974

[5] R.H.Doherty and J.R.Johler, "Loran-C System Dynamic Model, Temporal Propagation Variation Study", July 1979, Final Report, U.S. Department of Transportation, avail.: National Technical Information Service, Springfield, VA

[6] Robert L.Frank, "Current Developments in Loran-C", Proceedings Of The IEEE, Vol.71,No.10,Oct. 1983

[7] J.R. Johler, W.J.Kellar and L.C.Walters, "Phase of the Low Radiofrequency Ground Wave", NBS Circular 573, June 1956

[8] B.P. Lathi, "Modern Digital and Analog Communications Systems", Holt, Rinehart and Winston, 1983

[9] A.M.Law, W.D.Kelton, "Simulation Modelling Analysis" McGraw-Hill, 1985

[10] J.Makhoul, "Linear Prediction: A Tutorial Review", Proc. of IEEE, vol.63, 1975

[11] J.N.Newman, "Loran Navigation with a Hand Caculator", PROC. new England Sailing Yacht Symp. New London, Connecticut, Jan. 1979, pp. 6-1 - 6-13 Society of Naval Architects and Marine Engineers

[12] J.N.Newman, "Coordinate Conversion On A Simplified Razin Algorithm", 11th Annu. Symp., WGA, 1982

[13] A.Papoulis, "Probability, Random Variables, and Stochastic Processes", McGraw-Hill 1984

[14] S.N.Samaddar, "The Theory of Loran-C Ground Wave Propagation - A Review", Navigation:Journal of The Institute of Navigation, Vol.26, No.3, Fall 1979

[15] S.N.Samaddar, "Weather Effect on Loran-C Propagation", Navigation: Journal of The Institute of Navigation Vol.27,No.1, Spring 1980

[16] G.W.Snedecor, "Statistical Methods", Iowa State University Press, 1967

[17] U.S. Department Of Commerce, National Weather Service, "Daily Weather Maps", 6/25/1986 - 3/6/1987

[18] U.S. Department of Transportation, U.S. Coast Guards, "Specification of the Transmitted Loran-C Signal", July 1981

APPENDICES

Appendix I:
Derivation of the α-Factor:

The classical method of accounting for the effects of atmosphere refraction of radio waves is to assume an effective earth radius, $a_e = ka$, where a is the true radius of the earth and k is the effective earth's radius factor. This methods assumes an earth suitably larger than the actual earth so that the curvature of the radio ray may be absorbed in the curvature of the effective earth. The relative curvature of the two then remains the same, thus allowing that radio rays be drawn as straight lines over this earth rather than curved rays over the true earth, a tremendous simplification. It will now be shown that α is proportional to the gradient of the refractive index n:

In Fig. A.1 a wave front moves from AB to A'B' along the ray path.

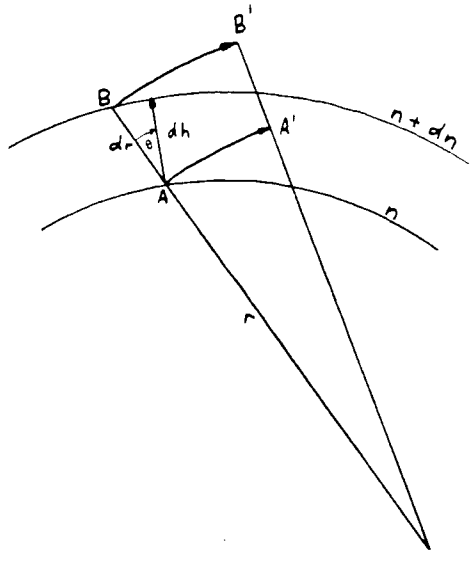

Figure A.1 Geometry to derive α-factor

If the phase velocity along AA' is v and v+dv along BB', then, from considering the angular velocity,

$$\frac{v}{r} = \frac{v + dv}{r + dr} \quad \text{or} \quad \frac{dv}{v} = \frac{dr}{r} \tag{A.1}$$

where r is the radius of the curvature of the arc AA'. Now, since the phase velocity, v, is

$$v = \frac{c}{n} \tag{A.2}$$

where c = velocity of light in vacuum and

n = refractive index of air, one obtains

$$\frac{dv}{v} = - \frac{dn}{n} \tag{A.3}$$

Combining (A.1) and (A.3) we obtain

$$\frac{1}{r} = - \frac{1}{n} \frac{dn}{dr} \tag{A.4}$$

If the ray path makes an angle Θ with the surface of constant refractive index

$$dh = dr \cos \Theta \tag{A.5}$$

where h is the height above the surface of the earth and the curvature of a radio ray is

$$\frac{1}{r} = - \frac{1}{n} \frac{dn}{dh} \cos \Theta \tag{A.6}$$

The curvature of the effective earth $1/a_e$ is defined as the curvature of the earth minus the curvature $1/r$ of a radio ray:

$$\frac{1}{a_e} = \frac{1}{a} - \frac{1}{r} \tag{A.7}$$

$$\text{then } a_e = a/\alpha = \frac{1}{1/a - 1/r} \tag{A.8}$$

$$\text{and } 1/\alpha = k = \frac{1}{1 + \frac{a}{n} \frac{dn}{dh} \cos \Theta} \tag{A.9}$$

For the small values of Θ normally used in tropospheric propagation, cos Θ may be set equally to unity.

The α-factor is then

$$\alpha = 1/k = 1 + \frac{a}{n}\frac{dn}{dh} \qquad (A.10)$$

By assuming that the gradient of n is constant, a linear model of N versus height has been adopted (N is called refractivity and is defined as $N = (n-1)\ 10^6$):

$$N = N_0 - \frac{h}{4a}\ 10^6$$

With equation (A.10) and $dn = dN \times 10^6 = -dh/4a$, the rough estimate, familiar factor of $k = 4/3$ or $\alpha = .75$ is obtained. Since it is not sufficient to assume a linear model of N versus height it is necessary to calculate the α-factor in more detail.

Appendix II:
The First Fresnel zone:

The first Fresnel zone is the spatial region in which an energy almost equivalent to that expected in free-space propagation can be transmitted from the transmitter to the receiver, its size expressed by the radius of its ellipsoid:

$$r1 = \sqrt{lamda\ d_1 d_2 / D} \qquad (A.11)$$

where r1 = radius of first Fresnel zone in distance d1 from the receiver

lamda = wavelength of the f=100 kHz signal

$$lamda = 3\ 10^5 / f \ [\ km\ ] = 3\ km \qquad (A.12)$$

D = distance from transmitter to receiver

$d_2 = D - d_1$

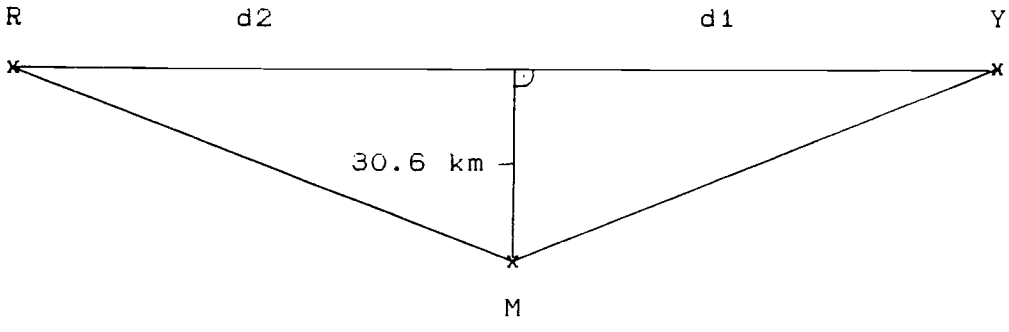

Figure A.2 First Fresnel Zone on the path YR

The direct path YR, which is $D=d_1+d_2=$ 1254.6 km (d1=588.4 km and d2=666.2km) long, has a radius of the first Fresnel zone in the distance d_1 of 30.62 km, almost the maximum Fresnel zone radius of 30.67 km. Fig. A.1 shows that the master station is only 32.6 km away from the direct path YR, only 2 km outside the first Fresnel zone. Our approximation in equation (1.5) can be made, since the paths YM and MR lie almost within the first Fresnel zone.

Appendix III:
Conversion Dew Point -> Partial Water Pressure

The dew point represents the temperature [°C], to which air would have to be cooled (with no change in air pressure or moisture content) for saturation to occur. Saturated air has a relative humidity of 100 percent, because it is filled to capacity with water.

The relative humidity is the ratio of the actual vapor pressure e [mbar] (a measure of the air's actual water vapor content) and the saturation water pressure e_s [mbar] (a measure of the air's total capacity for water vapor (saturation)). The relative humidity is then

$$\text{Relative Humidity} = \frac{e}{e_s} 100\% \qquad \text{(A.13)}$$

The following formula, called "Lowe Formula" estimates the vapor contents in mbar from the temperature in °C. The temperature [°C] converts to the saturation water pressure e_s [mbar] and the dewpoint [°C] to the actual water vapor content (partial water pressure) e [mbar].

a0=610.7799961	b0=486.6786841
a1=44.36518521	b1=31.52625546
a2=1.428945805	b2=.8640188586
a3=2.650648471e-2	b3=1.279669658e-2
a4=3.031240396e-4	b4=1.077955914e-4
a5=2.034080948e-6	b5=4.886796102e-7
a6=6.136820929e-9	b6=9.296950850e-10

Table A.1 Constants for Lowe Formula

For T > -50 °C: (A.14)

$$e=(a0+T*(a1+T*(a2+T*(a3+T*(a4+T*(a5+T*a6))))))/100$$

For -50 °C ≥ T > -100 °C (A.15)

$$e=(b0+T*(b1+T*(b2+T*(b3+T*(b4+T*(b5+T*b6))))))/100$$

Appendix IV:
Phase of the Low Frequency Ground Wave:

The source is assumed to be an elemental vertical electrical dipol as originally proposed by Hertz. The Hertz potential Π needs to fulfill:

$$(\nabla^2 + k^2)\,\Pi = -\Omega/K$$

where

∇ La Place operator

$k^2 = \frac{\epsilon w^2 + i4\pi\sigma w}{c^2}$ material constant of medium considered

ϵ dielectric constant

$w=2\pi f$ frequency of signal [rad/s]

σ conductivity

c speed of light in vacuum [m/s]

$\Omega = r\frac{I_o}{w}\exp\{i[kd-wt]\}$ source polarization

r radius (spherical earth theory coordinate) [m]

I_o amplitude of the source current [A]

$d=a\Theta$ distance from source [m]

a earth radius

Θ angular distance from the source over spherical earth

$K=\epsilon/(c^2\,\mu_o)$ permittivity [Farad/m]

μ_o permeability constant

There are 2 theories of calculating the field: the spherical earth theory and the plane-earth theory. It is known [14] that for distances > 5(wavelength [m])$^{1/3}$ km = 72 km the spherical earth theory gives best results:

The following refers to the spherical earth theory: The electric field is then

$$E_r = \frac{-1}{r\sin\Theta}\frac{\delta}{\delta\Theta}\left[\sin\Theta\frac{\delta\Pi}{\delta\Theta}\right]$$

$$E_\Theta = \frac{1}{r}\frac{\delta^2}{\delta\Theta\delta r}[r\Pi]$$

It has been convenient to express the total field E as a product of two factors [7]: (a) the primary field or free-space field Epr [V/m] and (b) the secondary factor F (dimensionless), which accounts for the disturbing influence of the source or the earth.

$$E = 2\,F\,Epr \qquad (A.16)$$

The primary field:

$$E_{pr} = \frac{I_0\ l\ k_1^2}{4\ \pi\ K\ w\ d} \exp\{i[k_1\ d - w\ t]\}\ [V/m] \qquad (A.17)$$

where

k1=w/c n wave number of the atmosphere at the surface of the earth [rad/m] (conductivity of air σ = 0 assumed)

n surface refractive index

d distance from transmitter to receiver [m]

l length of radio-transmitting antenna [m]

The secondary field:

$$F = R \exp\{i\,\Phi\} \qquad (A.18)$$

$$R = [\,2\pi\alpha^{2/3}(k_1 a)^{1/3}(\frac{d}{a})]^{1/2} \sum_{s=0}^{\infty} \frac{fs(h_1)\ fs(h_2)}{[2\tau_0 - 1/\ \xi_0]}$$

$$\Phi = (k_1 a)^{1/3}\ \tau_0\ \alpha^{2/3}\ \frac{d}{a} + \frac{\alpha d}{2a} + \frac{\pi}{4}$$

where

α α-factor (Appendix I)

a earth radius = 6370 10^3 m

h altitude of the source/receiver above the surface of the earth [m]

fs(h1) height-gain factor of source, needed, when receiver and transmitter not placed on earth surface

fs(h2) height-gain factor of receiver, needed, when receiver and transmitter not placed on earth surface

fs(h)=1, if at height h=0 (surface of earth)

The exponents 1/3 and 2/3 are a result of Hankel approximations of order 1/3 used.

τ_0 ground conductivity parameter

satisfies $\frac{d\,\xi_*}{d\,\tau_*} - 2\,\xi_*^2\,\tau_* + 1 = 0$,

a Ricati differential equation.

ξ_* conductivity and permittivity parameter for a vertical dipol source

$\xi_* = Ke \exp\{i[3\pi/4 - \Phi e]\}$

$$Ke = \frac{[c\alpha/(\epsilon_1^2 wa)]^{1/3}[\epsilon_2^2 + (\sigma^2\mu_0^2c^4)/w^2]^{1/2}}{[(\epsilon_2 - \epsilon_1)^2 + (\sigma^2\mu_0^2c^4)/w^2]^{1/4}}$$

$$\Phi e = \tan^{-1}[w\epsilon_2/(\mu_0 c^2\sigma)] - 1/2\,\tan^{-1}[w(\epsilon_2 - \epsilon_1)/(\mu_0 c^2\sigma)]$$

index 1: air index 2: earth

Approximation for τ_*, only term for s=0 used:

For $|\xi_*^2\,\tau| > 1/2$ and $Ke \gg 1$:

$\tau_0 = \tau_{0,0} - \xi_* - 2/3\,\tau_{0,0}\,\xi_*^3 + 1/2\,\xi_*^4$

For $|\xi_*^2\,\tau| < 1/2$ and $Ke \ll 1$:

$\tau_0 = \tau_{0,*} - [1/2\tau_{0,*}]\,1/\xi_* - [1/(2\tau_{0,*}^3)]\,1/\xi_*^2$

with $\tau_{0,0} = 1.8557$ and $\tau_{0,*} = 0.8086$

We are only interested in the phase not in the amplitude of the ground wave:

The primary phase is

$$\Phi_{pr} = k1\,d = w/c\,n\,d \qquad (A.20)$$

The secondary phase (neglecting the term $\alpha d/2a$ and the constant $\pi/4$) is:

$$\Phi_c = (k_1 a)^{1/3}\,\alpha^{2/3}\,\tau_0\,d/a \qquad (A.21)$$

Appendix V:

TD Plots

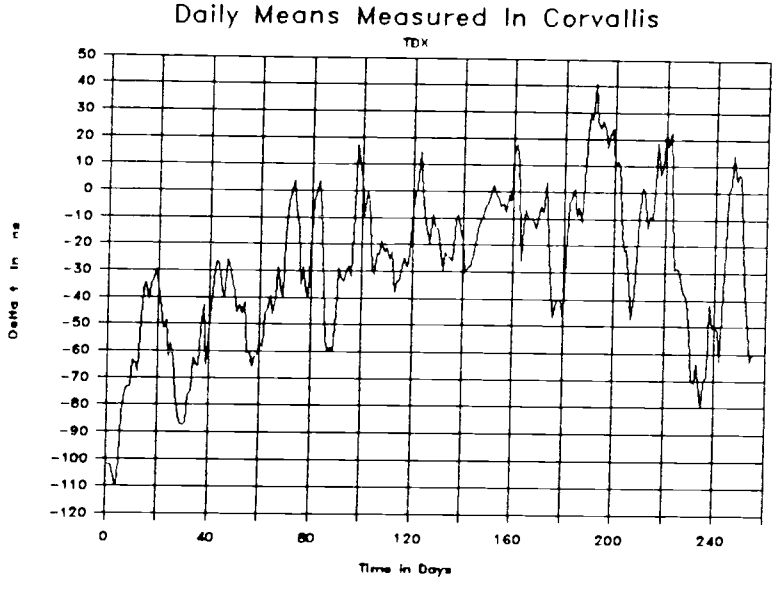

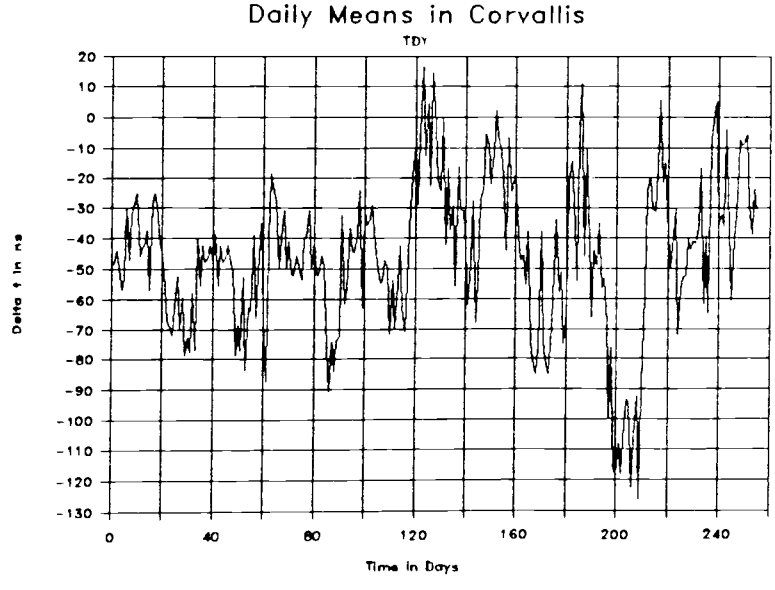

Appendix VI:

Distributions

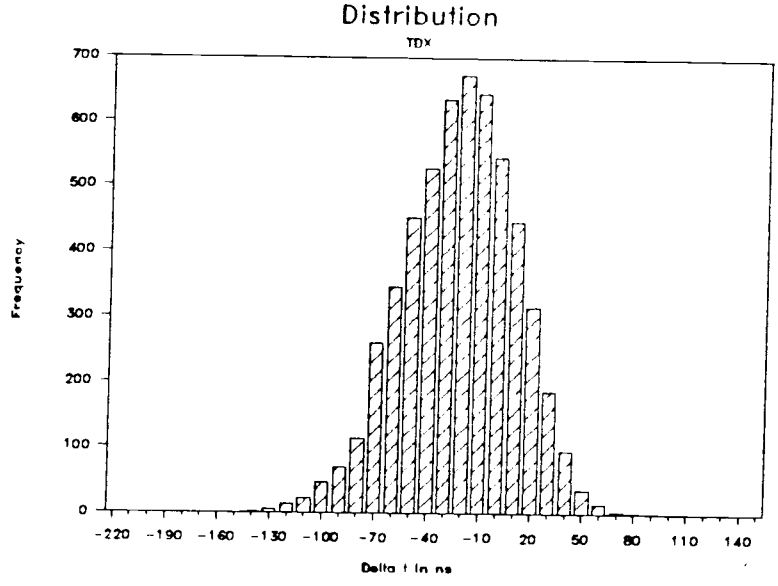

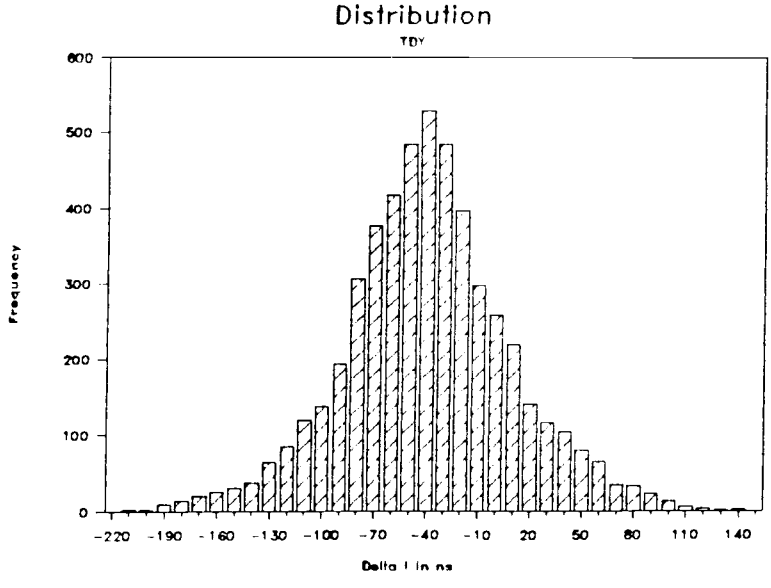

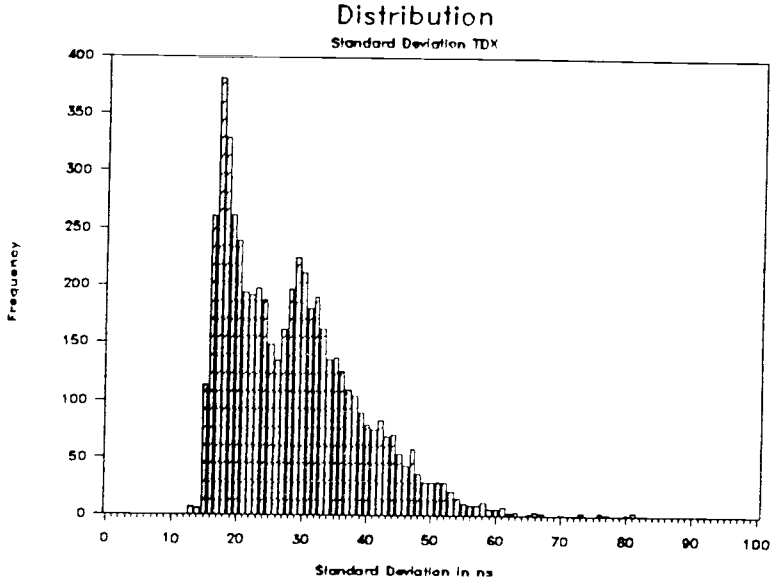
Distribution
Standard Deviation TDX
Frequency
400
350
300
250
200
150
100
50
0
0
10
20
30
40
50
60
70
80
90
100
Standard Deviation in ns

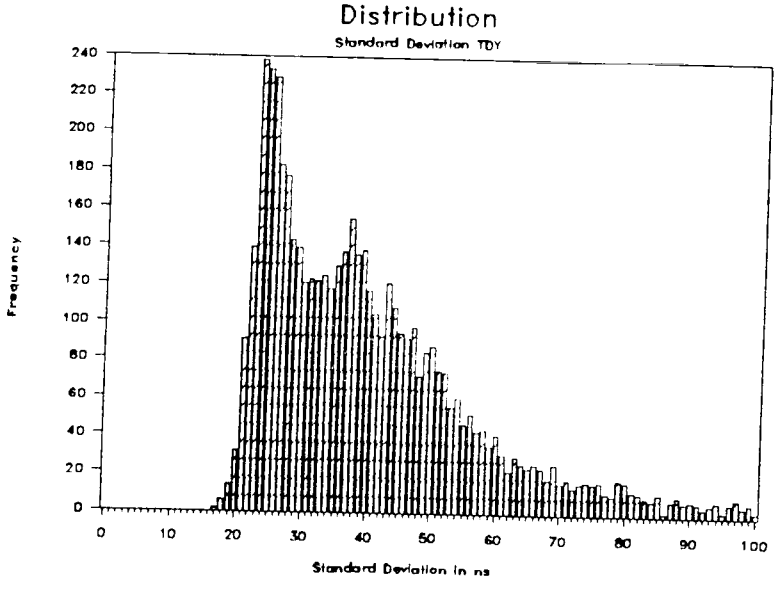
Distribution
Standard Deviation TDY
Frequency
240
220
200
180
160
140
120
100
80
60
40
20
0
0
10
20
30
40
50
60
70
80
90
100
Standard Deviation in ns

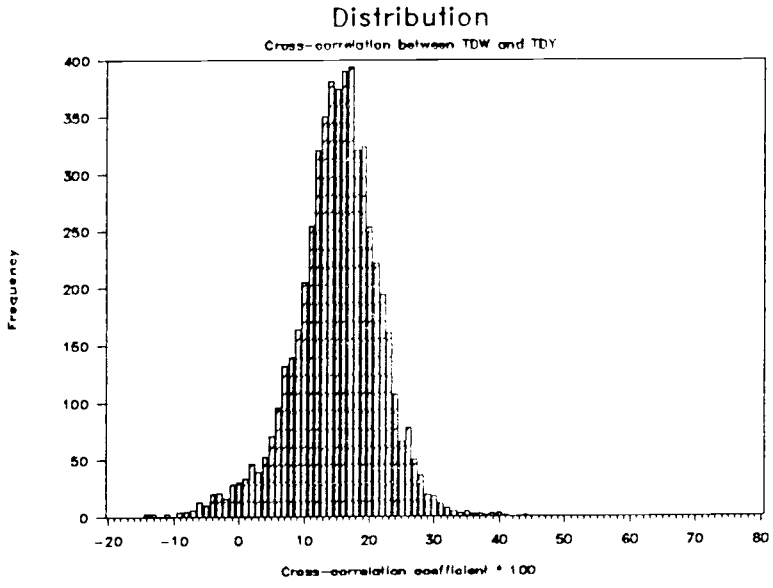
Distribution
Cross-correlation between TDW and TDY
Frequency
400
350
300
250
200
150
100
50
0
-20
-10
0
10
20
30
40
50
60
70
80
Cross-correlation coefficient * 100

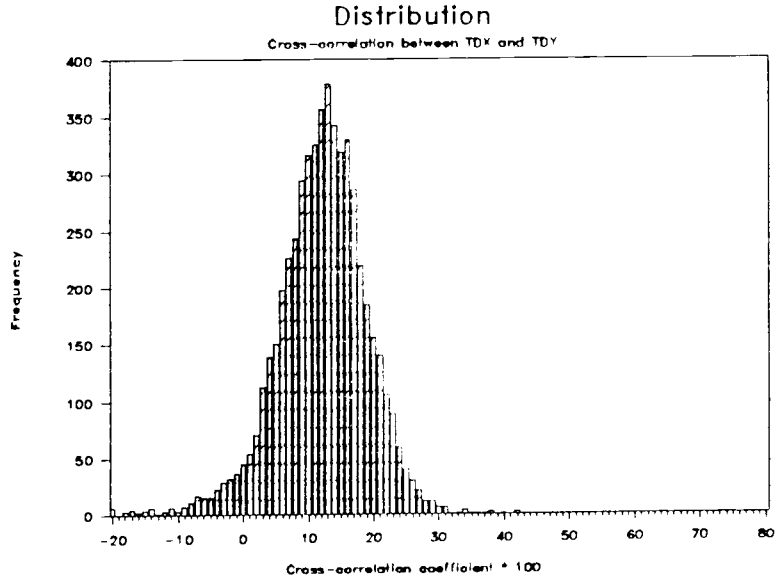
Distribution
Cross-correlation between TDX and TDY
Frequency
400
350
300
250
200
150
100
50
0
-20
-10
0
10
20
30
40
50
60
70
80
Cross-correlation coefficient * 100

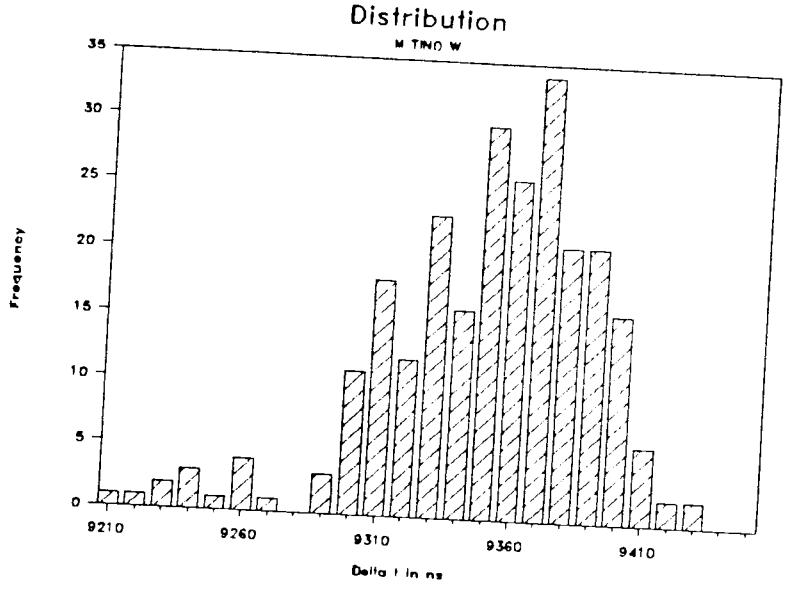
Distribution
M TIND W
Frequency
35
30
25
20
15
10
5
0
9210
9260
9310
9360
9410
Delta t in ns

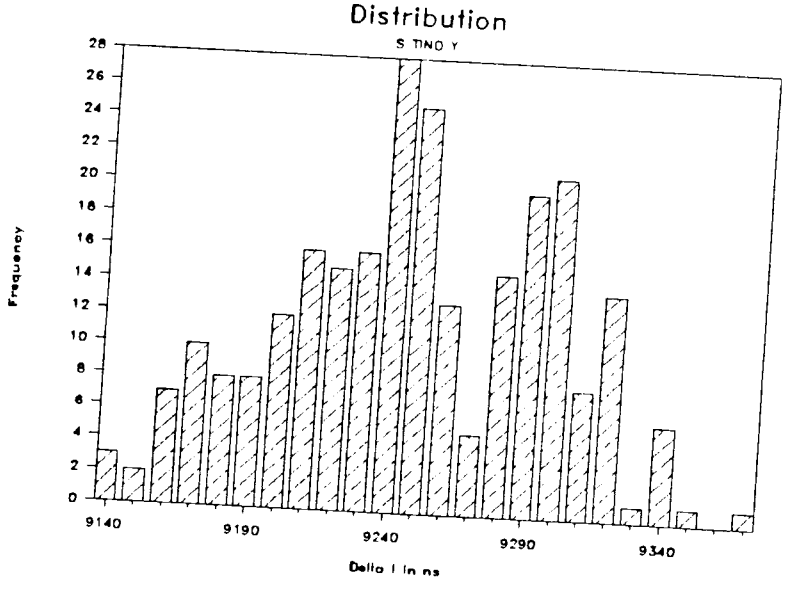
Distribution
S TIND Y
Frequency
28
26
24
22
20
18
16
14
12
10
8
6
4
2
0
9140
9190
9240
9290
9340
Delta t in ns

Appendix VII:

Monthly Means

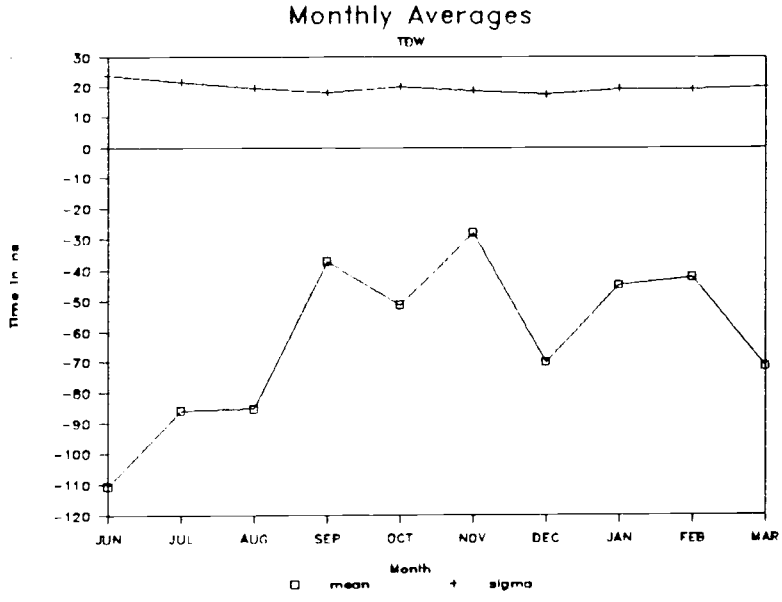

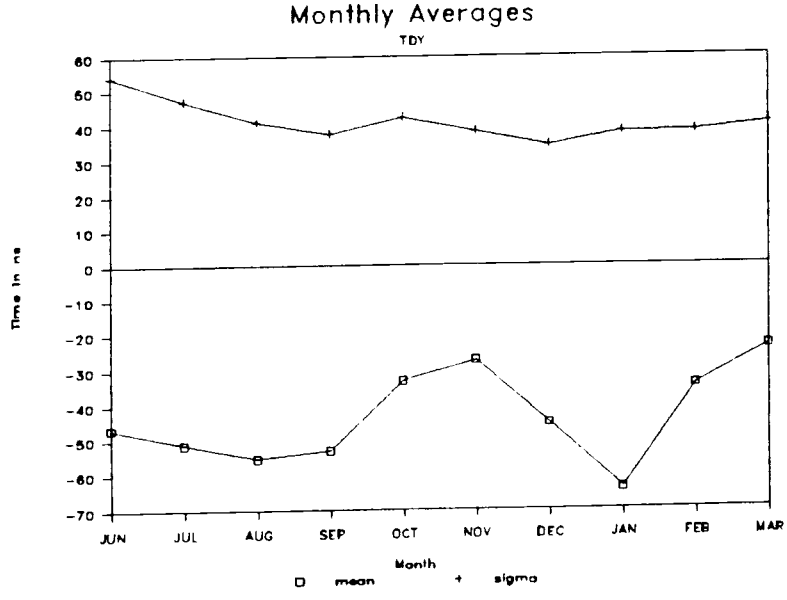

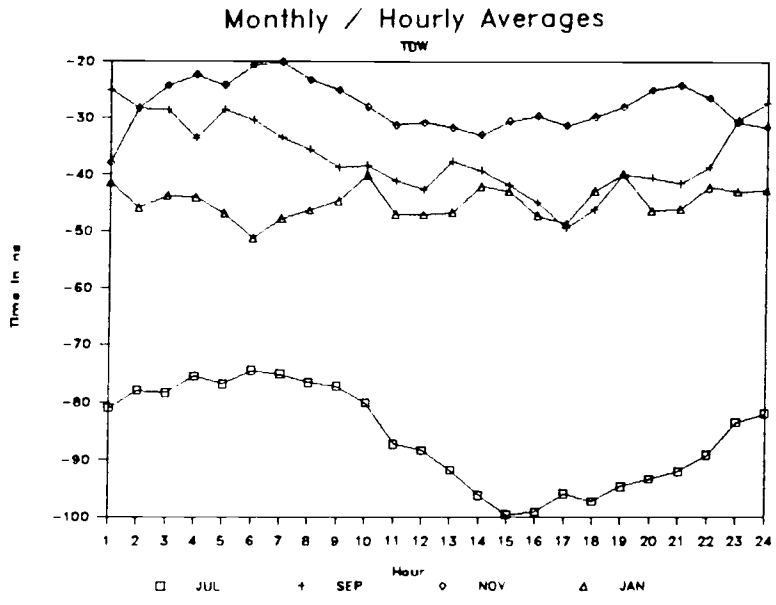
Monthly / Hourly Averages
TDW
Time in ns
-20
-30
-40
-50
-60
-70
-80
-90
-100
1 2 3 4 5 6 7 8 9 10 11 12 13 14 15 16 17 18 19 20 21 22 23 24
Hour
JUL
SEP
NOV
JAN

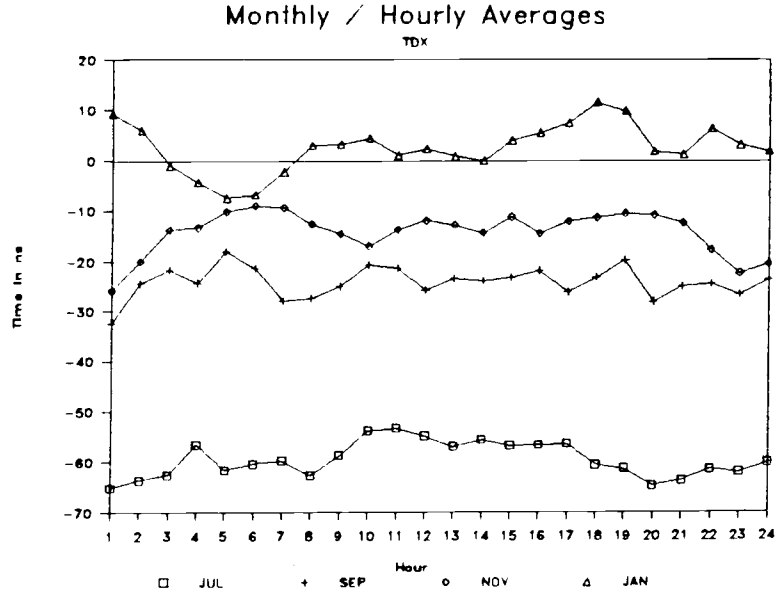
Monthly / Hourly Averages
TDX
Time in ns
20
10
0
-10
-20
-30
-40
-50
-60
-70
1 2 3 4 5 6 7 8 9 10 11 12 13 14 15 16 17 18 19 20 21 22 23 24
Hour
JUL
SEP
NOV
JAN

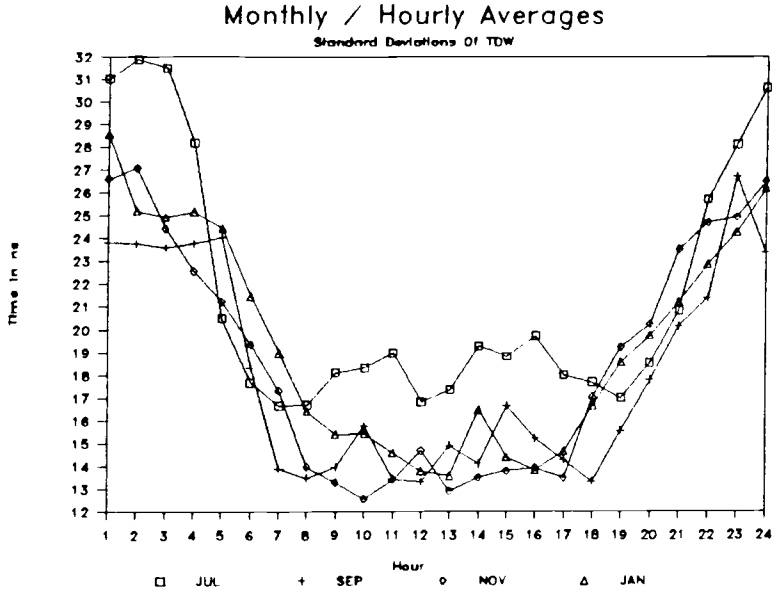
Monthly / Hourly Averages
Standard Deviations Of TDW
Time in ns
Hour
JUL
SEP
NOV
JAN

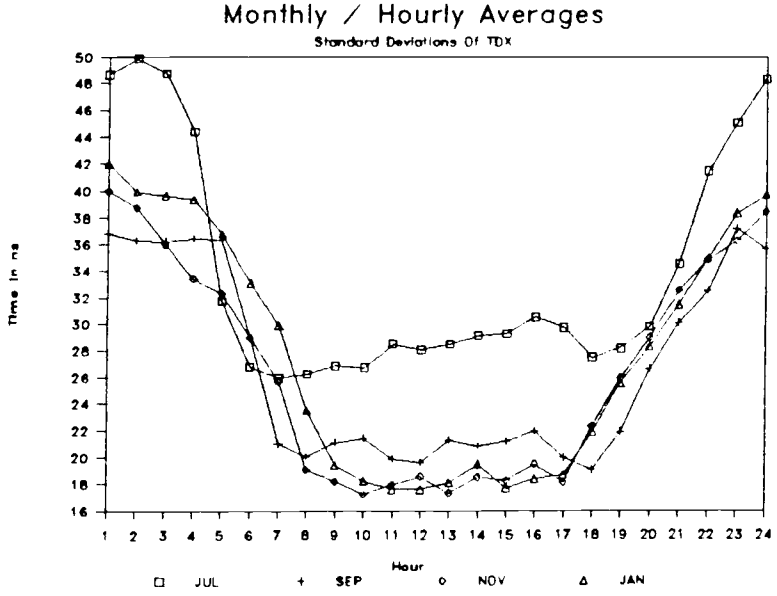
Monthly / Hourly Averages
Standard Deviations Of TDX
Time in ns
Hour
JUL
SEP
NOV
JAN

Appendix VIII:

TD Autocorrelations

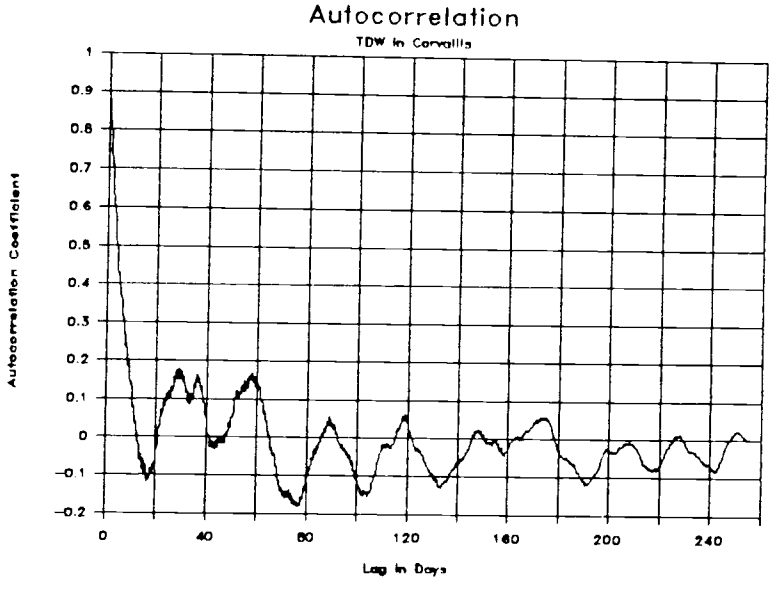

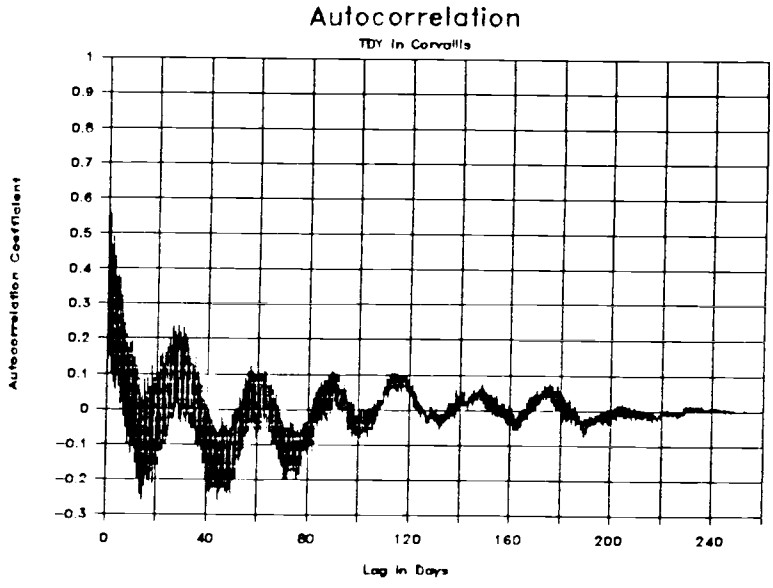
Autocorrelation
TDY in Corvallis
Autocorrelation Coefficient
1
0.9
0.8
0.7
0.6
0.5
0.4
0.3
0.2
0.1
0
-0.1
-0.2
-0.3
0
40
80
120
160
200
240
Lag in Days

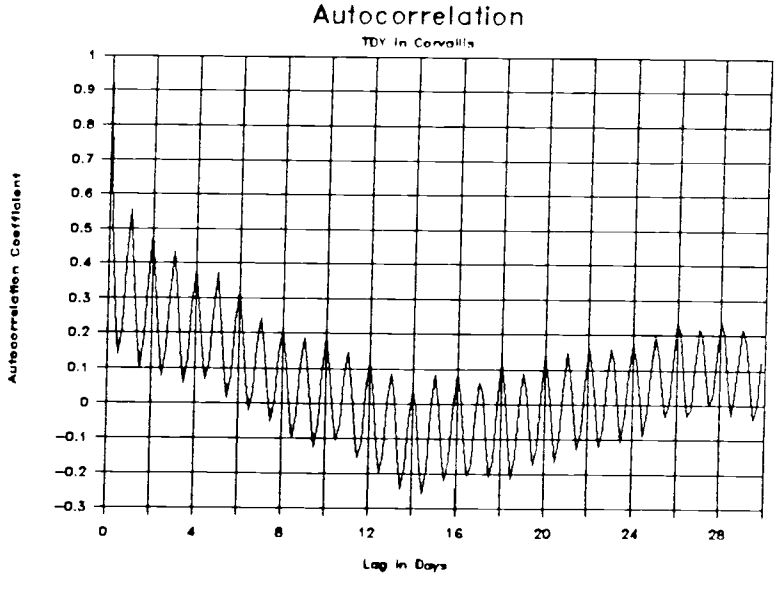
Autocorrelation
TDY in Corvallis
Autocorrelation Coefficient
1
0.9
0.8
0.7
0.6
0.5
0.4
0.3
0.2
0.1
0
-0.1
-0.2
-0.3
0
4
8
12
16
20
24
28
Lag in Days

Appendix IX:

TD Power Spectra

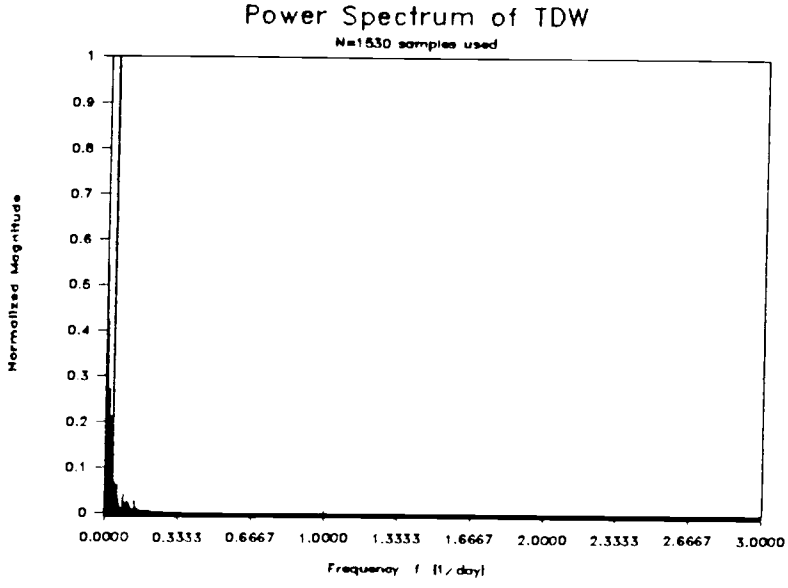

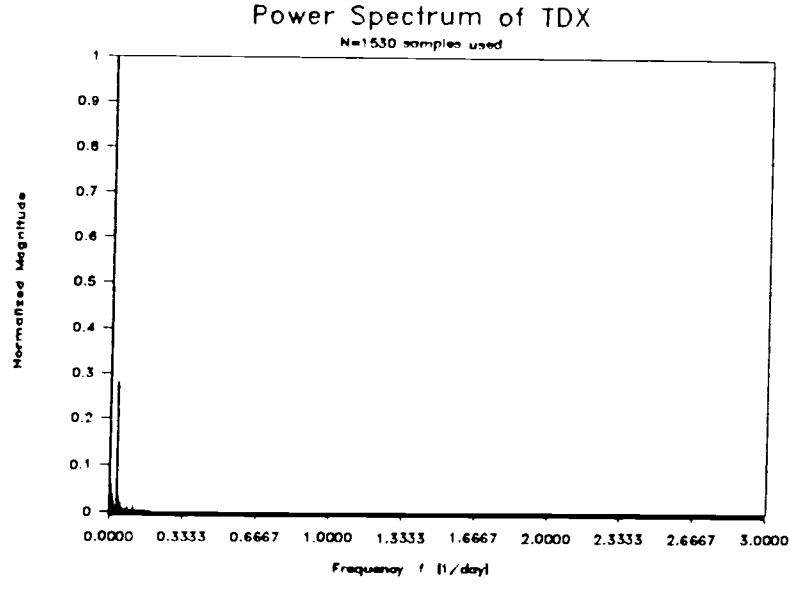

Appendix X:

TD Sample Autocorrelations

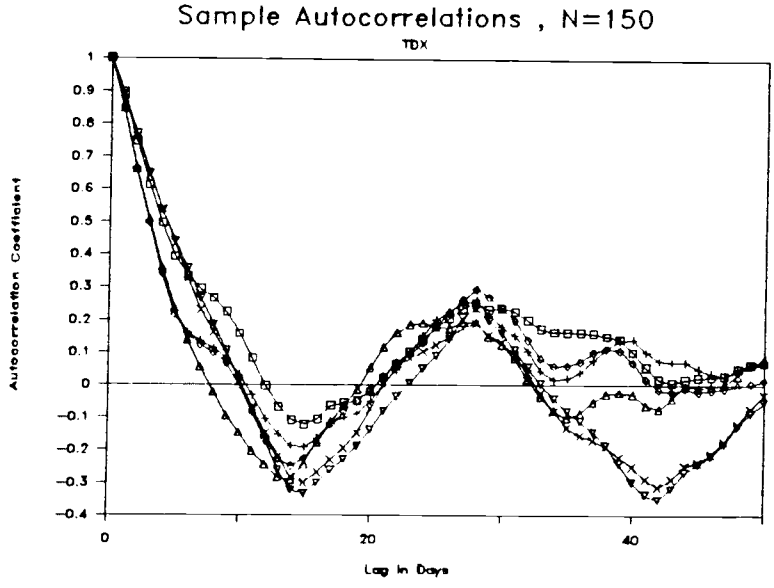

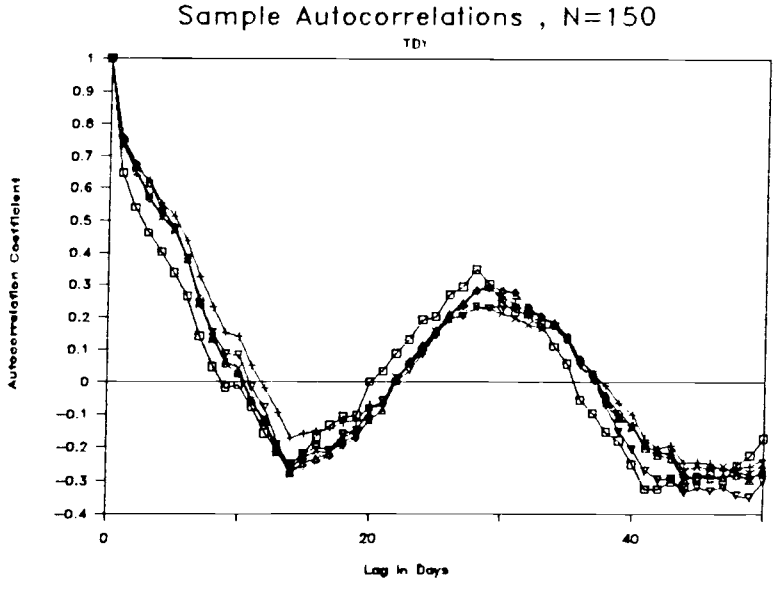

Appendix XI:

Weather Data Plots

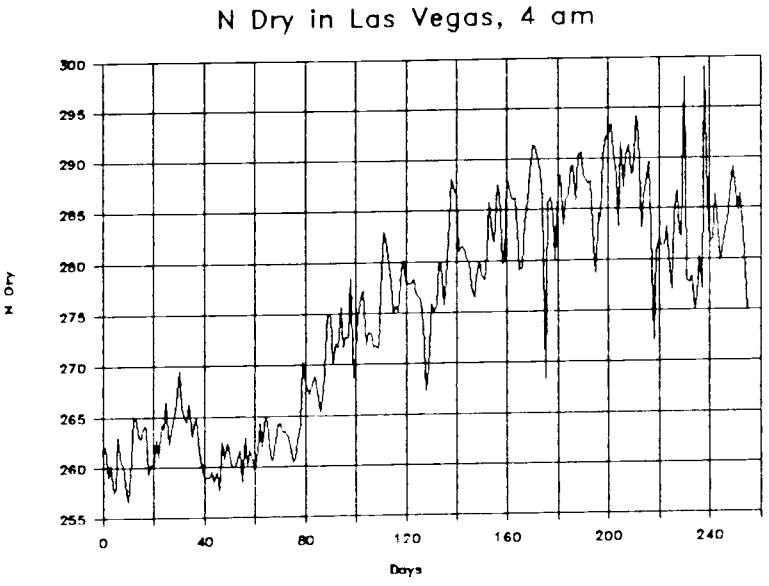

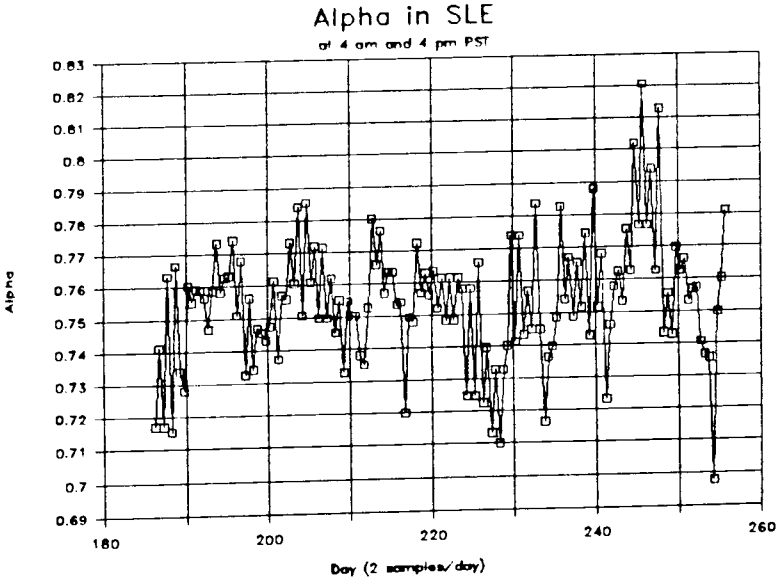

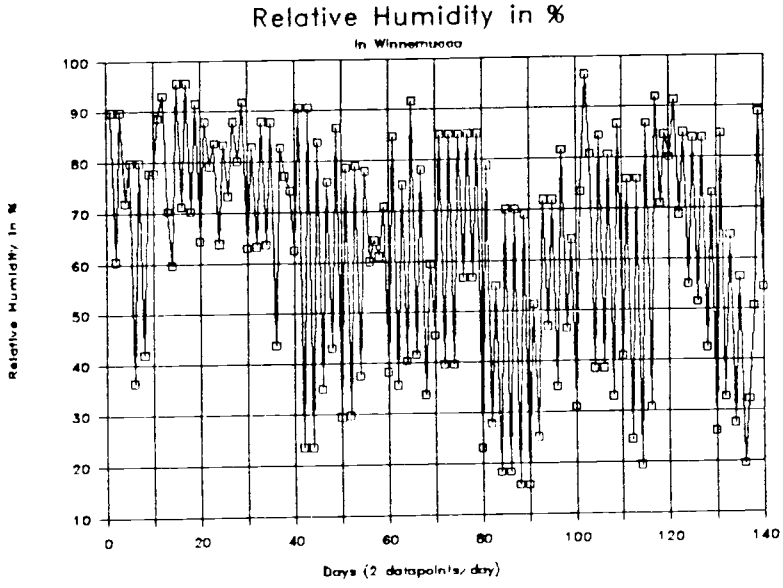
Relative Humidity in %
In Winnemucca
Relative Humidity in %
100
90
80
70
60
50
40
30
20
10
0
20
40
60
80
100
120
140
Days (2 datapoints/day)

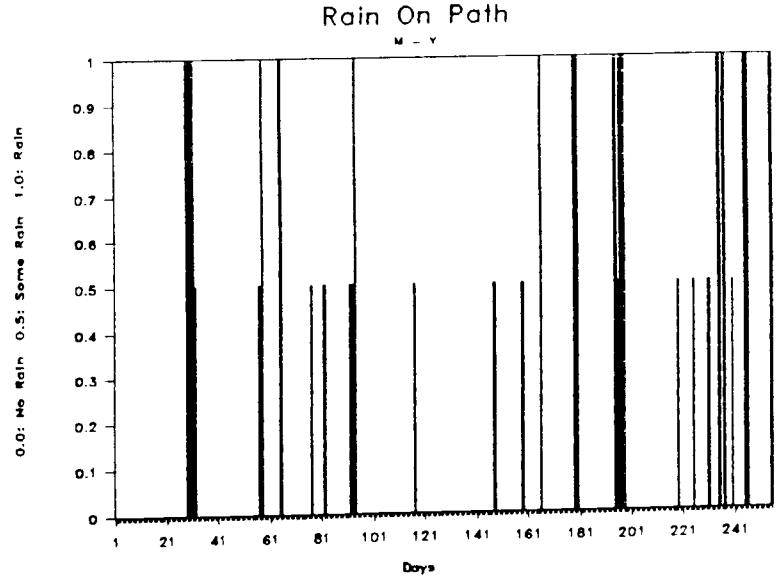
Rain On Path
M - Y
0.0: No Rain 0.5: Some Rain 1.0: Rain
1
0.9
0.8
0.7
0.6
0.5
0.4
0.3
0.2
0.1
0
1
21
41
61
81
101
121
141
161
181
201
221
241
Days

Appendix XII:

Weather Data: Autocorrelations and Power Spectra

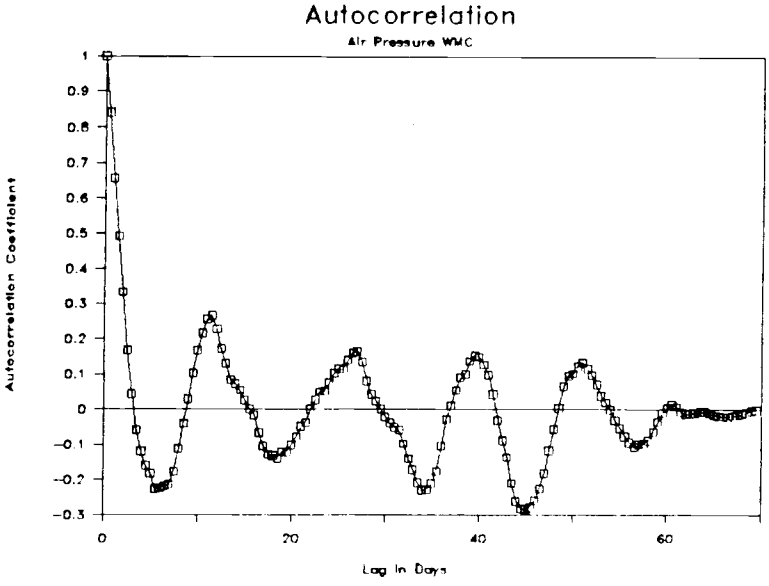

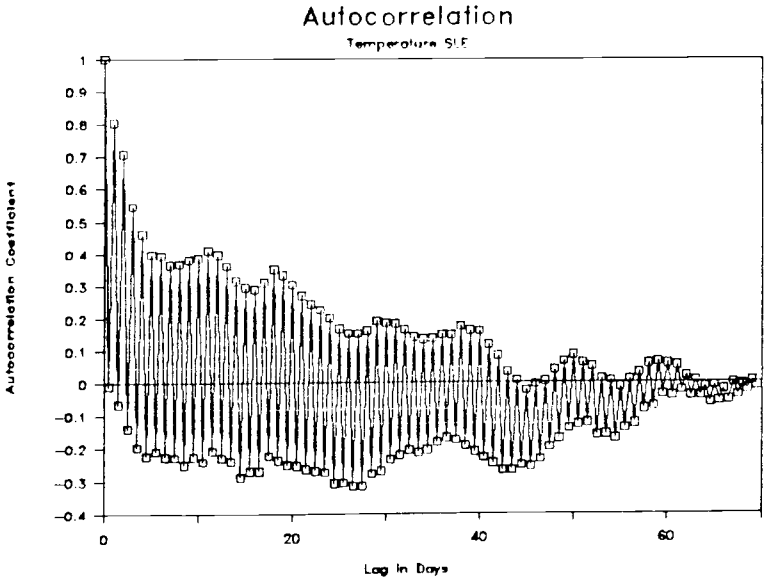

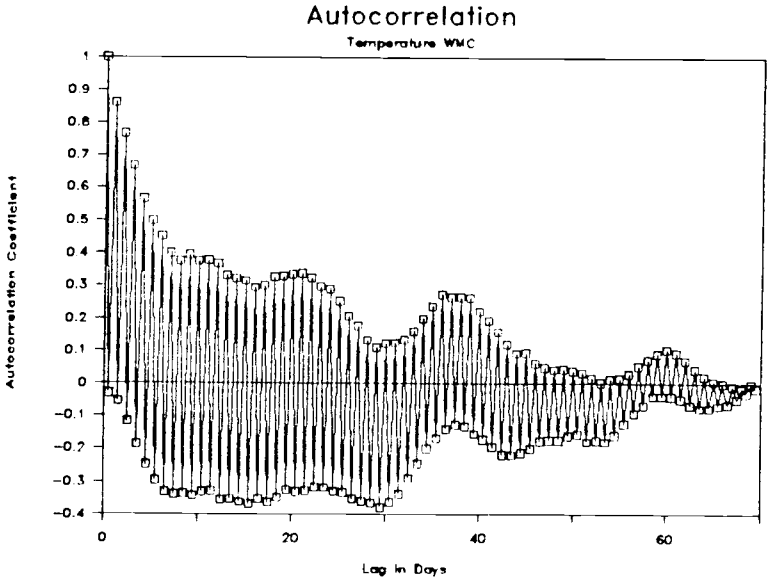
Autocorrelation
Temperature WMC
Autocorrelation Coefficient
1
0.9
0.8
0.7
0.6
0.5
0.4
0.3
0.2
0.1
0
-0.1
-0.2
-0.3
-0.4
0
20
40
60
Lag in Days

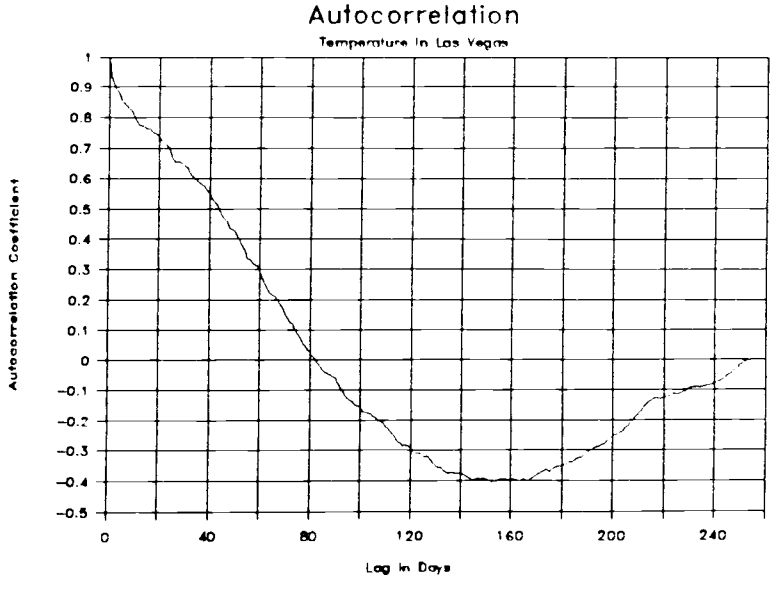
Autocorrelation
Temperature in Las Vegas
Autocorrelation Coefficient
1
0.9
0.8
0.7
0.6
0.5
0.4
0.3
0.2
0.1
0
-0.1
-0.2
-0.3
-0.4
-0.5
0
40
80
120
160
200
240
Lag in Days

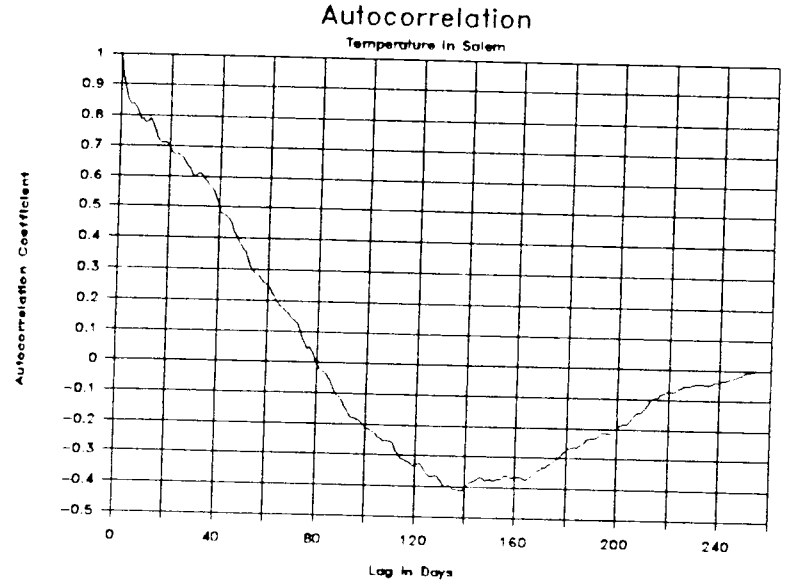
Autocorrelation
Temperature in Salem
Autocorrelation Coefficient
1
0.9
0.8
0.7
0.6
0.5
0.4
0.3
0.2
0.1
0
-0.1
-0.2
-0.3
-0.4
-0.5
0
40
80
120
160
200
240
Lag in Days

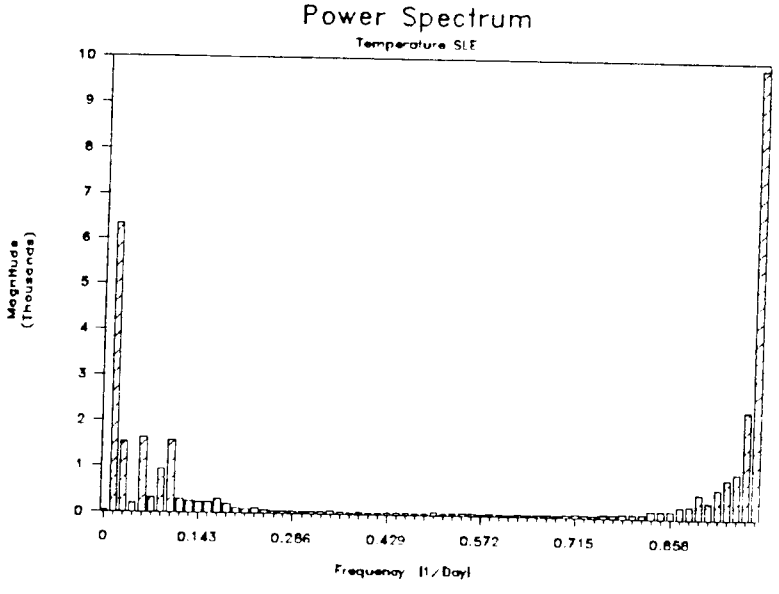
Power Spectrum
Temperature SLE
Magnitude (Thousands)
10
9
8
7
6
5
4
3
2
1
0
0
0.143
0.286
0.429
0.572
0.715
0.858
Frequency (1/Day)

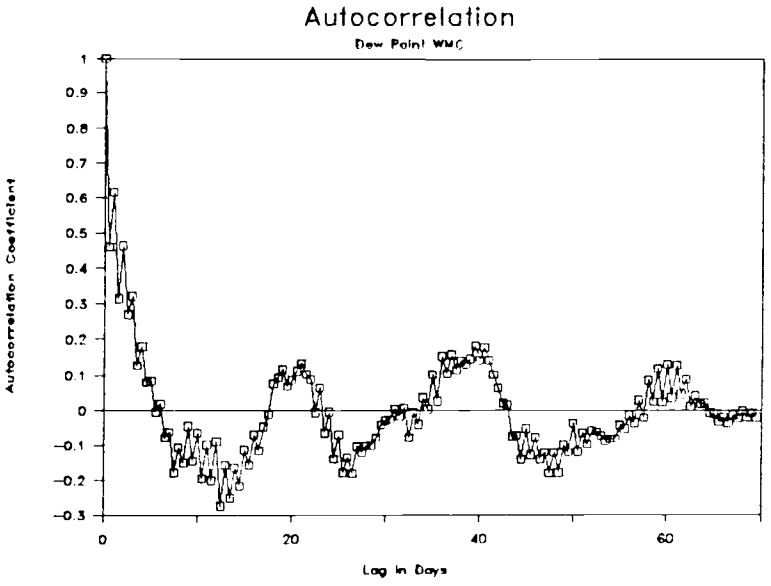
Autocorrelation
Dew Point WMC
Autocorrelation Coefficient
1
0.9
0.8
0.7
0.6
0.5
0.4
0.3
0.2
0.1
0
-0.1
-0.2
-0.3
0
20
40
60
Lag in Days

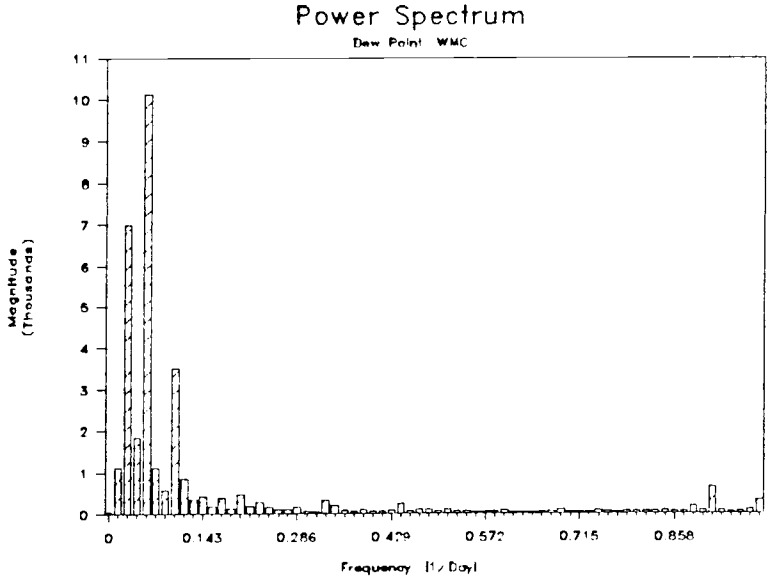
Power Spectrum
Dew Point WMC
Magnitude (Thousands)
11
10
9
8
7
6
5
4
3
2
1
0
0
0.143
0.286
0.429
0.572
0.715
0.858
Frequency (1/Day)

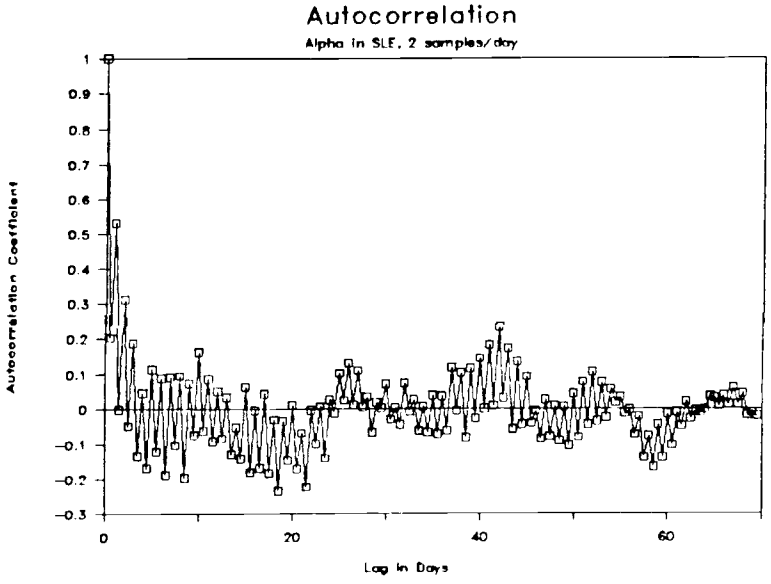
Autocorrelation
Alpha in SLE, 2 samples/day
Autocorrelation Coefficient
1
0.9
0.8
0.7
0.6
0.5
0.4
0.3
0.2
0.1
0
-0.1
-0.2
-0.3
0
20
40
60
Lag in Days

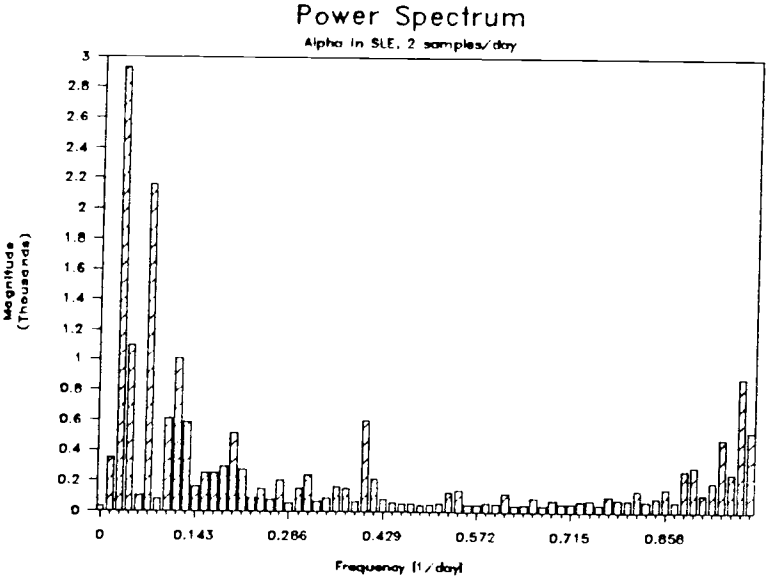
Power Spectrum
Alpha in SLE, 2 samples/day
Magnitude (Thousands)
3
2.8
2.6
2.4
2.2
2
1.8
1.6
1.4
1.2
1
0.8
0.6
0.4
0.2
0
0
0.143
0.286
0.429
0.572
0.715
0.858
Frequency (1/day)

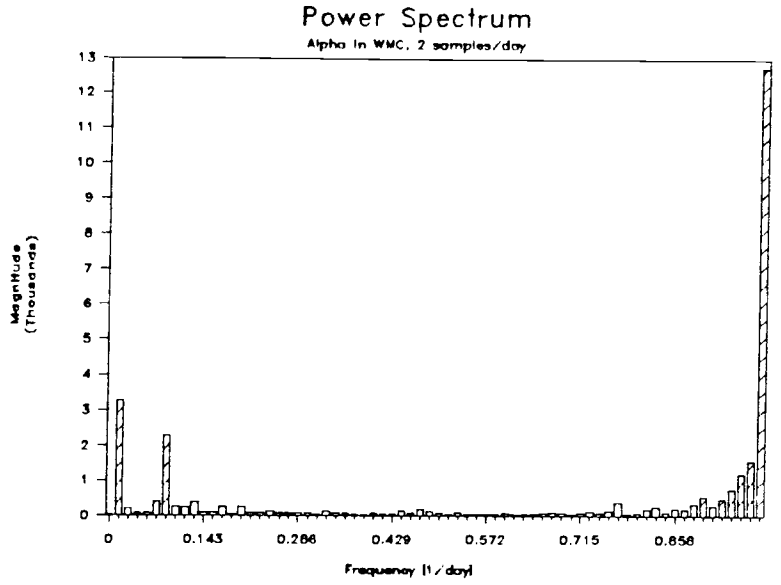
Power Spectrum
Alpha in WMC, 2 samples/day
Magnitude (Thousands)
13
12
11
10
9
8
7
6
5
4
3
2
1
0
0
0.143
0.286
0.429
0.572
0.715
0.858
Frequency (1/day)

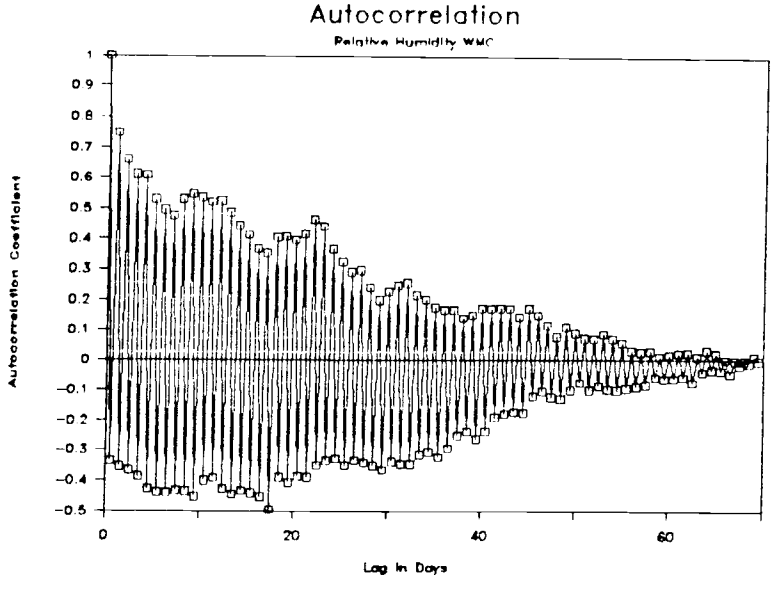
Autocorrelation
Relative Humidity WMC
Autocorrelation Coefficient
1
0.9
0.8
0.7
0.6
0.5
0.4
0.3
0.2
0.1
0
-0.1
-0.2
-0.3
-0.4
-0.5
0
20
40
60
Lag in Days

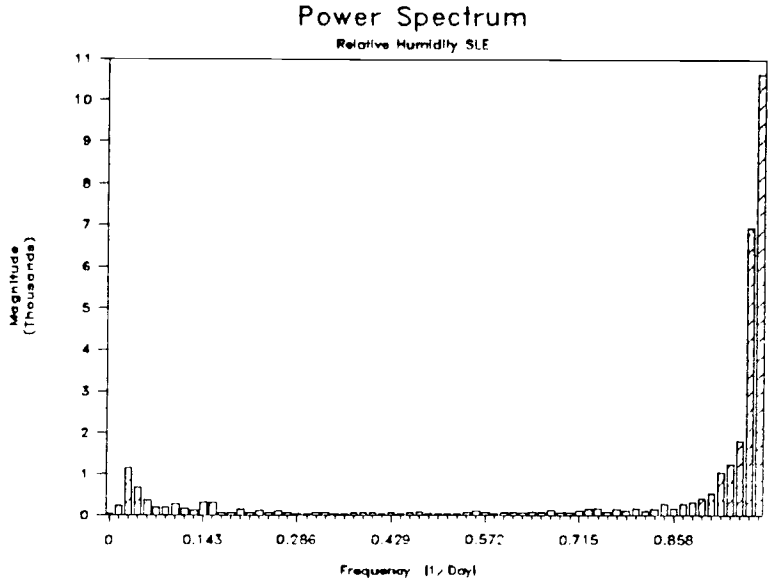
Power Spectrum
Relative Humidity SLE
Magnitude (Thousands)
11
10
9
8
7
6
5
4
3
2
1
0
0
0.143
0.286
0.429
0.572
0.715
0.858
Frequency (1 / Day)

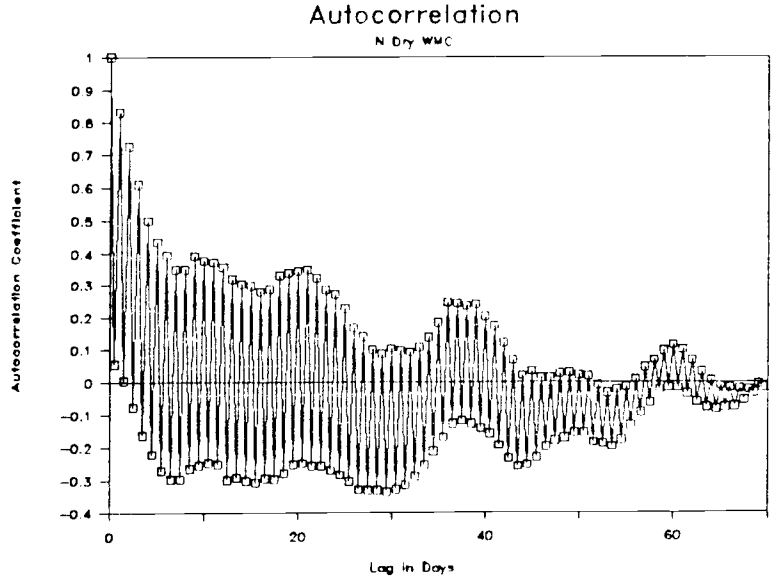
Autocorrelation
N Dry WMC
Autocorrelation Coefficient
1
0.9
0.8
0.7
0.6
0.5
0.4
0.3
0.2
0.1
0
-0.1
-0.2
-0.3
-0.4
0
20
40
60
Lag in Days

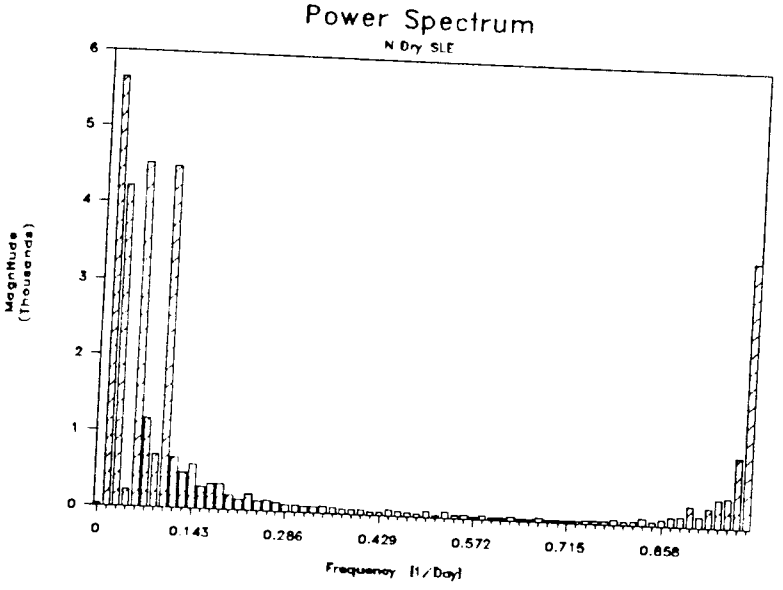
Power Spectrum
N Dry SLE
Magnitude (Thousands)
0
1
2
3
4
5
6
0
0.143
0.286
0.429
0.572
0.715
0.858
Frequency (1/Day)

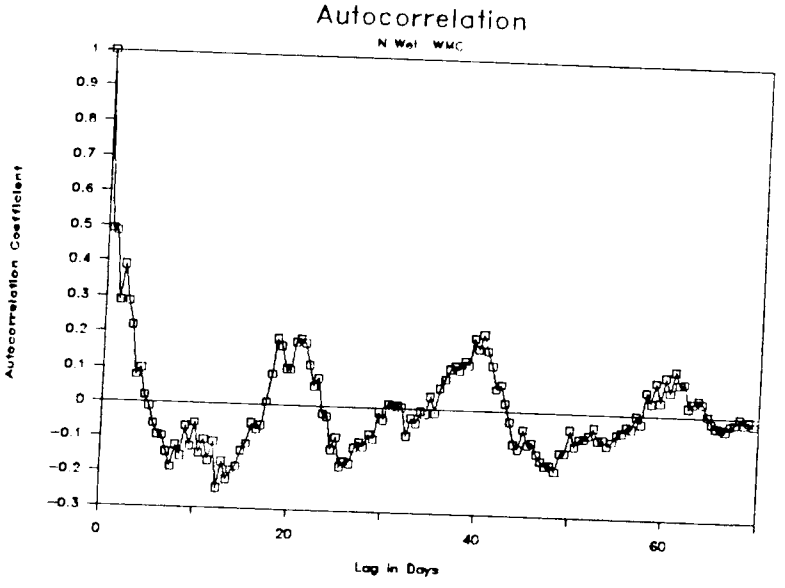
Autocorrelation
N Wet WMC
Autocorrelation Coefficient
1
0.9
0.8
0.7
0.6
0.5
0.4
0.3
0.2
0.1
0
-0.1
-0.2
-0.3
0
20
40
60
Lag in Days

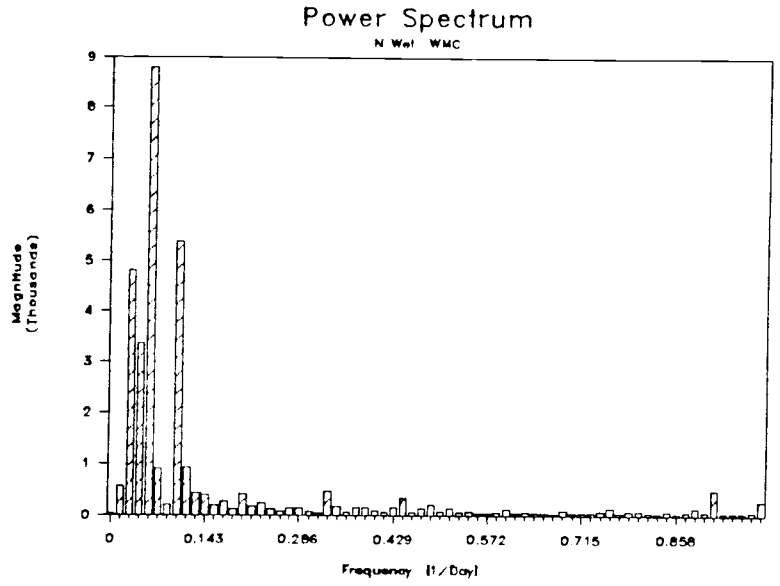
Power Spectrum
N Wat WMC
Magnitude (Thousands)
0
1
2
3
4
5
6
7
8
9
0
0.143
0.286
0.429
0.572
0.715
0.858
Frequency (1/Day)

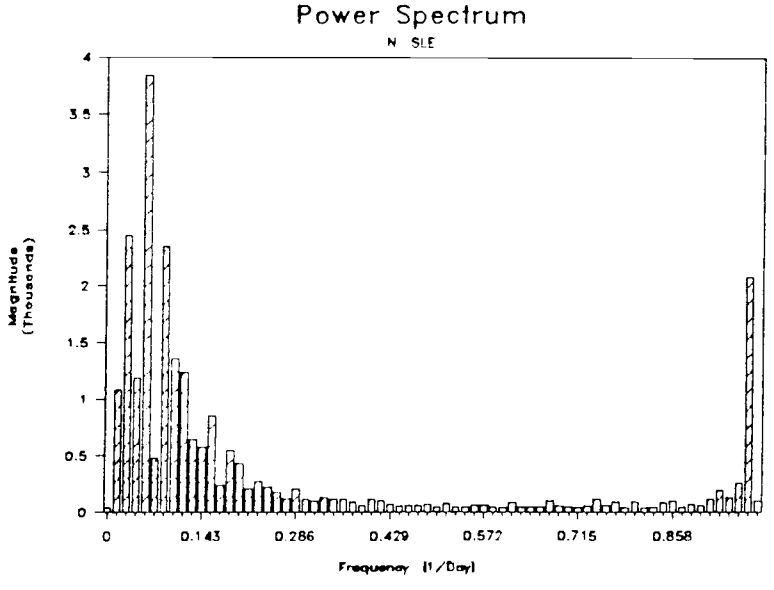
Power Spectrum
N SLE
Magnitude (Thousands)
0
0.5
1
1.5
2
2.5
3
3.5
4
0
0.143
0.286
0.429
0.572
0.715
0.858
Frequency (1/Day)

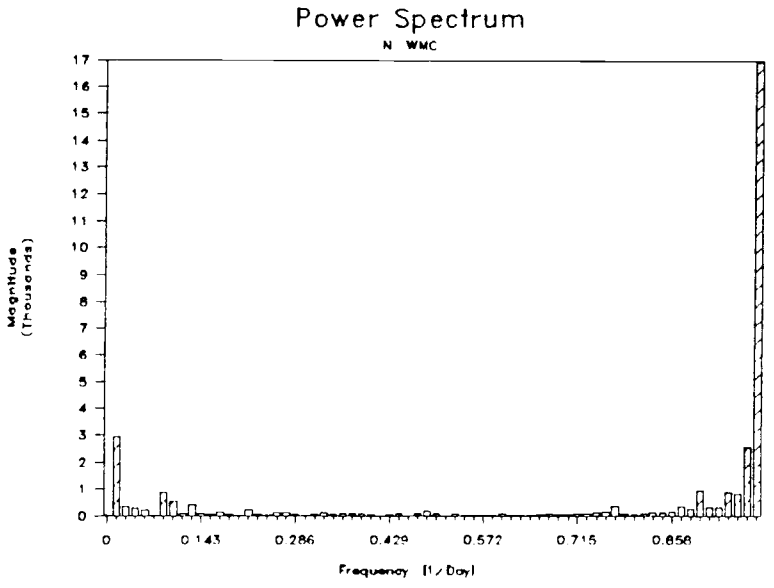
Power Spectrum
N WMC
Magnitude (Thousands)
17
16
15
14
13
12
11
10
9
8
7
6
5
4
3
2
1
0
0
0.143
0.286
0.429
0.572
0.715
0.858
Frequency (1 / Day)

Appendix XIII:

Transmitter Station Data and Power Spectra

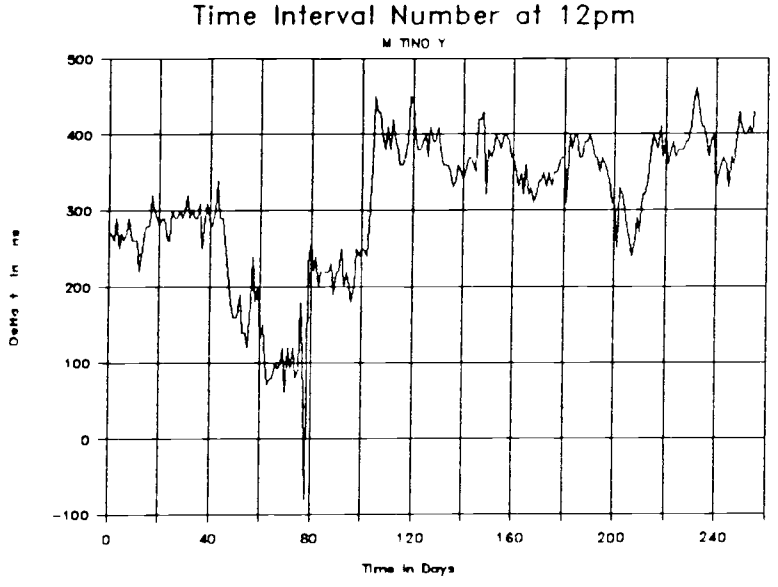

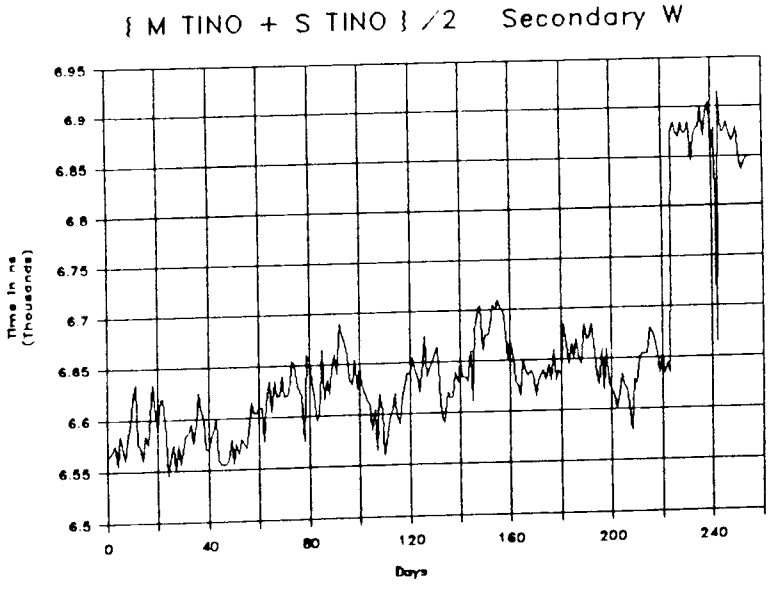

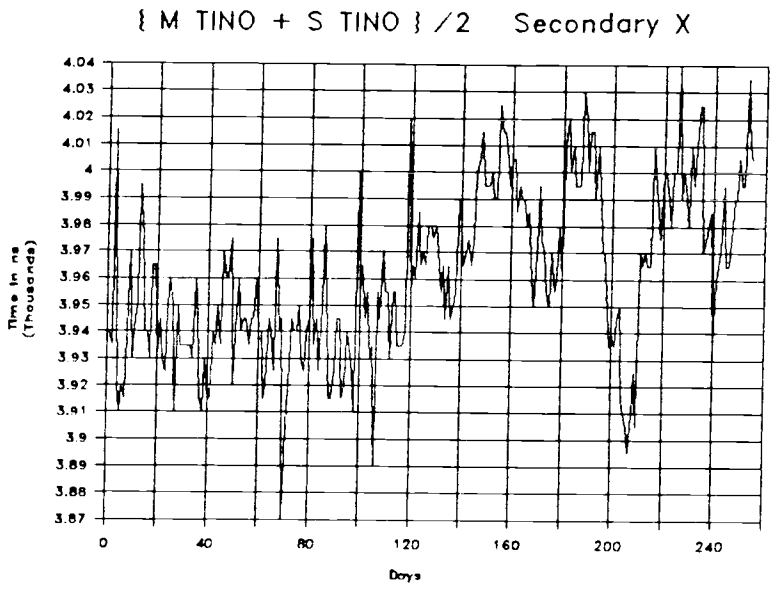
{ M TINO + S TINO } /2 Secondary X
Time in ns (Thousands)
4.04
4.03
4.02
4.01
4
3.99
3.98
3.97
3.96
3.95
3.94
3.93
3.92
3.91
3.9
3.89
3.88
3.87
0
40
80
120
160
200
240
Days

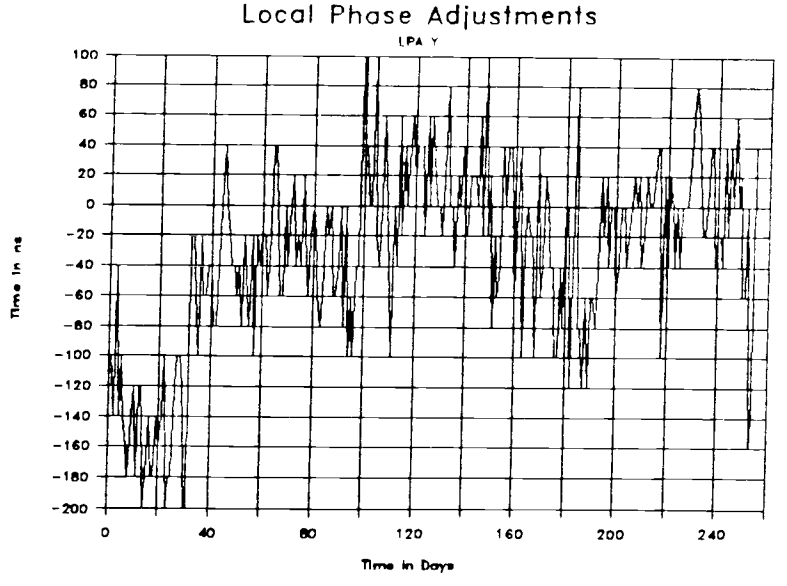
Local Phase Adjustments
LPA Y
Time in ns
100
80
60
40
20
0
-20
-40
-60
-80
-100
-120
-140
-160
-180
-200
0
40
80
120
160
200
240
Time in Days

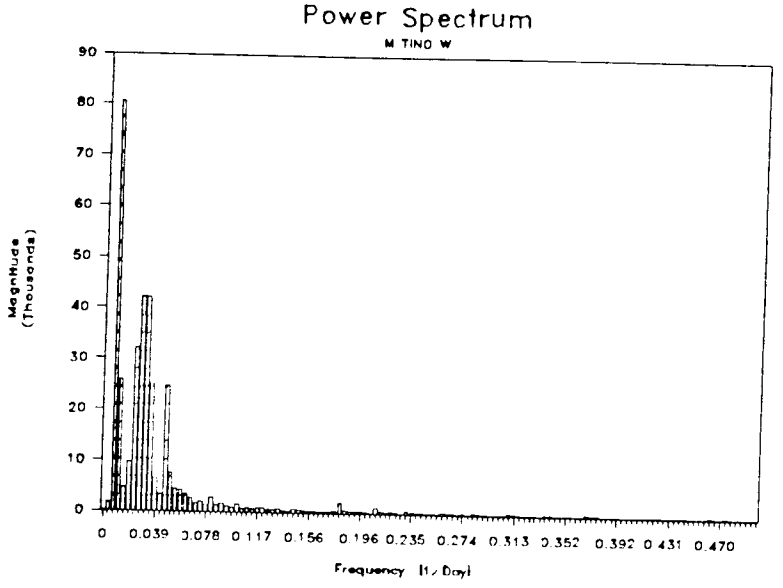
Power Spectrum
M TINO W
Magnitude (Thousands)
90
80
70
60
50
40
30
20
10
0
0 0.039 0.078 0.117 0.156 0.196 0.235 0.274 0.313 0.352 0.392 0.431 0.470
Frequency (1 / Day)

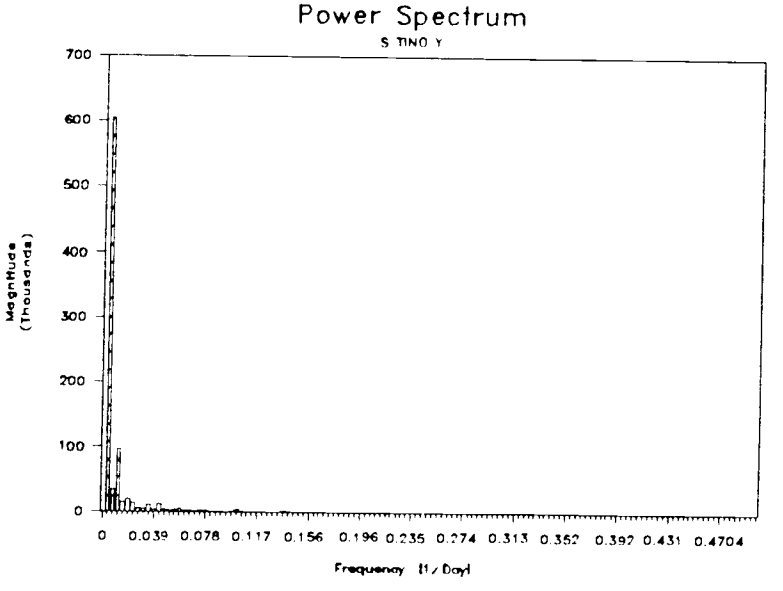
Power Spectrum
S TINO Y
Magnitude (Thousands)
700
600
500
400
300
200
100
0
0 0.039 0.078 0.117 0.156 0.196 0.235 0.274 0.313 0.352 0.392 0.431 0.4704
Frequency (1 / Day)

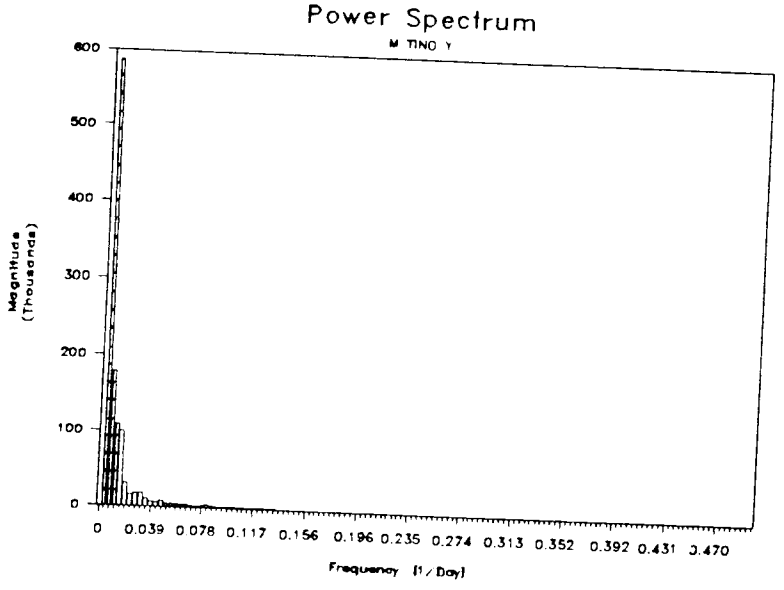
Power Spectrum
M TINO Y
600
500
400
300
200
100
0
Magnitude (Thousands)
0
0.039
0.078
0.117
0.156
0.196
0.235
0.274
0.313
0.352
0.392
0.431
0.470
Frequency (1 / Day)

Appendix XIV:

Transmitter Switching Times and Power Spectra

TDW and Switching Times of Secondary W

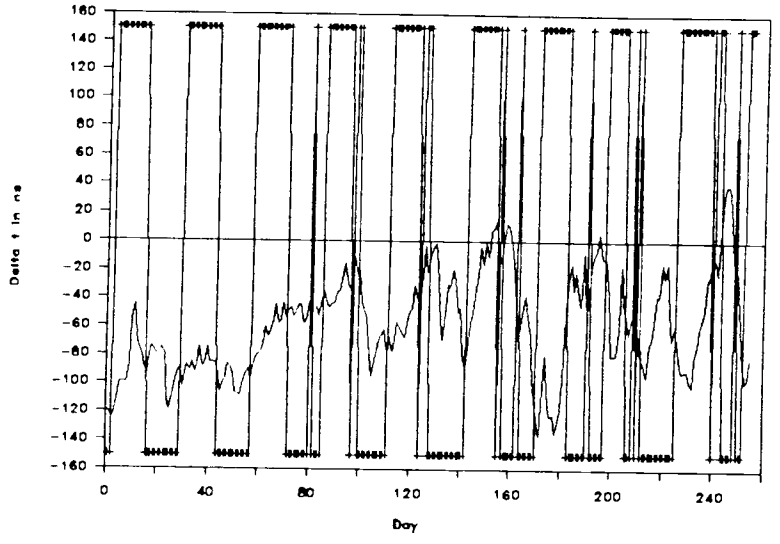

TDX and Master Transmitter Switching Times

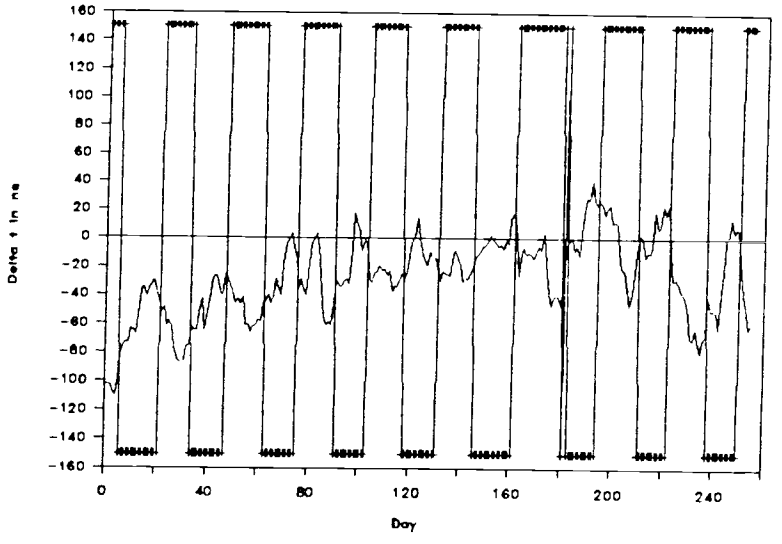

TDX and Switching Times of Secondary X

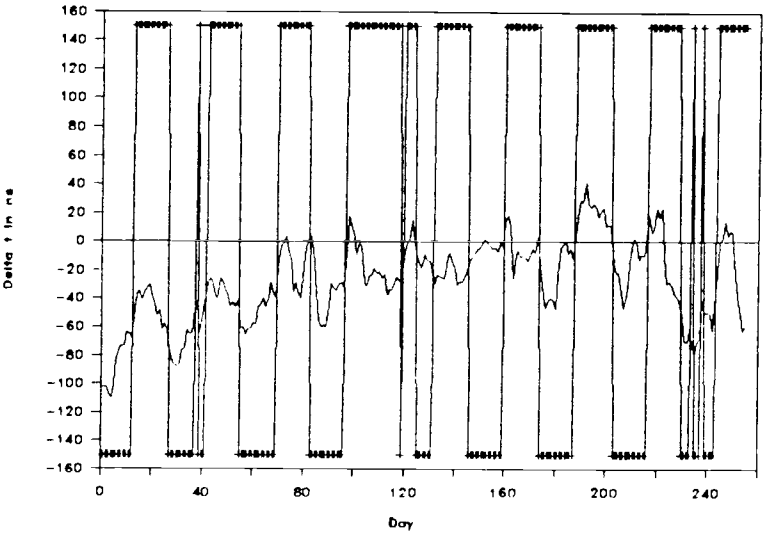

TDY and Master Transmitter Switching Times

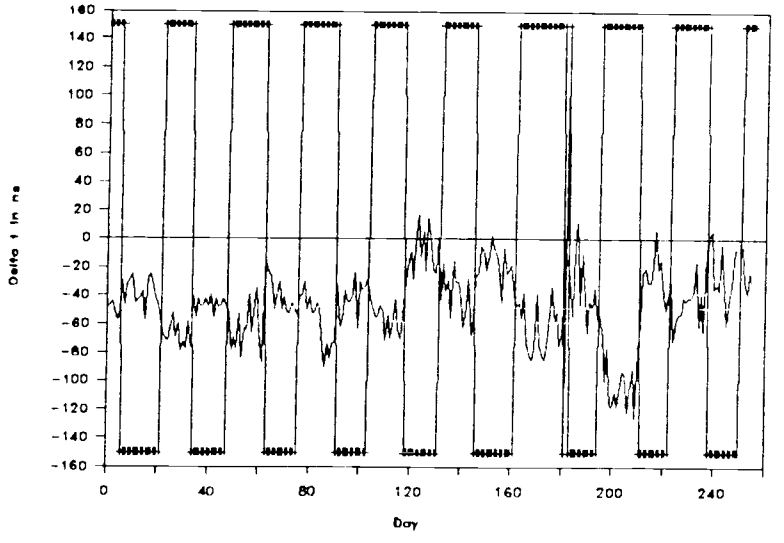

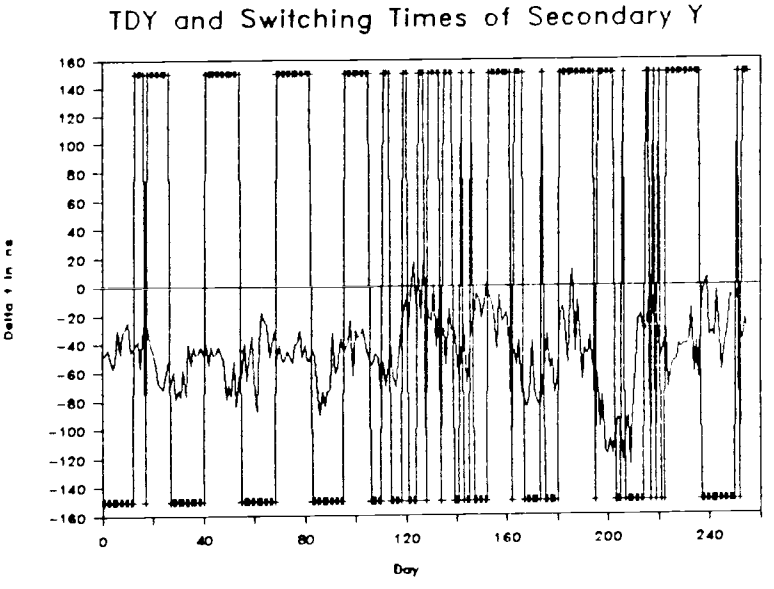
TDY and Switching Times of Secondary Y
Delta t in ns
160
140
120
100
80
60
40
20
0
-20
-40
-60
-80
-100
-120
-140
-160
0
40
80
120
160
200
240
Day

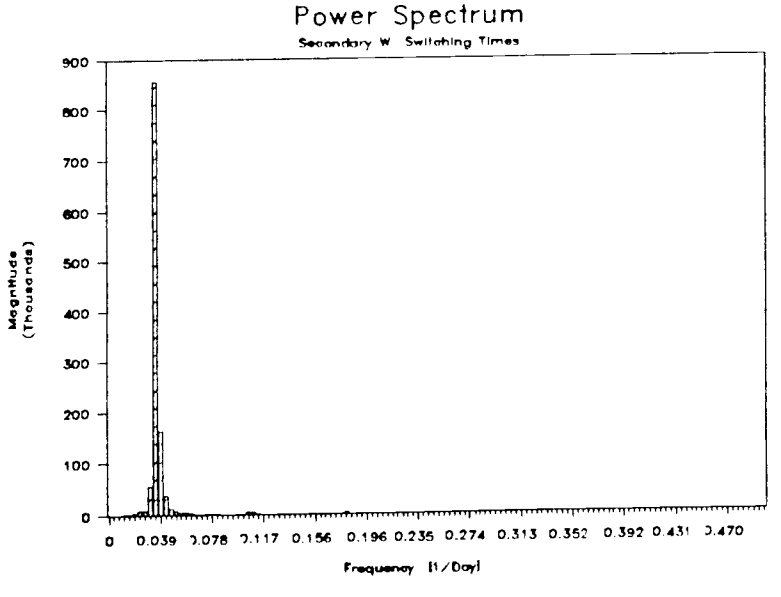
Power Spectrum
Secondary W Switching Times
Magnitude (Thousands)
900
800
700
600
500
400
300
200
100
0
0
0.039
0.078
0.117
0.156
0.196
0.235
0.274
0.313
0.352
0.392
0.431
0.470
Frequency (1/Day)

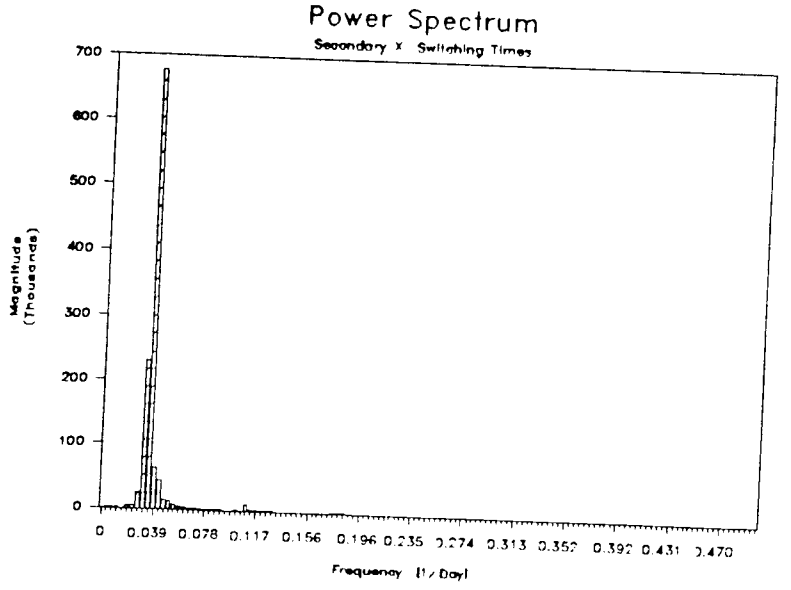
Power Spectrum
Secondary X Switching Times
Magnitude (Thousands)
700
600
500
400
300
200
100
0
0 0.039 0.078 0.117 0.156 0.196 0.235 0.274 0.313 0.352 0.392 0.431 0.470
Frequency (1/Day)

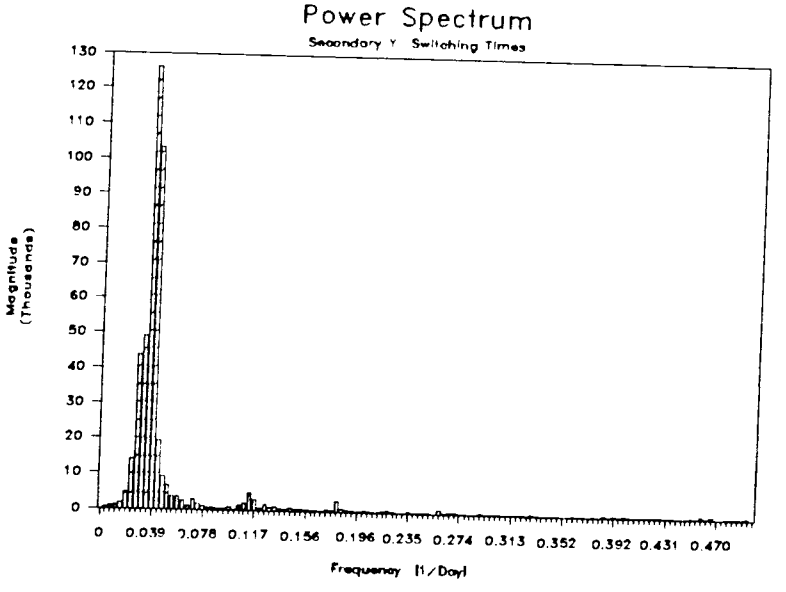
Power Spectrum
Secondary Y Switching Times
Magnitude (Thousands)
130
120
110
100
90
80
70
60
50
40
30
20
10
0
0 0.039 0.078 0.117 0.156 0.196 0.235 0.274 0.313 0.352 0.392 0.431 0.470
Frequency (1/Day)

Appendix XV:

Weather and TINO Data: Sample Autocorrelations

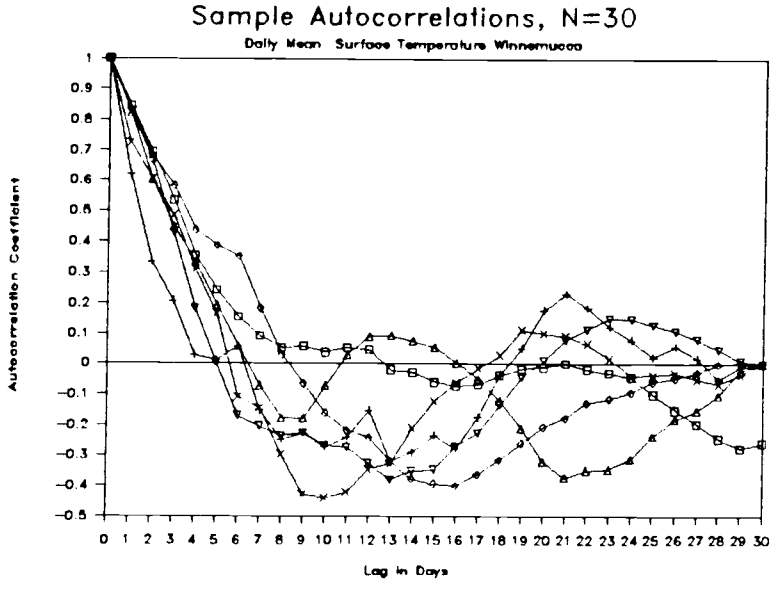

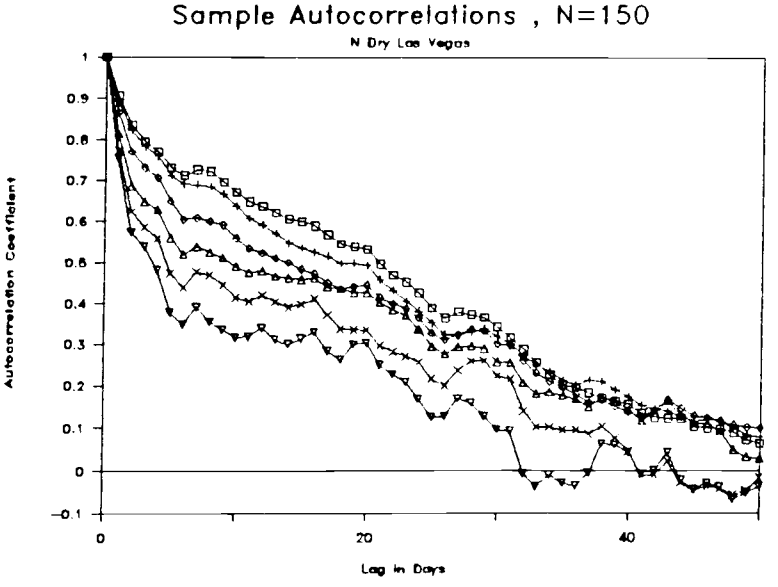

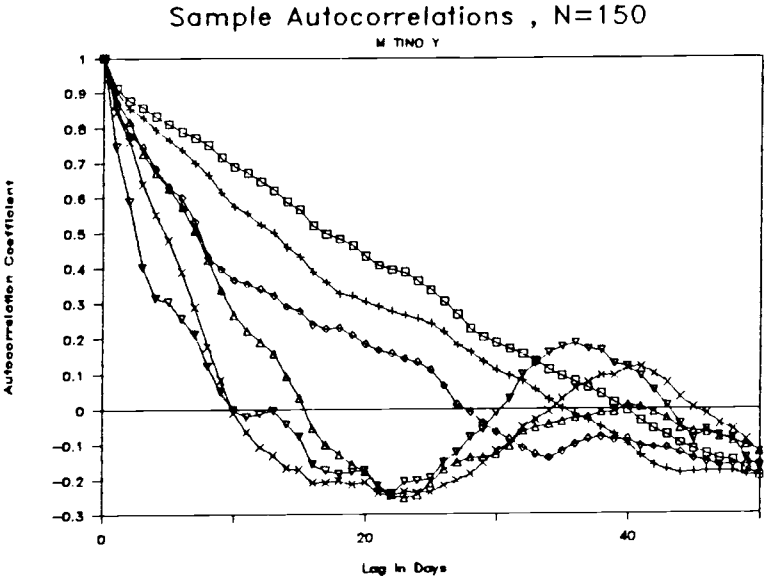
Sample Autocorrelations , N=150
M TINO Y
Autocorrelation Coefficient
1
0.9
0.8
0.7
0.6
0.5
0.4
0.3
0.2
0.1
0
-0.1
-0.2
-0.3
0
20
40
Lag in Days

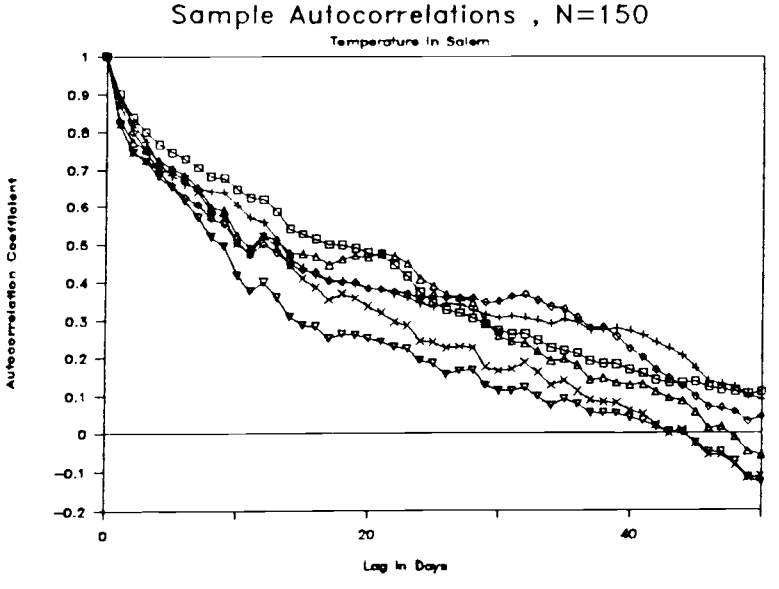
Sample Autocorrelations , N=150
Temperature in Salem
Autocorrelation Coefficient
1
0.9
0.8
0.7
0.6
0.5
0.4
0.3
0.2
0.1
0
-0.1
-0.2
0
20
40
Lag in Days

Appendix XVI:

Linear Predictions of CVs

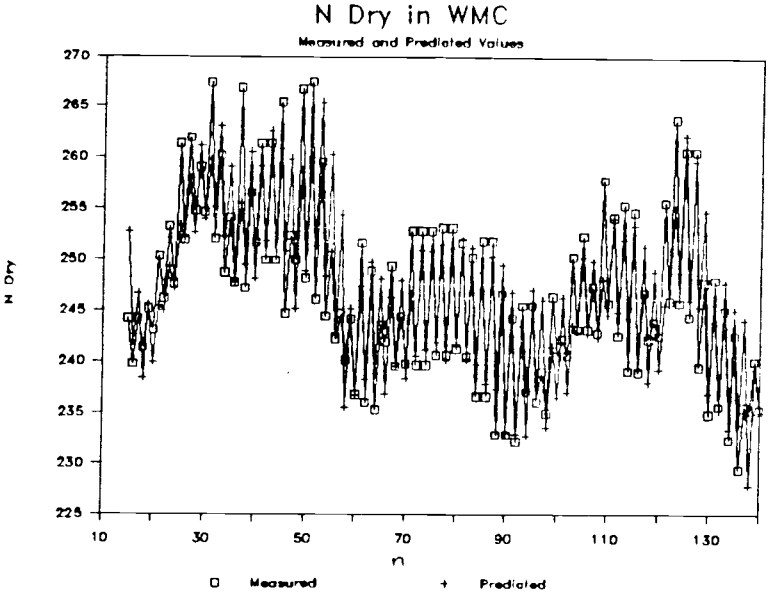

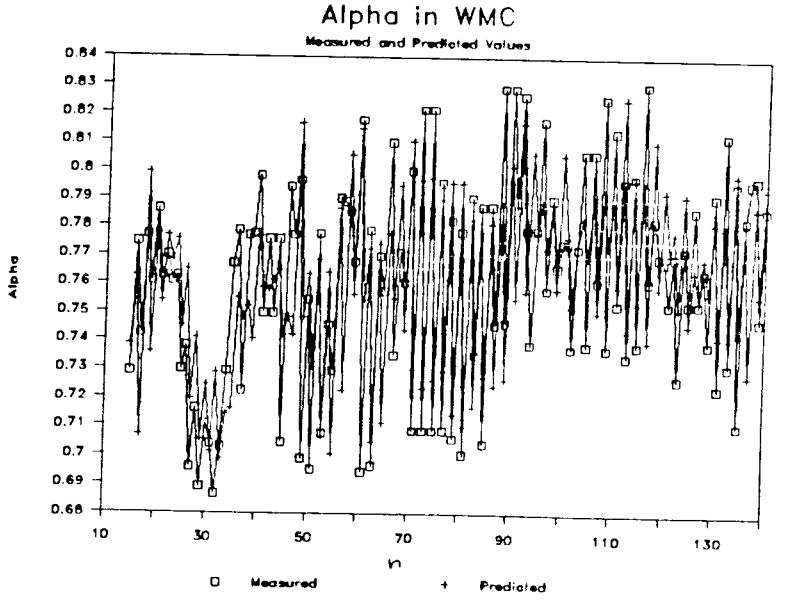

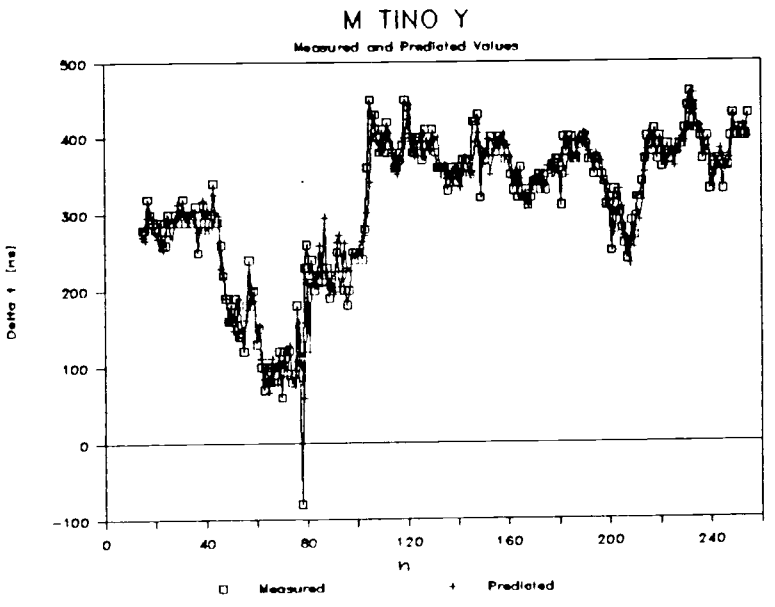
M TINO Y
Measured and Predicted Values
500
400
300
200
100
0
-100
Delta t [ns]
0
40
80
120
160
200
240
n
Measured
Predicted

Appendix XVII:

Residual TDs

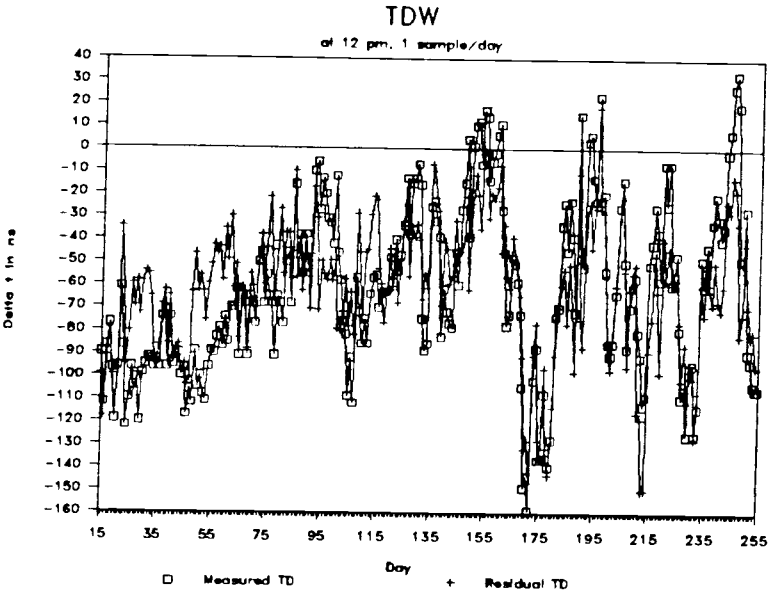

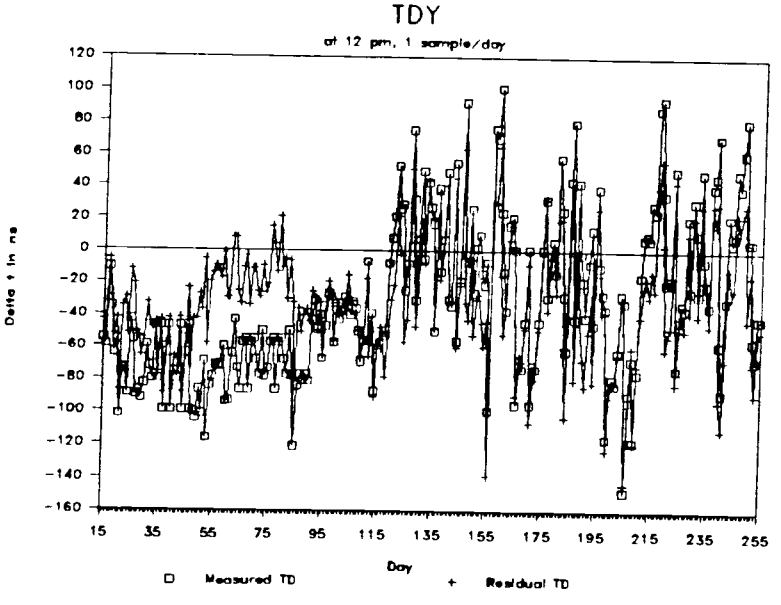

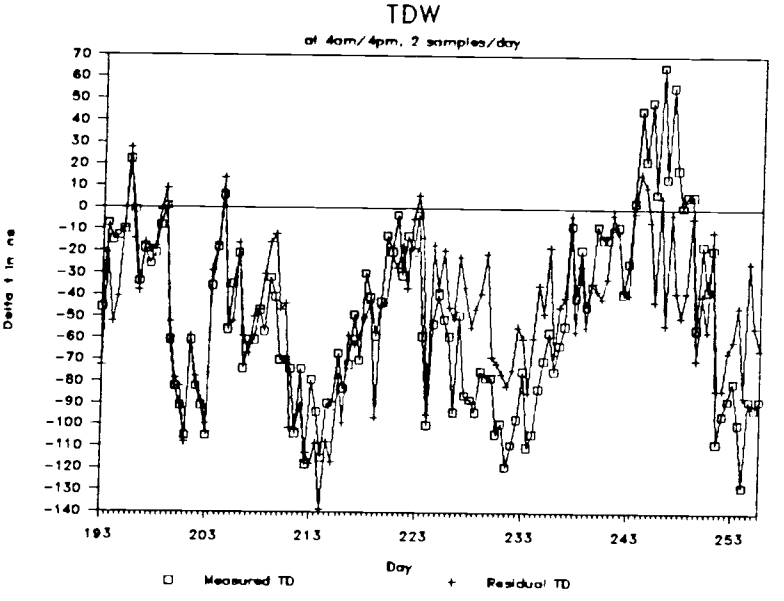
TDW
at 4am/4pm, 2 samples/day
Delta t in ns
70
60
50
40
30
20
10
0
-10
-20
-30
-40
-50
-60
-70
-80
-90
-100
-110
-120
-130
-140
193
203
213
223
233
243
253
Day
Measured TD
Residual TD

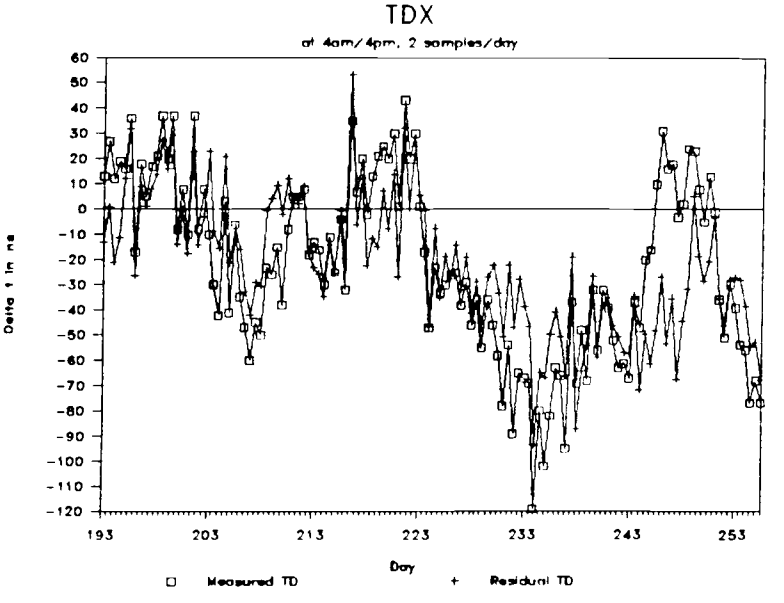
TDX
at 4am/4pm, 2 samples/day
Delta t in ns
60
50
40
30
20
10
0
-10
-20
-30
-40
-50
-60
-70
-80
-90
-100
-110
-120
193
203
213
223
233
243
253
Day
Measured TD
Residual TD

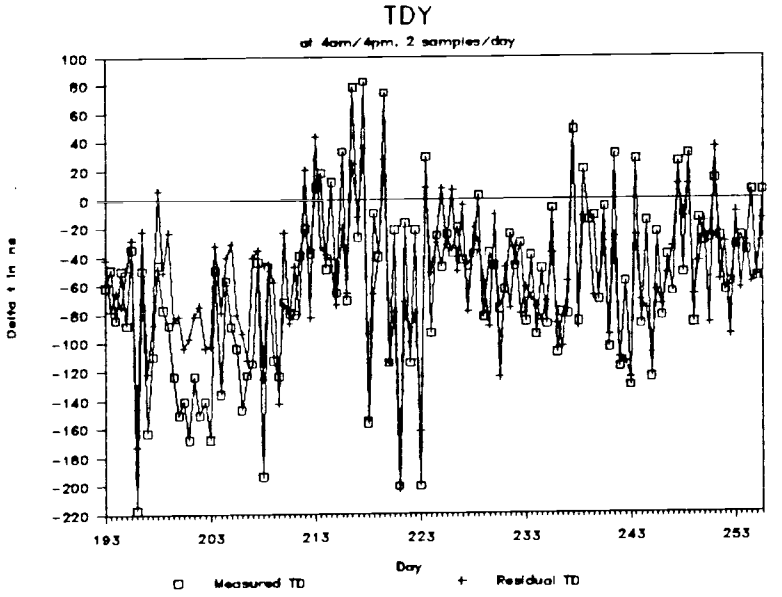
TDY
at 4am/4pm. 2 samples/day
Delta t in ns
100
80
60
40
20
0
-20
-40
-60
-80
-100
-120
-140
-160
-180
-200
-220
193
203
213
223
233
243
253
Day
Measured TD
Residual TD

Appendix XVIII:

Residual TDs: Autocorrelations and Power Spectra

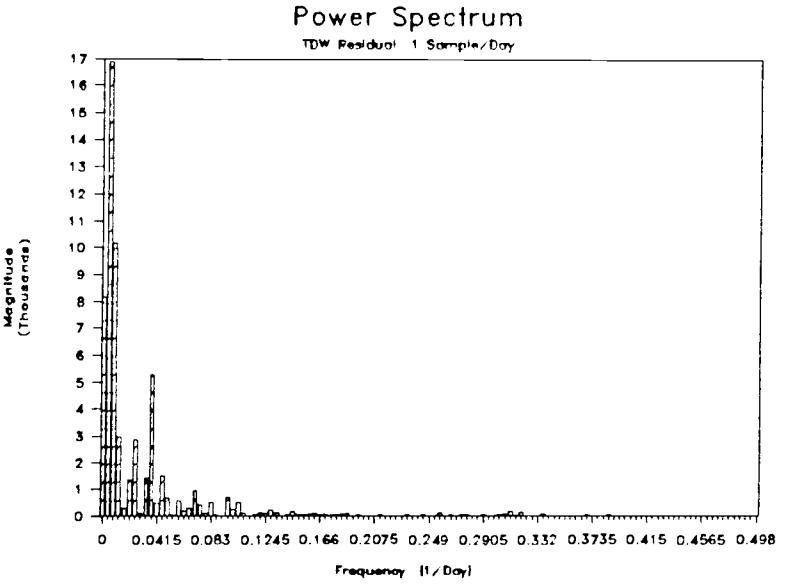

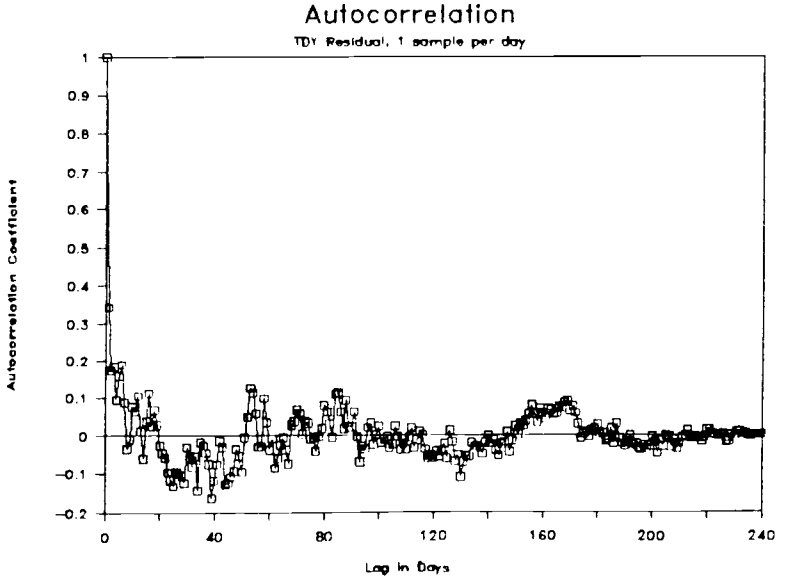

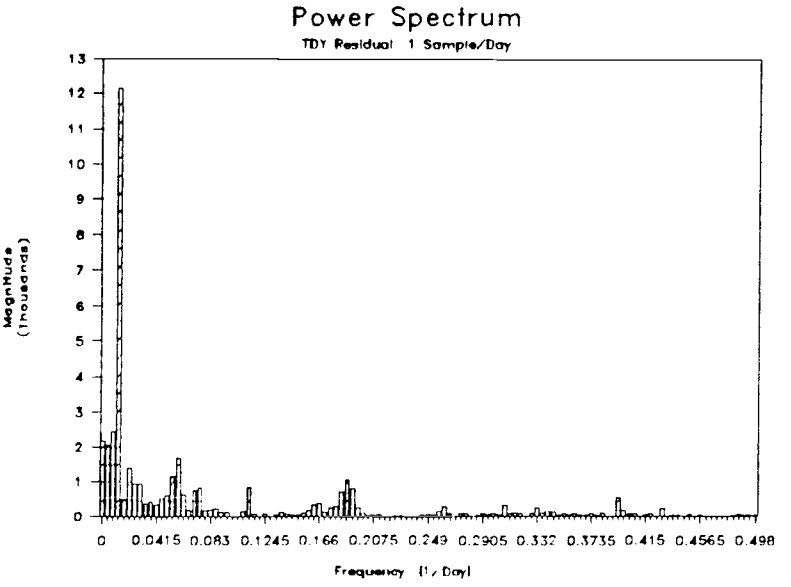
Power Spectrum
TDY Residual 1 Sample/Day
Magnitude (Thousands)
13
12
11
10
9
8
7
6
5
4
3
2
1
0
0
0.0415
0.083
0.1245
0.166
0.2075
0.249
0.2905
0.332
0.3735
0.415
0.4565
0.498
Frequency (1 / Day)